PhD Thesis

Novel redox probes for electrochemistry at the three-phase junction

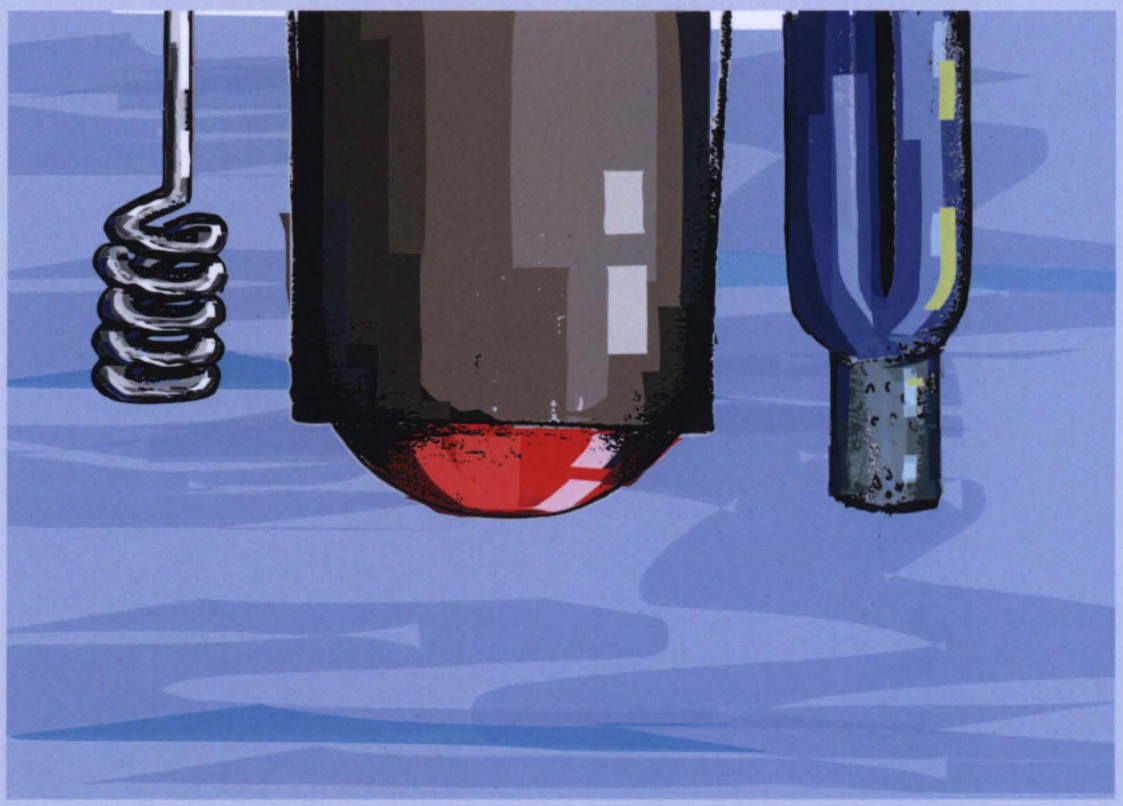

Vishwanath Rudregowda Sarojamma

Institute of Physical Chemistry

Polish Academy of Sciences

Institute of Physical Chemistry
Polish Academy of Sciences
Kasprzaka 44/52
01-224 Warsaw, Poland

PhD Thesis

Novel redox probes for electrochemistry at the three-phase junction

Vishwanath Rudregowda Sarojamma
(Vishwanath R. S)

Supervisor: dr hab. Martin Jönsson-Niedziółka, prof. IPC PAS

This dissertation was prepared within the International PhD in Chemistry Studies at the Institute of Physical Chemistry of the Polish Academy of Sciences in Warsaw

Warsaw, June 2020

Acknowledgements

I express my most profound gratitude to many people. Foremost, I thank my doctoral advisor, **dr hab. Martin Jönsson-Niedziółka**, he introduced me to the field of electrochemistry at liquid|liquid interfaces and microfluidic devices. Thank you for being an excellent guide, constant support, and mentorship during my PhD studies. Moreover, I acknowledge you for sharing your expertise with me; we had an excellent scientific discussion around the chalkboard. Besides the PhD topic, you allowed me to work on different projects for my benefit.

I thank all my colleagues and former members of Charge Transfer Processes in Hydrodynamic Systems group. In particular, **Marta Podrażka**, **Magdalena Kundys-Siedlecka**, **Dr Magdalena Z. Wiloch**, **Dr Wojciech Adamiak**, and **Dr Dawid Kałuża** for their help during my research. My special thanks to **Dr Emilia Witkowska Nery**, for motivating me throughout my doctoral studies to do better than I thought. Thank you for many suggestions and questions that encouraged different directions in my Ph D studies.

I acknowledge all the professors and staff of the **Institute of Physical Chemistry**, **Polish Academy of Sciences**, for offering essential physical chemistry courses, internships, seminars, and assistance.

I express gratitude to all my collaborators. Thanks to **prof. Mas-aaki Haga**, Chuo University, Tokyo, Japan, for offering an internship and guiding in the synthesis of electroactive metal complexes. Also, I extend my thanks to the master students from Chuo University with whom I worked many long night shifts on the synthesis of ruthenium complexes. I am thankful to my other collaborator **Dr Sakthivel Kandaiah**, REVA University, India, for providing the opportunity of working and having publication with me.

I thank my doctoral commission and thesis reviewers comprising of **prof. Włodzimierz Kutner**, **prof. Piotr Garstecki**, **prof. Dorota Gryko**, **dr hab. inż. Łukasza Górskiego**, and **prof. Zbigniew Stojek**.

I want to express my special thanks to my parents **Mr G. Thipperudre Gowda** and **Mrs G. Sarojamma**, for their constant support and love. Last but not least, I thank my wife, brother, and friends from India, Poland, and everywhere.

This research work was funded by the National Science Centre and the Institute of Physical Chemistry, Polish Academy of Sciences, Poland.

NATIONAL SCIENCE CENTRE
POLAND

I am very grateful to the **National Science Centre**, Poland, for the provision of a doctoral scholarship in grant no **NCN 2015/18/E/ST4/00319**.

I am genuinely thankful to the **Institute of Physical Chemistry**, **Polish Academy of Sciences** for the part-time employment, a doctoral fellowship (2019), the outstanding PhD student scholarship (2019), and supporting my doctoral research during the past four years.

Abstract

This thesis aimed to investigate the electrochemistry of different compounds at the organic|aqueous|electrode three-phase interface. For three-phase electrochemistry, I used the microdroplet based three-phase electrode (TPE) configuration and TPE configuration created in microfluidic devices.

In the microdroplet based TPE system, a microdroplet volume of a water-immiscible organic solvent containing a neutral lipophilic redox compound (without supporting electrolyte) is deposited on the working electrode and immersed in the aqueous electrolyte. The electron transfer across the electrode|organic interface results in the ions transfer from aqueous to the organic phase to maintain the electroneutrality in the organic droplet. This method enables determining the lipophilicity of different transferring ions at various organic|aqueous interfaces. Further, the lipophilicity of moving ions can be correlated with their biological and pharmacological activities. Additionally, the lipophilic|hydrophilic interface formed at TPE is the simple design of complex biological systems, hence studying electrochemistry of biologically relevant compounds and ions at TPE is required.

The first section of my work concerns the use of different quinones for cation transfer studies. Generally, electroactive organic and metallorganic compounds have been used to study ion transfer at TPE system. However, the redox behaviour of biologically essential compounds is not often studied at the TPE setup. Hence, I studied the reduction of essential quinone derivatives such as 1-aminoanthraquinone (AQ), and 2,3-dichloro-1,4-naphthoquinone (NQ) at glassy carbon (GC) working electrode|n-octyl-2-pyrrolidone (NOP)|aqueous electrolyte three-phase interface for cation transfer studies. Both AQ and NQ functional groups are present in various biomolecules, and the activities of these biomolecules depend on the redox behaviour of the quinone moieties (AQ and NQ). At the three-phase junction, AQ exhibited a single step two-electron reduction to AQ^{2-}, which was supported by the cations transfer from the aqueous to NOP. However, NQ reduction occurred in two steps; in the first step (NQ to $NQ^{\bullet-}$ radical anion), $NQ^{\bullet-}$ transferred to the interface with the reduction potential dependent on the hydrophobicity of the aqueous anion due to salting-out effects. In the second reduction ($NQ^{\bullet-}$ to NQ^{2-}), cations transferred from the aqueous phase to NOP. With AQ and NQ, the cation transfer potential depends on the ionic potential of the aqueous cation due to the ion-pair formation between the transferred cation with the reduced quinone in NOP.

The second section comprises the study of 7,7,8,8-tetracyanoquinodimethane (TCNQ) for cation transfer at GC|NOP|aqueous TPE configuration. TCNQ is an organic redox probe, employed in the studies of heterogeneous electron and alkylammonium cation transfer across the organic|aqueous interfaces. To examine TCNQ's applicability

for TPE cation transfer reactions, it is essential to investigate for both inorganic and organic cations. Consequently, I studied the reduction of TCNQ at GC|NOP|aqueous three-phase interface for both inorganic and organic cations transfer reactions. At the three-phase junction, the reduction of TCNQ to $TCNQ^{\bullet-}$ and $TCNQ^{2-}$ leads to the reduced TCNQ anions ($TCNQ^{\bullet-}$ and $TCNQ^{2-}$) expulsion to water instead of cation transfer from the aqueous phase to NOP. TCNQ anion expulsion was confirmed by the decrease of current in the continuous scans, and the reduction potentials did not depend on the nature of the aqueous cation. Moreover, the reduction potential of TCNQ to $TCNQ^{\bullet-}$ varied with the hydrophobicity of the aqueous anion because of the salting-out effect when $TCNQ^{\bullet-}$ transferred to the water. Therefore, TCNQ is not a suitable redox probe for TPE cation transfer studies.

The third part of my work includes the three-phase anion transfer studies using a highly lipophilic mononuclear ruthenium(II) complex $[Ru^{II}(LR)(L)]^0$ having two tridentate ligands of 2,6-bis(1-(2-octyldodecan)benzimidazol-2-yl)pyridine (LR) and 2,6-bis(benzimidazol-2-yl)pyridine (L). So far, commercially available decamethylferrocene (DMFc) and tetraphenylporphyrinato-metal complexes (TPP-metal) have been used for anion transfer studies. It is known that the expulsion of oxidised DMFc to water is possible when the aqueous phase contains hydrophilic anions (Cl^-); also, TPP-metal complexes interact with the transferring nucleophilic anions (F^- and SCN^-). Thus, a new, highly lipophilic non-interacting redox probe is needed. Therefore, during my internship in Japan, I synthesised $[Ru^{II}(LR)(L)]^0$ complex and investigated the anion transfer studies at GC|nitrobenzene(NB)|aqueous TPE setup. The oxidation of $[Ru^{II}(LR)(L)]^0$ to $[Ru^{III}(LR)(L)]^+$ in NB is followed by the anion transfer from the water to NB. Anion transfer was verified by examining the dependence of oxidation potential on the hydrophobicity and concentration of the aqueous anion. Usually, Ru complexes are not used in anion transfer studies since they do not undergo $Ru^{II/III}$ oxidation before the water oxidation at TPE. In this work, by choosing bis(benzimidazolyl)pyridine based ligands, the lower $Ru^{II/III}$ oxidation potential and high lipophilicity of $[Ru^{II}(LR)(L)]^0$ complex was achieved.

The last section of the thesis constitutes the investigation of the ion transfer voltammetry in the microfluidic TPE setup of different geometries. In the microfluidic device, the parallel flow of the organic|aqueous interface across the microband electrode creates the three-phase junction; which is used to study the ion transfer across the interface in hydrodynamic condition. D. Kałuza et al. from our group have performed a comparison ion transfer study between a droplet-based TPE system and a microfluidic TPE system. Also, they investigated the strange effect of flow rate with the limiting current in three-phase cyclic voltammetry. To contribute further, I tried to examine the voltammetry in the T-junction microfluidic TPE system; where one phase is stationary, and the other is flowing. I fabricated different models of T-junction and chemically hydrophobised the microchannel to have the stationary organic phase and flowing

aqueous phase. The interface was not stable at T-junction and always moved back-and-forth. Hence the ion transfer voltammetry was not reproducible. Besides, increasing the hydrophobicity and providing PDMS micropillar structures to the organic microchannel could not able to prevent the tiny back-and-forth vibration of the interface.

Streszczenie

Celem niniejszej pacy doktorskiej było zbadanie procesów elektrodowych zachodzących w układach trójfazowych typu: faza organiczna|faza wodna|powierzchnia elektrody dla różnych związków. Badania zostały przeprowadzone zarówno w układach stacjonarnych jak i przepływowych. W układach stacjonarnych stosowałem elektrody, których powierzchnię modyfikowałem mikrokroplami, tak aby uzyskać granice trzech faz (ang. three-phase electrode - TPE). Granicą trzech faz uzyskuje się poprzez modyfikację powierzchni elektrody pracującej za pomocą naniesienia mikrolitowej objętości cieczy organicznej niemieszającej się z wodą. Faza organiczna zawiera lipofilowy, elektrycznie obojętny związek ulegający reakcjom utlenienia i redukcji, natomiast pozbawiona jest elektrolitu. Tak przygotowaną elektrodę zanurza się do wodnego roztworu elektrolitu podstawowego. Zastosowanie układu typu TPE umożliwia określenie lipofilowości jonów przenoszących przez różne granice faz typu ciecz|ciecz, gdzie jedną z faz stanowi rozpuszczalnik organiczny, a drugą woda. TPE z powadzeniem może być stosowany do określania liofilowości, parametru określającego aktywność biologiczną i farmakologiczną, cząsteczek obdarzonych ładunkiem. Układ typu TPE może być również stosowany jako prosty model membran biologicznych (np. błony komórkowej) ze względu na występowanie obok siebie dwóch faz, w których jedna ma charakter lipofilowy a druga hydrofilowy.

W pierwszym rozdziale części eksperymentalnej niniejszej rozprawy opisałem badania transportu kationów z wykorzystaniem różnego typu chinonów. Najczęściej badanymi substancjami w układach typu TPE są elektroaktywne związki organiczne oraz związki metaloorganiczne. Niewiele doniesień literaturowych opisujących pomiary na granicy trzech faz dotyczy badań substancji biologicznie istotnych. Dlatego podjąłem się próby scharakteryzowania odpowiedzi prądowej związków będących pochodnymi chinonu: 1-aminoantrachinon (AQ) i 2,3-dichloro-1,4-naftochinon (NQ). Związki te osadzałem na powierzchni elektrody z węgla szklistego, po wcześniejszym ich rozpuszczeni w n-oktylo-2-pirolidonie (NOP). Badania procesów reakcji redukcji wykonałem w wodnych elektrolitach podstawowych. Wspomniane grupy AQ i NQ są obecne w różnych biomolekułach, a aktywność tych biocząsteczek zależy od zachowania redoks ugrupowań chinonowych (AQ i NQ).

Na granicy trzech faz AQ ulega jednoetapowej, dwuelektronowej reakcji redukcji do AQ^{2-}, czemu towarzyszy przeniesienie kationów z roztworu wodnego do NOP. W przypadku NQ redukcja zachodzi w dwóch etapach. W pierwszym etapie NQ ulega reakcji redukcji do anionorodnika $NQ^{\bullet-}$. Utworzony anionorodnik $NQ^{\bullet-}$ jest transportowany do granicy faz: faza organiczna|faza wodna, a potencjał redukcji tego anionorodnika zależy od hydrofobowości anionu obecnego w fazie wodnej, zgodnie z tzw. efektem wysalania. Drugiemu etapowi reakcji redukcji z formy $NQ^{\bullet-}$ do NQ^{2-} towarzyszy przeniesienie kationów z fazy wodnej do NOP. Zarówno w przypadku AQ jak i NQ potencjał przejścia kationu zależny od siły jonowej związanej z obecnością różnych kationów w fazie wodnej oraz tworzeniem sie par jonowych pomiędzy

przenoszonym kationem z fazy wodnej oraz zredukowaną formą chinonu rozpuszczoną w NOP.

Drugi rozdział części eksperymentalnej rozprawy obejmuje badania z wykorzystaniem granicy trzech faz transportu kationów z fazy wodnej do organicznej zawierającej 7,7,8,8-tetracyanochinodimetanu (TCNQ). TCNQ to organiczny próbnik redoks, stosowany zarówno w badaniach heterogenicznego transportu elektronów jak i w badaniach przeniesienia jonów alkiloamoniowych przez granice faz: ciecz|ciecz gdzie jedną z faz stanowi faza organiczna a drugą wodna. Celem badań opisanych w tym rozdziale było sprawdzenie czy cząsteczka TCNQ może być stosowana jako próbnik redoks do badania przeniesienia kationu z fazy wodnej do organicznej w układzie TPE. W tym celu zbadałem reakcje przeniesienia różnych kationów organicznych i nieorganicznych zachodzące podczas redukcji TCNQ. Otrzymane wyniki wskazują, że reakcje redukcji TCNQ do $TCNQ^{\bullet-}$ i $TCNQ^{2-}$ skutkowały przeniesieniem zredukowanych związków do fazy wodnej, a nie tak jak zakładano pierwotnie transportem kationów do NOP. Świadczył o tym spadek wartości natężania prądu w kolejnych cyklach pomiarowych oraz brak zmiany wartości potencjału przejścia dla różnych kationów obecnych w fazie wodnej. Ponadto zauważyłem, że potencjał reakcji redukcji TCNQ do $TCNQ^{\bullet-}$ zmieniał się zależnie od hydrofobowości anionu obecnego w fazie wodnej, co związane było z tzw. efektem wysalania. Na podstawie uzyskanych wyników stwierdziłem że TCNQ nie jest odpowiednim próbnikiem redoks do badań w układzie typu TPE.

Trzecia część prac eksperymentalnych przestawiona w tej rozprawie obejmuje badania na granicy trzech faz z przeniesieniem anionów. W trakcie realizacji moje pracy doktorskiej badałem liofilowy kompleksu rutenu(II) $[Ru^{II}(LR)(L)]^0$ z podstawionymi dwoma ligandami trójwartościowymi: 2,6-bis(1-(2-oktyldodekanu))benzimidazol-2-ilo)pirydyna (LR) i 2,6-bis(benzimidazol-2-ilo)pirydyna (L). Do tej pory w celu badania przeniesienia anionów w układzie z granicą trzech faz stosowano powszechnie dostępny dekametyloferrocen (DMFc) i kompleksy metali z tetrafenyloporfirynami (TPP-metal). Na podstawie przeprowadzonych prac udowodniono, że utleniona forma DMFc może przechodzić z fazy organicznej do wodnej gdy w tej ostatniej obecne są aniony hydrofilowe (Cl^-). Wykazano również, że możliwe jest oddziaływanie kompleksów TPP-metal z anionami nukleofilowymi (F^- i SCN^-), przenoszonymi z fazy wodnej do organicznej – co jest zjawiskiem niepożądanym. Niezbędne było zatem otrzymanie nowego próbnika redoks, który posiadałby właściwości lipofilowe i jednocześnie nie oddziaływał z transportowanymi z fazy wodnej anionami. Synteza takiego związku była kolejnym celem mojej pracy doktorskiej. W trakcie zagranicznego stażu w Japonii zsyntezowałem związek kompleksowy rutenu: $[Ru^{II}(LR)(L)]^0$, którego właściwości elektrochemiczne zbadałem w układzie typu TPE (elektroda GC|nitrobenzen(NB)|faza wodna). Zgodnie z oczekiwaniami reakcji utlenienia $[Ru^{II}(LR)(L)]^0$ do $[Ru^{III}(LR)(L)]^+$ zachodzącej w NB, towarzyszyło przeniesienie anionów z fazy wodnej do organicznej.

W celu pełnego scharakteryzowania otrzymanego próbnika redoks zbadałem jak hydrofobowość oraz stężenie anionów obecnych w fazie wodnej wpływa na potencjał utleniania $[Ru^{II}(LR)(L)]^0$. Należy podkreślić że zazwyczaj związki kompleksowe rutenu nie są wykorzystywane w badaniach nad przeniesieniem anionów, ponieważ w układach typu TPE utlenianie wody jest bardziej prawdopodobne niż reakcja utlenienia Ru^{II} do Ru^{III}. Jednak zsyntezowany przeze mnie związek $[Ru^{II}(LR)(L)]^0$, zawiera w swojej strukturze ligandy oparte na bis(benzimidazolilo)pirydynie przez co wykazuje się nie tylko wysoką lipofilowością, ale również posiada znacznie niższy potencjał utleniania centrum metalicznego niż inne związki kompleksowe rutenu.

W ostatnim rozdziale części eksperymentalnej niniejszej rozprawy opisane są badania przeprowadzone w układach mikroprzepływowych o różnych geometriach. W układach mikroprzepływowych, granica trzech faz tworzy się między strumieniami fazy wodnej i organicznej oraz elektrodą wbudowaną w układ dzięki czemu możliwe jest badania przeniesienia jonów w warunkach hydrodynamicznych. W grupie badawczej, w której wykonywałem swoją pracę doktorską podjedliśmy się porównania dwóch układów typu TPE, pierwszy z nich oparty był na kropli i badaniach opisanych powyżej, drugi powstawał w specjalnie do tego celu przygotowanych mikroukładach. Zbadałem wpływ szybkości przepływu cieczy na rejestrowany prąd graniczny. Stworzyłem również specjalne układy z mikrokanałami w kształcie litery T, w których tylko faza wodna była ruchoma. Aby uniknąć tworzenia mikroemulsji w takim układzie oraz aby ustabilizować fazę organiczną zwiększyłem hydrofobowość mikrokanałów poprzez ich chemiczną modyfikację. Niestety nie udało się osiągnąć stabilnej granicy trzech faz, co powodowało brak powtarzalności uzyskiwanych wyników. Ponadto ani zwiększenie hydrofobowości mikrokanałów, ani wykorzystanie podłoża wykonanego z PDMS nie zapobiegło drobnym i niepożądanym mikro drganiom granicy faz.

Major abbreviations

Abbreviations:	Description
ITIES	Interface between two immiscible electrolyte solutions
DCB	Dichlorobenzene
DCE	1,2-dichloroethane
NB	Nitrobenzene
NOP	1-octyl-2-pyrrolidone
WE	Working electrode
RE	Reference electrode
CE	Counter electrode
TPE	Three-phase electrode
GC	Glassy carbon
Ox^+	The oxidised form of the compound
Red^-	The reduced form of the compound
An^-	Aqueous electrolyte anion
Cat^+	Aqueous electrolyte cation
TRPDs	*N*,*N*,*N*′,*N*′-tetraalkylphenylenediamines
THPD	*N*,*N*,*N*′,*N*′-tetrahexylphenylenediamine
DMFc	Bis(pentamethylcyclopentadienyl)iron(II)
TPP	Tetraphenylporphyrinato
Fe(III)TPP-Cl	Iron(III) tetraphenyl porphyrine chloride
TCNQ	Tetracyanoquinodimethane
$TCNQ^{\bullet-}$	Tetracyanoquinodimethane radical anion
$TCNQ^{2-}$	Tetracyanoquinodimethane dianion
LBPC	Lutetium bis(tetra-tert-butylphthalocyaninato)
DPPH	2,2-diphenyl-1-picrylhydrazyl
TMACl	Tetramethylammonium chloride
TEACl	Tetraethylammonium chloride
TPACl	Tetrapropylammonium chloride
TBACl	Tetrabutylammonium chloride
$TBAClO_4$	Tetrabutylammonium perchlorate

AQ	1-Aminoanthraquinone
$AQ^{\bullet-}$	1-Aminoanthraquinone radical anion
AQ^{2-}	1-Aminoanthraquinone dianion
NQ	2,3-Dichloro-1,4-naphthoquinone
$NQ^{\bullet-}$	2,3-Dichloro-1,4-naphthoquinone radical anion
NQ^{2-}	2,3-Dichloro-1,4-naphthoquinone dianion
LH_2	2,6-Bis(benzimidazol-2-yl)pyridine
LR	2,6-Bis(1-(2-octyldodecan)benzimidazol-2-yl)pyridine)
$[Ru^{II}(LR)(L)]^0$	Ru complex having two tridentate LR and L ligands
CV	Cyclic voltammogram
SWV	Square wave voltammogram
PDMS	Polydimethylsiloxane
OTS	Octadecyltrichlorosilane

List of contents

Publications

This thesis is based on the following publications:

1) **R.S. Vishwanath**, E. Witkowska Nery, M. Jönsson-Niedziółka, Electrochemistry of selected quinones at immiscible n-octyl-2-pyrrolidone/aqueous interface using a three-phase electrode system, Electrochim. Acta. 306 (2019) 54–60.
2) **R.S. Vishwanath**, E. Witkowska Nery, M. Jönsson-Niedziółka, Electrochemical reduction of 7,7,8,8-tetracyanoquinodimethane at the n-octyl pyrrolidone/water/electrode three-phase junction, J. Electroanal. Chem. 854 (2019) 113558.
3) **R.S. Vishwanath**, Masa-aki Haga, Takumi Watanabe, E. Witkowska Nery, M. Jönsson-Niedziółka, Three-phase electrochemistry of a highly lipophilic neutral Ru-complex having tridentate bis(benzimidazolate)pyridine ligand, ChemRxiv , http://doi.org/10.26434/chemrxiv.12170136.v2, (**Under review**).

Other publications during the PhD studies:

4) I. Udachyan, P. Kumara, **R.S. Vishwanath**, S. Kandaiah, Visible-Light-Active Mixed-Valent Copper-Ion-Coordinated 2,5-Dimercapto-1,3,4-thiadiazole-Based p-Type Metallopolymer, ChemElectroChem. 5 (2018) 3847–3853.
5) I. Udachyan, **R.S. Vishwanath**, C.S. Pradeepa Kumara, S. Kandaiah, Ruthenium ion containing N and S rich triazine based metallopolymer as a low overpotential acid stable electrocatalyst for hydrogen evolution, J. Catal. 357 (2018) 138–146.
6) M. Mallappa, M.A. Savanur, B.G. Gowda, **R.S. Vishwanth**, B. Puthusseri, Molecular Interaction of Hemorrheologic Agent, Pentoxifylline with Bovine Serum Albumin: An Approach to Investigate the Drug Protein Interaction Using multispectroscopic, Voltammetry and Molecular Modelling Techniques, Zeitschrift Für Phys. Chemie. 233 (2019) 973–994.
7) I. Udachyan, **Vishwanath. R. S.**, P.K. C. S., S. Kandaiah, Anodic fabrication of nanostructured Cu_xS and $CuNiS_x$ thin films and their hydrogen evolution activities in acidic electrolytes, New J. Chem. 43 (2019) 7674–7682.
8) I. Udachyan, **R.S. Vishwanath**, C.S. Pradeepa Kumara, S. Kandaiah, Potential dependent growth of $Cu(OH)_2$ nanostructures on Cu and their thermal conversion to mixed-valent copper oxides p-type photoelectrode, Int. J. Hydrogen Energy. 44 (2019) 7181–7193.

Publications before starting PhD studies:

9) **R.S. Vishwanath**, S. Kandaiah, Metal ion-containing $C_3N_3S_3$ coordination polymers chemisorbed to a copper surface as acid stable hydrogen evolution electrocatalysts, J. Mater. Chem. A. 5 (2017) 2052–2065.
10) **R.S. Vishwanath**, S. Kandaiah, Electrochemical growth of triazine based metal ion containing polymers on nanostructured nickel electrodeposits and their hydrogen evolution activities in acidic condition, Int. J. Hydrogen Energy. 41 (2016) 8829–8838.
11) **R.S. Vishwanath**, S. Kandaiah, Chemically Immobilized Triazine Based $Cu^{II}S_3C_3N_3$ Metallopolymer on Copper as a Photocathode for Photoelectrochemical Hydrogen Evolution, J. Electrochem. Soc. 163 (2016) H402–H409.
12) **R.S. Vishwanath**, S. Kandaiah, Electrochemical preparation of crystalline γ-CuI thin films through potential-controlled anodization of copper and its photoelectrochemical investigations, J. Solid State Electrochem. 20 (2016) 2093–2102.
13) **R.S. Vishwanath**, S. Kandaiah, Facile electrochemical growth of nanostructured copper phthalocyanine thin film via simultaneous anodic oxidation of copper and dilithium phthalocyanine for photoelectrochemical hydrogen evolution, J. Solid State Electrochem. 20 (2016) 767–773.

Chapter 1. Electrochemistry at liquid|liquid interfaces

1.1 Introduction

This chapter gives an introduction to the structure and dynamics at the liquid|liquid interface. The fundamental aspects related to my research, such as ion partition, types of interfaces, and several ion transfer reactions at the liquid|liquid interface, are summarised.

According to the electrochemical literature, the liquid|liquid interface or an interface between two immiscible electrolyte solutions (ITIES) refers to the interface established between two immiscible/low mutually miscible liquid solvents. Generally, one of these solvents is water, and the other is a polar liquid organic solvent having high/moderate dielectric permittivity such as 1,2-dichloroethane (DCE), dichlorobenzene (DCB), nitrobenzene (NB), 1-octyl-2-pyrrolidone (NOP), and 2-nitrophenyl octyl ether (NPOE). Liquid|liquid interfaces establish not only between water and liquid organic solvents but, can also be present between some of the liquid noble gases and liquid nitrogen systems. However, the interfaces of organic|aqueous and room-temperature ionic liquid|aqueous are generally studied for both applied and fundamental science [1–3].

Electrochemistry at an ITIES gained interest due to its wide range of scope in biochemical and chemical domains. In biological systems, ion transport across lipophilic|hydrophilic (i.e., organic|aqueous) interfaces is vital for several biological activities. The relevant thermodynamic data, namely, the standard Gibbs energies of transfer of ions across the interface, are essential to determine their lipophilicities, which further related the pharmacological activities [4,5]. In living systems, the organic phase is generally in the form of a molecular membrane; molecules are not dispersed like in the bulk of a liquid. Although, both organic phase and molecular membrane have similar properties (e.g., lower polarity and immiscibility with water) [1]. Hence, the organic|aqueous interface is a simple model of the more complex biological system.

The electrochemical charge transfer reactions at the liquid|liquid interface are the necessary aspects of several practical applications in chemistry: especially electro-assisted solvent extraction, phase-transfer catalysis, electrocatalysis, pharmacokinetics and electrochemical sensors [6].

When the interface is formed between two immiscible solutions having compounds dissolved in them, the partition of the compounds takes place according to their solvation in both the phases (the thermodynamic aspect) with a fixed rate (the kinetic aspect). In another case, where ions are present in one or both phases, ions also undergo partition, which leads to the development of the interfacial potential difference. Such interfaces merely show electrochemical effects, and various electrochemical techniques are there to study them [1]. They are discussed in detail in this chapter.

1.2 Theoretical and methodological concepts in the structure and dynamics of the ITIES

The structure of the liquid|liquid interface is complex to imagine when electrolytes are present in the adjacent phases. Few comprehensive reviews by Z. Samec [3,7] and F. Scholz [1], give us a detailed overview of the theoretical modellings and experimental results in the study of the ITIES, primarily concerned with the structure and dynamics of the ITIES. Most of the understandings about the molecular structure of the interface are from the molecular dynamic (MD) and Monte Carlo (MC) simulations.

The initial structural descriptions of the liquid|liquid interface were developed from the existing solid|liquid interface models. In 1939, the first theoretical approach by Verwey and Niessen [8], represented the ITIES as two back-to-back, diffuse double layers with one phase comprising plenty of the positive space charge and the other phase having an equal extra of the negative space charge (**Fig. 1.1a**) [3,7]. The diffuse double layer in the Verwey and Niessen (VN) model was analysed by the Gouy and Chapman theory. Gouy and Chapman model explains a situation of the solid charged surface in contact with oppositely charged ions in the solution; where the ions concentration decreases with a distance from the solid charged surface (diffuse double layer). Gavach and co-workers proposed the presence of an ion-free inner solvent layer, which separates two diffuse layers at liquid|liquid interface (a modified Verwey–Niessen model, MVN) (**Fig. 1.1b** and **1.2**) [9]. According to the MVN and VN models, the interface was hypothetically sharp, which means the step change in the density of the solvent at the Gibbs dividing surface [3]. Later Girault et al. proposed the concept of the mixed solvent and ion layer comprising a constant change in composition on moving from one phase to another [10].

Benjamin's MD simulations of the DCE|water interfacial ion transfer showed the existence of capillary wave distortions (capillary waves), and the interface was rough but sharp on a molecular scale [3,11] (**Fig. 1.1c**). Minimal displacement of molecules concerning their in-plane position, give rise to an increase in the interfacial area, the interfacial tension reverses back this displacement to build up capillary waves [1]. There can also be an additional effect which is the bending rigidity of the interface. On both sides of the interface, the dipole molecules line up in the energetically preferred position. Which means the positive and negative ends of the molecules are positioned opposite to each other. Any distortion will increase the free energy due to a non-ideal alignment of the dipoles, and the offsetting distortions are assumed as an additional rigidity [1].

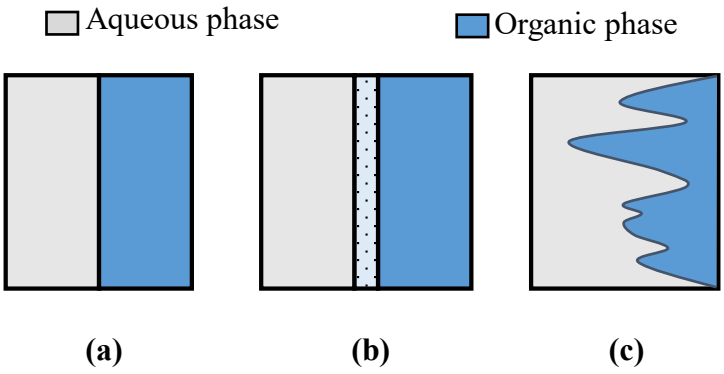

Figure 1.1 Sketches of the ITIES. **(a)** Verwey and Niessen model showing two back-to-back GC diffuse double layers. **(b)** Modified Verwey–Niessen model showing the ion-free solvent inner layer between two diffuse layers. **(c)** Molecular dynamic or capillary waves model. Adapted from Ref. [3].

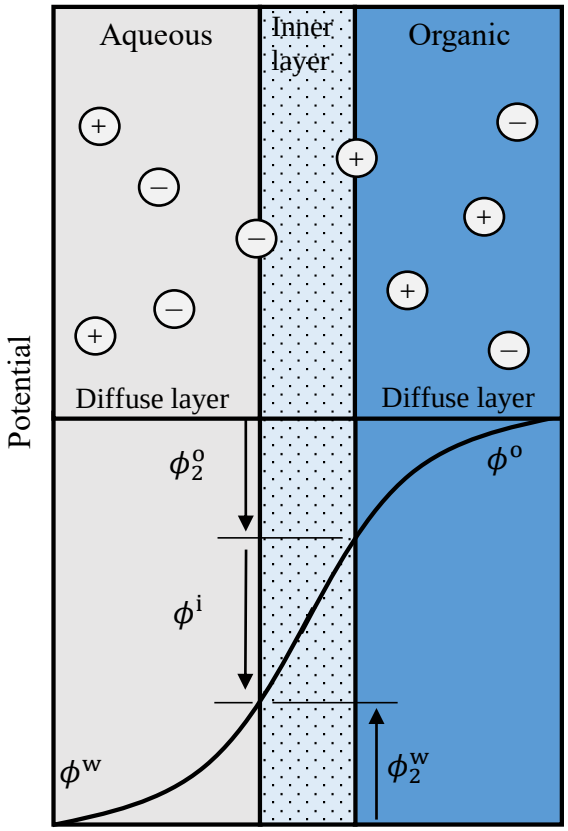

Figure 1.2 Modified Verwey and Niessen model showing the Galvani potentials of the aqueous (ϕ^{w}) and the organic phases (ϕ^{o}). Where, ϕ^{i} is the potential difference across the inner layer, ϕ_2^{o} and ϕ_2^{w} are the potential differences across the space charge regions in the organic and aqueous phases, respectively. Adapted from [7].

MD simulations of hydrogen bond dynamics at the interface between water and a series of organic liquids have been reported [12]. MC simulations showed that the water molecules near the organic phase prefer to align perpendicular to the interface plane [13]. Few models developed in which ions allowed to penetrate the inner layer and interactions have studied [14,15].

Many experimental attempts had made to understand the structure of the interface, which discussed in the critical reviews and a book chapter by Z. Samec [2,3,7,16]. However, the structure of liquid|liquid interface has not yet understood completely, but the research along this line is making progress.

1.3 Thermodynamics for the ions partition

The fundamental concepts related to the thermodynamics of ions partition and development of Galvani potential difference at ITIES are well described in the review articles by Z Samec [2], P. Peljo et al. [17], and L. J. S. Vallejo et al. [18]. This section has been adapted from the references mentioned above.

Ions can partition between immiscible organic (org) and aqueous (aq) electrolyte solutions due to the difference in the ion energy in both the phases. This simple ion transfer at org|aq interface is represented as [18]:

$$I^{z_i}(\text{aq}) \leftrightharpoons I^{z_i}(\text{org}) \qquad 1.1$$

Where the ion (I^{z_i}) can transfer from aqueous to the organic phase or reverse, z_i represents the charge of the species *i*.

The thermodynamic equilibrium maintains the equality of electrochemical potentials ($\tilde{\mu}$) of *i* in each phase at constant temperature and pressure [18]:

$$\tilde{\mu}_i^{\text{aq}} = \tilde{\mu}_i^{\text{org}} \qquad 1.2$$

For ions, the electrochemical potential has a chemical term and an electrical term [18]:

$$\tilde{\mu}_i^j = \mu_i^j + z_i F \phi^j \qquad 1.3$$

Where, $z_i F \phi^j$ is the electrical term; z_i represents the charge number of the ion, *F* indicates the Faraday constant, and ϕ^j is the Galvani potential of the *j* phase (*j* = aq and org phase). The chemical potential term μ_i^j is given by [17,18]:

$$\mu_i^j = \mu_i^{0,j} + RT \ln(a_i^j) \qquad 1.4$$

Where, $\mu_i^{0,j}$ signifies the standard chemical potential, *R* refers to the universal gas constant, and *T* is the absolute temperature. The term a_i^j represents the activity of *i* in the *j*-phase.

At the interface, the electrochemical potentials are at equilibrium. Hence, Eq. 1.2 can be written as follows [17,18]:

$$\mu_i^{0,\mathrm{aq}} + RT\ln\left(a_i^{\mathrm{aq}}\right) + z_i F\phi^{\mathrm{aq}} = \mu_i^{0,\mathrm{org}} + RT\ln\left(a_i^{\mathrm{org}}\right) + z_i F\phi^{\mathrm{org}} \qquad 1.5$$

By rearranging the above expression, it is possible to express the Galvani potential difference ($\Delta_{\mathrm{org}}^{\mathrm{aq}}\phi$) between aqueous and the organic phases [18]:

$$\Delta_{\mathrm{org}}^{\mathrm{aq}}\phi = \frac{\Delta \mathrm{G}_{\mathrm{tr},i}^{0,\mathrm{aq}\rightarrow\mathrm{org}}}{z_i F} + \frac{RT}{z_i F}\ln\left(\frac{a_i^{\mathrm{org}}}{a_i^{\mathrm{aq}}}\right) \qquad 1.6$$

Where, $\Delta_{\mathrm{org}}^{\mathrm{aq}} = (\phi^{\mathrm{aq}} - \phi^{\mathrm{org}})$ and $\Delta \mathrm{G}_{\mathrm{tr},i}^{0,\mathrm{aq}\rightarrow\mathrm{org}} = (\mu_i^{0,\mathrm{org}} - \mu_i^{0,\mathrm{aq}})$ is the standard Gibbs energy of ion transfer from aqueous to the organic phase.

From Eq. 1.6, the Nernst ion transfer equation can be obtained on org|aq interfaces as follows [18]:

$$\Delta_{\mathrm{org}}^{\mathrm{aq}}\phi = \Delta_{\mathrm{org}}^{\mathrm{aq}}\phi_i^0 + \frac{RT}{z_i F}\ln\left(\frac{a_i^{\mathrm{org}}}{a_i^{\mathrm{aq}}}\right) \qquad 1.7$$

Where, $\Delta_{\mathrm{org}}^{\mathrm{aq}}\phi_i^0 = \frac{\Delta \mathrm{G}_{\mathrm{tr},i}^{0,\mathrm{aq}\rightarrow\mathrm{org}}}{z_i F}$ is the standard Galvani potential difference of ion transfer for species *i*.

1.4 Ideally non-polarizable ITIES

An ideally non-polarizable interface forms when the same salt (e.g., tetrabutylammonium bromide) is present in both immiscible solvents which are in contact. The partition of salt between adjacent phases causes the polarisation of the interface. In this case, the obtained Galvani potential difference/liquid junction potential ($\Delta_{\mathrm{org}}^{\mathrm{aq}}\phi$) is the distribution potential, and it is determined by the partitioning equilibrium of common ions present in both the phases. $\Delta_{\mathrm{org}}^{\mathrm{aq}}\phi$ is defined by applying equation 1.7 to both cation and anion (Eq. 1.8) [17].

$$\Delta_{\mathrm{org}}^{\mathrm{aq}}\phi = \Delta_{\mathrm{org}}^{\mathrm{aq}}\phi_{\mathrm{cat}^+}^0 + \frac{RT}{F}\ln\left(\frac{a_{\mathrm{cat}^+}^{\mathrm{org}}}{a_{\mathrm{cat}^+}^{\mathrm{aq}}}\right) = \Delta_{\mathrm{org}}^{\mathrm{aq}}\phi_{\mathrm{an}^-}^0 + \frac{RT}{F}\ln\left(\frac{a_{\mathrm{an}^-}^{\mathrm{org}}}{a_{\mathrm{an}^-}^{\mathrm{aq}}}\right) \qquad 1.8$$

For dilute solutions, the above equation shortens to (Eq. 1.9):

$$\Delta_{\mathrm{org}}^{\mathrm{aq}}\phi = \frac{1}{2}(\Delta_{\mathrm{org}}^{\mathrm{aq}}\phi_{\mathrm{cat}^+}^0 + \Delta_{\mathrm{org}}^{\mathrm{aq}}\phi_{\mathrm{an}^-}^0) \qquad 1.9$$

The distribution of salt causes the interface polarisation at a fixed potential, which is determined by the standard transfer potentials of the different ionic species. Since the polarisation potential has a fixed value, it is impossible to polarise the interface without

altering the chemical composition of both phases. Hence the polarisation of ideally non-polarizable interface causes the transfer of ions to maintain the equilibrium value [17].

1.5 Ideally polarisable ITIES

Ideally polarisable interfaces can be obtained by dissolving a hydrophilic salt (e.g., lithium sulphate) in water and a hydrophobic salt (e.g., tetrabutylammonium tetraphenylborate) in the organic phase so that the hydrophilic salt concentration in the organic solvent is insignificant compared with that of the hydrophobic salt concentration. On the other hand, the hydrophobic salt concentration in water is negligible when compared to hydrophilic salt concentration. In this case, the interface can be polarised by an external voltage source without changing the chemical composition of the adjacent phases. Because none of the phases has common ions; moreover, the electrolyte ions have high standard Gibbs energies of transfer. The applied Galvani potential difference by the external source results in the arrangement of two back-to-back, diffuse double layers [17]. Which somewhat looks like a capacitor with an excess of cations in one phase and anions in the other phase. These ions cannot transfer across the interface (to offset the changes of interfacial potential) within a specific potential window called the polarisation range.

In the 1970s, Claude Gavach showed that the ITIES is polarisable, like an interface between an electrode and an electrolyte. He used electrochemical methods to study the ion transfer reactions at the liquid|liquid interfaces [19–21]. Later, more studies were carried out by Koryta [22–24], he introduced the concept of standard Gibbs energy of ion transfer. After these two significant breakthrough contributions, this field has developed to become a new branch in electrochemistry.

1.6 Charge transfer reaction across the ITIES

Electrochemistry performed at the ITIES mainly includes three types of charge transfer processes. Namely: (1) Simple ion-transfer from one phase to another; (2) Ion-transfer facilitated by a complexing agent; (3) The electron-transfer reaction between redox probes present in the two phases [6,17]. However, both the facilitated ion-transfer and the electron-transfer reactions are beyond the scope of this thesis.

1.6.1 Simple ion transfer

As discussed in the earlier section 1.5, the ITIES is polarisable using an external voltage source. Experimentally, polarisation can be performed by using a four-electrode potentiostat having two reference (REs) and two counter electrodes (CEs) (**Fig. 1.3**). Also, by using the three-phase electrode system with a conventional three-electrode cell setup [17].

1.6.1.1 Four-electrode setup for ion transfer across the ITIES

Up till 2000, the direct polarisation of the liquid|liquid interface using a four-electrode setup was the exclusive electrochemical method to investigate the ion transfer reactions across the ITIES [1]. This setup is equipped with a pair of current-supplying (CEs) and a pair of potential measuring (REs) electrodes, as shown in **Fig. 1.3**. The organic RE requires an unpolarised liquid junction containing a common ion of either organic cation or anion. Moreover, four electrode ion transfer measurements are not easy to perform; working with cell requires the experience [25].

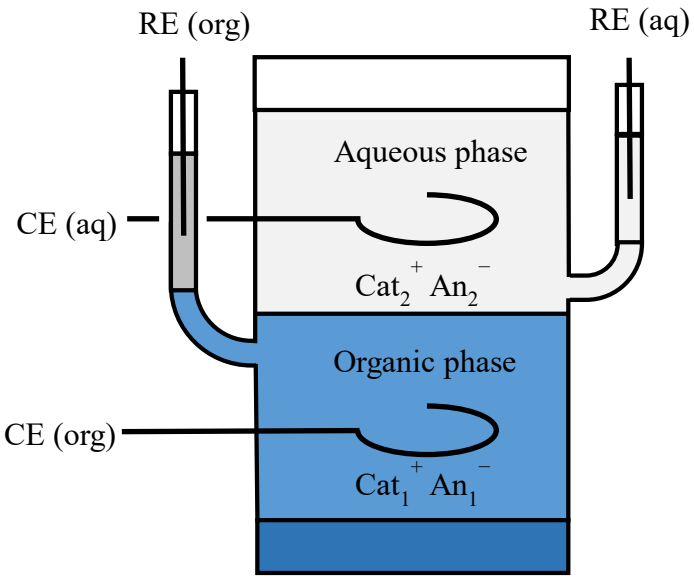

Figure 1.3 Four-electrode electrochemical cell setup for the study of ion transfer across the ITIES; RE = reference electrode and CE = counter electrode; $Cat_1^+An_1^-$ is a highly hydrophilic salt and $Cat_2^+An_2^-$ is a highly lipophilic salt. Adapted from [25].

For the polarisable ITIES, the $\Delta_{aq}^{org}\phi$ is determined by the electrostatic equilibrium. The polarisation of a polarisable interface to further positive or negative than the equilibrium potential results in the no net current flow; since the standard transfer potential values of the cation ($\Delta_{aq}^{org}\phi_{cat^+}^0$) and anion ($\Delta_{aq}^{org}\phi_{an^-}^0$) are high. Nevertheless, when the applied potential approaches high positive values, the aqueous cations or the organic anions gain sufficient energy to transfer to the adjacent phase. In the same manner, highly negative applied potentials provide the necessary energy for aqueous anions or organic cations to transfer to the other phase [17]. Such ions transfer across the ITIES result in the increase of net ionic current in the voltammograms. The shape of the voltammogram for polarisable ITIES with schematic illustrations of ion transfer is shown in **Fig. 1.4**.

The significant drawbacks of this method are: 1) The potential range is less due to the need of different electrolytes in both solvents; 2) Usually a large volume of organic solvent is required; 3) There are few organic solvents with suitable electrolytes could form a polarisable interface with an aqueous solution [25]. Hence, the traditional n-octanol|water interface (which mimics the biological membrane) cannot be polarisable

using a four-electrode technique. The reason is not having the appropriate lipophilic electrolyte for n-octanol [25].

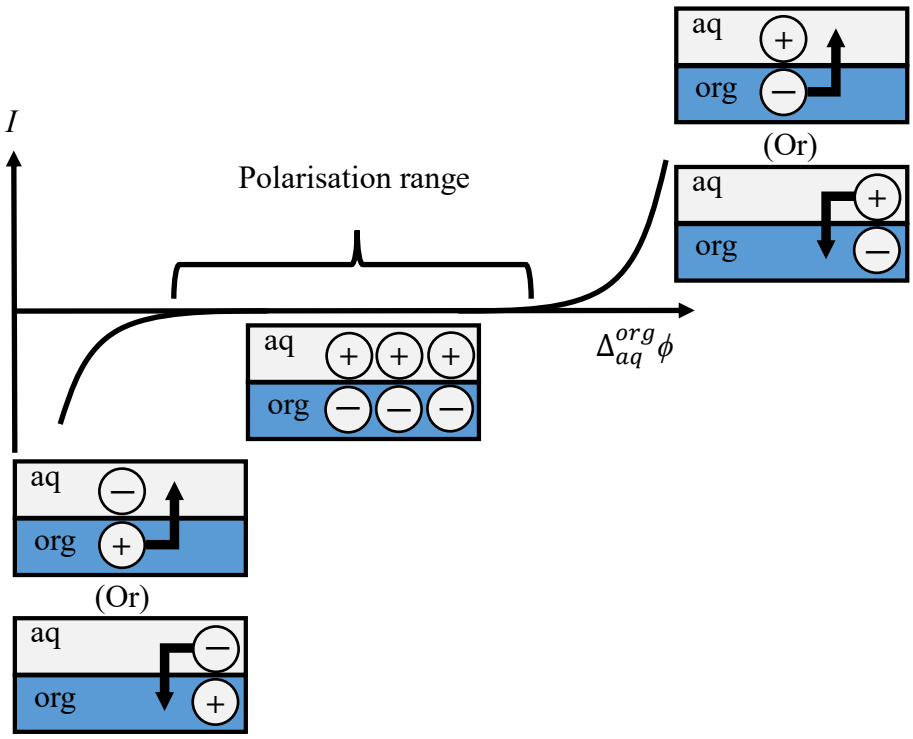

Figure 1.4 Voltammogram of a polarisable ITIES shown with the scheme of ion transfer reactions.

1.6.1.2 Three-phase electrode configuration for the ion transfer across the organic|aqueous interface

The basic principles of three-phase electrode (TPE) configuration, a detailed literature review, and the theoretical treatments on TPE ions transfer are well explained in a book (chapter 6) [26] and review by F. Scholz et al. [25]. Some of the figures and all the mathematical expressions used in this section are from the references mentioned above. TPE configuration for ion transfer across the interface has few advantages over the four-electrode system: 1) TPE setup does not require the RE in the organic phase; 2) A small volume of the organic phase is enough; 3) Most of the water-immiscible organic solvents can be used (including n-octanol) [25].

The liquid|liquid|solid three-phase junction is created when two immiscible liquids meet each other on the solid electrode surface. Each phase must share an interface with the other two phases. The situation of organic|aqueous|electrode three-phase junction participating in an electrode reaction is common in surface-modified, thin-film, and fuel cell electrode systems. The instance of an organic droplet attached to a solid electrode surface and immersed in an aqueous electrolyte solution is shown in **Fig. 1.5.** The shape

of the organic droplet at TPE setup depends on the interfacial tensions among the three phases, which is defined by the Young equation [26]:

$$\cos\theta = \frac{\sigma_{\mathrm{I-III}} - \sigma_{\mathrm{I-II}}}{\sigma_{\mathrm{II-III}}} \qquad 1.10$$

When the contact angle is minimal (θ is going to zero), the organic droplet would form a thin film on the electrode. If the contact angle is too large (approaching 180^0), then the organic droplet detaches from the electrode [26].

From the relation between the electrode potential and the interfacial tension [26]:

$$\sigma = -\frac{1}{2}C_d E^2 + \text{const.} \qquad 1.11$$

Where C_d indicates the differential double layer capacity, and E represents the electrode potential. Eq. 1.11 describes that altering the electrode potential will change the interfacial tensions of $\sigma_{\mathrm{I-II}}$ and $\sigma_{\mathrm{I-III}}$. Luckily, these changes are negligible when lipophilic microdroplets are attached to lipophilic surfaces like graphite, glassy carbon (GC), and paraffin-impregnated electrode. In another instance, where an organic droplet deposited on a metal electrode (Pt or Au), it is challenging to keep the droplet stable during the voltammetric experiments [26]. Hence, I used the GC working electrode (WE) for the three-phase junction electrochemistry.

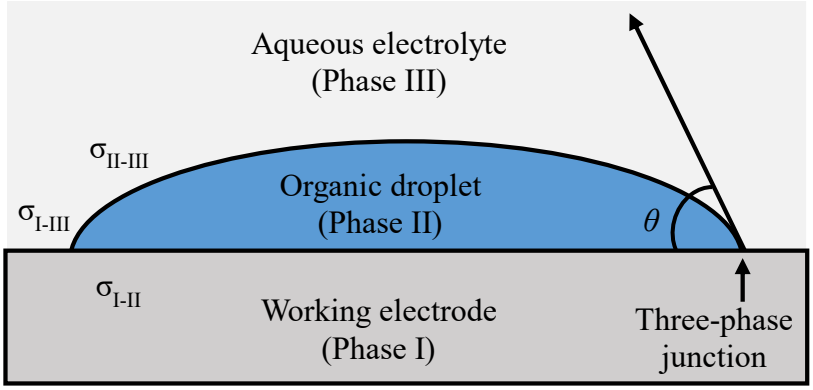

Figure 1.5 The three-phase electrode system of an organic droplet immobilized on a solid electrode and immersed in an aqueous electrolyte solution; where θ is the contact angle and σ represents the interfacial tension between the phases designated in the subscripts (adapted from page 226 of [26]).

1.6.1.2.1 The principle and experiment of TPE ion transfer

The principle of three-phase electrochemistry is similar to that of the insertion electrochemistry, which occurs at many solid compounds in batteries. For example, the

electrochemical reduction of solid manganese(IV) oxide in contact with an aqueous electrolyte solution (Eq. 1.12) [1].

$$MnO_{2(solid)} + e^- + H^+_{(solution)} \leftrightharpoons MnOOH_{(solid)} \qquad 1.12$$

The electron transfer from a current supply to the solid MnO_2 compound is accompanied by the transfer of the H^+ ion from a solution to the solid MnO_2. Insertion electrochemistry is studied very handily using a technique where electroactive solid particles are immobilised on the surface of the inert WE [26]. Similar electrochemistry can be performed by attaching an electroactive water-immiscible organic droplet (without supporting electrolyte) to WE instead of an electroactive solid compound. The latter method helps us to determine the standard Gibbs energy of ion transfer across an organic|aqueous interface [25].

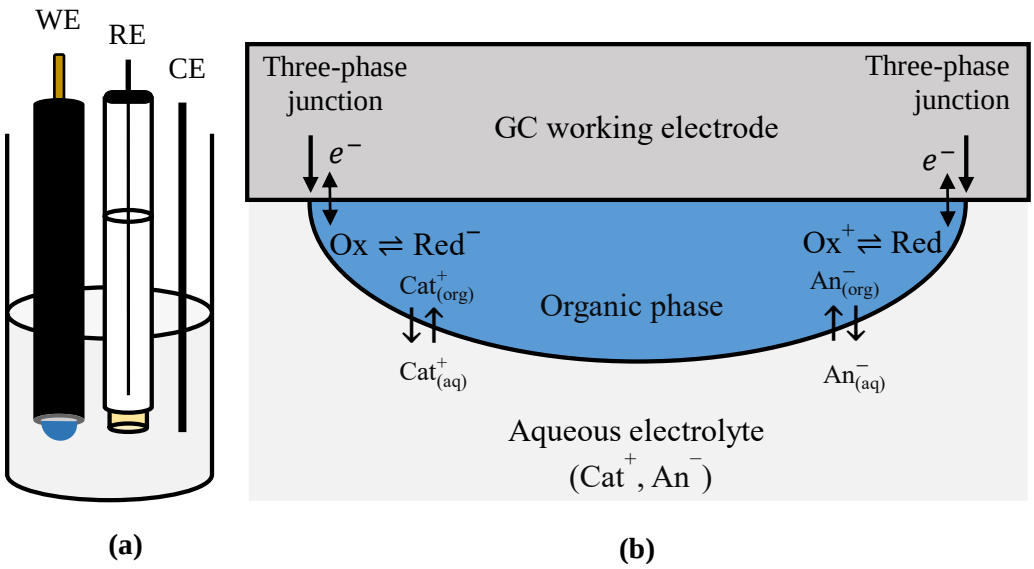

Figure 1.6 (a) The electrochemical cell set up for the TPE voltammetry. **(b)** Blown-up image of the TPE configuration created by immobilizing a droplet on the WE and the schematic representation of the ion transfer processes occurring at the three-phase junction (adapted from pages 248 and 260 of [26]).

A conventional three-electrode cell setup with an inert working, a reference, and a counter electrode is used to study the three-phase ion transfer reactions (**Fig. 1.6a**). A neutral lipophilic electroactive compound (without supporting electrolyte) is dissolved in the water-immiscible organic solvent; a microdroplet (1−5 µL) of this organic solvent is attached to the surface of a WE and immersed in an aqueous electrolyte to create the TPE configuration (**Fig. 1.6b**). The three-phase junction forms where the WE surface, organic, and aqueous solution meet each other. At this junction, the electron transfer across the WE and the organic phase is followed by the counterions transfer from aqueous to the organic droplet; to maintain the charge neutrality of the organic phase

[25,26]. The electron and ion transfer processes are simultaneous, and both are recorded in the voltammetric experiments. The ion transfer mechanisms of most commonly observed cases are as follows:

When a neutral oxidisable compound Red is dissolved in an organic droplet. The oxidation of Red to Ox^+ can be accompanied by the transfer of An^- (anion) from aqueous to the organic droplet (Eq. 1.13) only if the free energy for such transfer is smaller than that for the expulsion of an Ox^+ from the organic to the aqueous phase (Eq. 1.14).

$$Red_{(org)} + An^-_{(aq)} \rightleftharpoons Ox^+_{(org)} + An^-_{(org)} + e^- \quad 1.13$$

$$Red_{(org)} \rightleftharpoons Ox^+_{(aq)} + e^- \quad 1.14$$

When a neutral reducible compound Ox is dissolved in an organic droplet. The reduction of Ox to Red^- may be associated with the transfer of Cat^+ (cation) from aqueous to the organic phase (Eq. 1.15) or the expulsion of Red^- from organic to an aqueous phase (Eq. 1.16). Again the free energies will decide the process; lower free energy process takes place, but the reduced probe expulsion is the most probable pathway [26].

$$Ox_{(org)} + Cat^+_{(aq)} + e^- \rightleftharpoons Red^-_{(org)} + Cat^+_{(org)} \quad 1.15$$

$$Ox_{(org)} \rightleftharpoons Red^-_{(aq)} + e^- \quad 1.16$$

Also, the solvation of the electrochemically generated (cationic or anionic) species in the organic droplet should be stronger than the hydration of ionic species in the aqueous phase. Then the ion transfer is possible from aqueous to the organic droplet (Eq. 1.13 and 1.15) at the three-phase junction [26]. **Fig. 1.6b** displays the mechanism of ion transfer reactions.

1.6.1.2.2 Thermodynamics of TPE

The organic droplet does not contain supporting electrolyte; therefore, the initial conductivity at the three-phase junction comes from the partition of the electrolyte present in the aqueous phase [26]. Hence the applied potential between the WE and RE can primarily act at the three-phase junction. **Fig. 1.7** illustrates the potential drops at TPE system.

The following expression gives the potential drop at the GC|org interface ($\Delta\phi_{GC|org}$) [26].

$$\Delta\phi_{GC\,|\,org} = \Delta\phi_{GC\,|\,aq} - \Delta U_{ohmic} - \Delta\phi_{aq\,|\,org} \quad 1.17$$

The potential drop at GC|aqueous interface ($\Delta\phi_{GC|aq}$) is controlled potentiostatically; hence, $\Delta\phi_{GC|org}$ is the applied potential difference ($\Delta\phi_{GC|aq}$) reduced by the value of ohmic drop (ΔU_{ohmic}) of the organic droplet and potential drop ($\Delta\phi_{aq|org}$) due to partitioning of ions at aqueous|organic interface. Except at the three-phase junction, ΔU_{ohmic} is substantial over the GC|organic interface because droplet contains no supporting electrolyte in it. The thin layer at the aqueous|organic interface will have

ionic conductivity due to the partitioning of the salts present in the aqueous phase. For this reason, the electrochemical redox reaction can initiate without the obstacle of an ohmic drop [26].

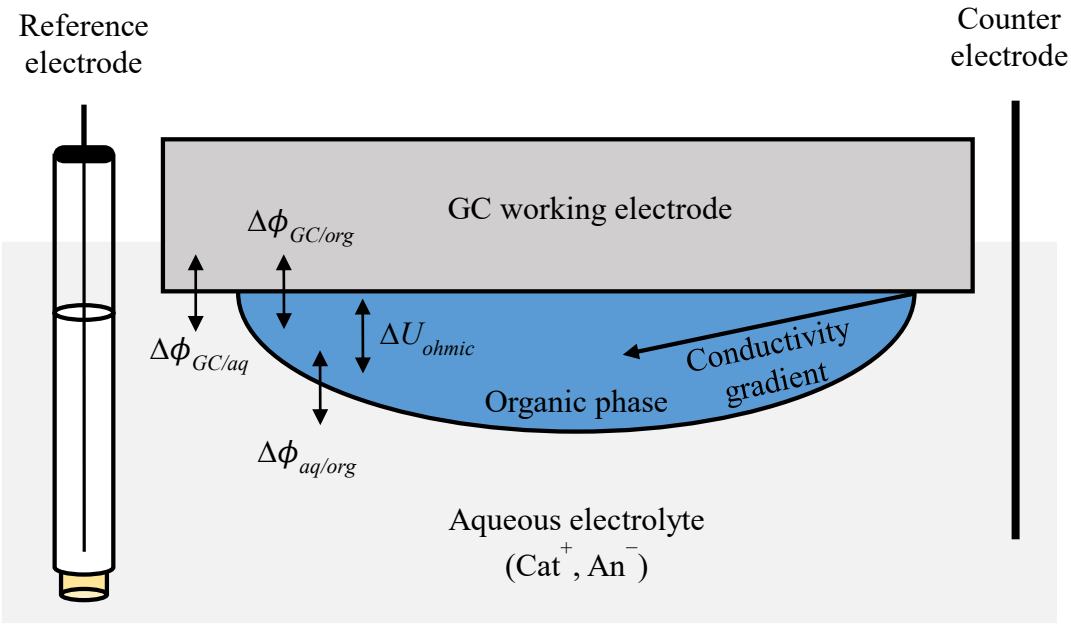

Figure 1.7 Potential drops at the three-phase interface (adapted from page 250 of [26]).

The Nernst equation obtained by the thermodynamic treatment to anion transfer reaction given in Eq. 1.13 is as follows [25,26]:

$$E = E^{\ominus}_{Ox^+_{(org)}/Red_{(org)}} + \Delta\phi^{(org)\ominus}_{(aq),An^-} + \frac{RT}{F}\ln\frac{a_{Ox^+_{(org)}}\, a_{An^-_{(org)}}}{a_{Red_{(org)}}\, a_{An^-_{(aq)}}} \qquad 1.18$$

In the above equation, E indicates the applied potential between the WE and RE; $E^{\ominus}_{Ox^+_{(org)}/Red_{(org)}}$ represents the standard potential of the redox couple in the organic phase; $\Delta\phi^{(org)\ominus}_{(aq),An^-}$ is the standard potential for anions transfer from aqueous to the organic phase; while $a_{Ox^+_{(org)}}$ and $a_{Red_{(org)}}$ denote the activities of the redox compound in the organic phase; whereas $a_{An^-_{(org)}}$ and $a_{An^-_{(aq)}}$ are the anion activities in the organic and aqueous solutions, respectively. The activities can be replaced by concentrations in the Nernst equation in the first approximation. Because the anion concentration in the aqueous phase during the experiment does not change significantly; hence the anion concentration term is separated and Eq. 1.18 is rewritten as follows:

$$E = E^{\ominus}_{\frac{Ox^+_{(org)}}{Red_{(org)}}} + \Delta\phi^{(org)\ominus}_{(aq),An^-} - \frac{RT}{F}\ln c_{An^-_{(aq)}} + \frac{RT}{F}\ln\frac{c_{Ox^+_{(org)}}\, c_{An^-_{(org)}}}{C_{Red_{(org)}}} \qquad 1.19$$

The electroneutrality principle needs that:

$$c_{Ox^{+}_{(org)}} = c_{An^{-}_{(org)}} \quad 1.20$$

The mass conservation law of the organic phase leads to the following Eq.:

$$c_{Red_{(org)}} + c_{Ox^{+}_{(org)}} = c^{*}_{Red_{(org)}} \quad 1.21$$

In Eq. 1.21, $c^{*}_{Red_{(org)}}$ is the initial concentration of the oxidisable compound in the organic phase. When the applied potential becomes equal to the formal potential of the redox compound present in the organic phase, then

$$c_{Red_{(org)}} = c_{Ox^{+}_{(org)}} \quad 1.22$$

By substitution Eqs. 1.20, 1.21 and 1.22 in Eq. 1.19 gives the formal potential ($E_c^{\ominus'}$) of the system:

$$E_c^{\ominus'} = E^{\ominus}_{Ox^{+}_{(org)}/Red_{(org)}} + \Delta\phi^{(org)\ominus}_{(aq),An^{-}} - \frac{RT}{F}\ln c_{An^{-}_{(aq)}} + \frac{RT}{F}\ln\frac{c^{*}_{Red_{(org)}}}{2} \quad 1.23$$

Eq. 1.23 describes the formal potential of the three-phase voltammograms depends on the nature of the aqueous anions through $\Delta\phi^{(org)\ominus}_{(aq),An^{-}}$. In general, more lipophilic anions have a more negative value of $\Delta\phi^{(org)\ominus}_{(aq),An^{-}}$. Therefore, as the lipophilicity of the transferring anions increases, oxidation of compound Red in the organic phase occurs at more negative potentials, i.e., more facile oxidation. Additionally, for the ten-fold increase in the concentration of aqueous anions, the formal oxidation potential should shift negatively by about 59 mV [25,26].

Similar to the anion transfer case, a thermodynamic treatment of the cation transfer reaction given in Eq. 1.15 leads the Nernst equation in the following form.

$$E_c^{\ominus'} = E^{\ominus}_{Ox_{(org)}/Red^{-}_{(org)}} + \Delta\phi^{(org)\ominus}_{(aq),Cat^{+}} + \frac{RT}{F}\ln c_{Cat^{+}_{(aq)}} + \frac{RT}{F}\ln\frac{2}{c^{*}_{Ox_{(org)}}} \quad 1.24$$

The more lipophilic aqueous cations will have a more positive value of $\Delta\phi^{(org)\ominus}_{(aq),Cat^{+}}$. As the lipophilicity of the cations in the aqueous phase increases, the reduction of the compound Ox in the organic phase occurs at a more positive potential. Also, the formal reduction potential shift in a positive direction by 59 mV for a 10-fold increase in the concentration of transferring cations in the aqueous phase.

1.7 Conclusion

This chapter aims to introduce TPE ion transfer at the organic|aqueous interface. The principle, experimental setup, and mechanisms related to the three-phase junction ion transfer reactions have been provided.

TPE configuration for ion transfer studies is easy to use as compared with the four-electrode system. Most of the water-immiscible organic solvents can be used as the organic phase, and less volume of the organic phase is required. Besides, no need for supporting electrolytes in the organic phase and ion transfer measurements are faster at the TPE system.

Oxidation of the redox probe at the three-phase junction is associated with the transfer of anion transfer from aqueous to the organic phase. The formal oxidation potential for the coupled electron-ion reaction depends on the lipophilicity of the transferring anion and its concentration. The more lipophilic the anion is, the oxidation occurs at a more negative potential, i. e. easier ion transfer process (Eq. 1.23). Likewise, the reduction of a compound at the three-phase junction is coupled with the cation transfer from aqueous to the organic phase. The reduction potential depends on the lipophilicity and concentration of the aqueous cation. For more hydrophobic cation, the reduction occurs at a more positive potential; means a more easy ion transfer process (Eq. 1.24).

The next chapter delivers a literature review of three-phase ion transfer studies.

1.8 References

[1] F. Scholz, Recent advances in the electrochemistry of ion transfer processes at liquid–liquid interfaces, Annu. Rep. Prog. Chem., Sect. C Phys. Chem. 102 (2006) 43–70. doi:10.1039/B417141C.

[2] Z. Samec, Electrochemistry at the Interface between Two Immiscible Electrolyte Solutions (IUPAC Technical Report), Chem. Int. -- Newsmag. IUPAC. 27 (2005) 2147–2180. doi:10.1515/ci.2005.27.2.26.

[3] Z. Samec, Dynamic electrochemistry at the interface between two immiscible electrolytes, Electrochim. Acta. 84 (2012) 21–28. doi:10.1016/j.electacta.2012.03.118.

[4] A. Leo, C. Hansch, D. Elkins, Partition coefficients and their uses, Chem. Rev. 71 (1971) 525–616. doi:10.1021/cr60274a001.

[5] R. Gulaboski, K. Riedl, F. Scholz, Standard Gibbs energies of transfer of halogenate and pseudohalogenate ions, halogen substituted acetates, and cycloalkyl carboxylate anions at the water|nitrobenzene interface, Phys. Chem. Chem. Phys. 5 (2003) 1284–1289. doi:10.1039/b210356g.

[6] F. Reymond, D. Fermín, H.J. Lee, H.H. Girault, Electrochemistry at liquid/liquid interfaces: methodology and potential applications, Electrochim. Acta. 45 (2000)

2647–2662. doi:10.1016/S0013-4686(00)00343-1.

[7] Z. Samec, Electrical double layer at the interface between two immiscible electrolyte solutions, Chem. Rev. 88 (1988) 617–632. doi:10.1021/cr00086a003.

[8] E.J.W. Verwey, K.F. Niessen, XL. The electrical double layer at the interface of two liquids, London, Edinburgh, Dublin Philos. Mag. J. Sci. 28 (1939) 435–446. doi:10.1080/14786443908521199.

[9] C. Gavach, P. Seta, B. D'epenoux, The double layer and ion adsorption at the interface between two non miscible solutions, J. Electroanal. Chem. Interfacial Electrochem. 83 (1977) 225–235. doi:10.1016/S0022-0728(77)80168-X.

[10] H.H. Girault, D.J. Schiffrin, Thermodynamic surface excess of water and ionic solvation at the interface between immiscible liquids, J. Electroanal. Chem. Interfacial Electrochem. 150 (1983) 43–49. doi:10.1016/S0022-0728(83)80188-0.

[11] l. Benjamin, Mechanism and Dynamics of Ion Transfer Across a Liquid-Liquid Interface, Science (80-.). 261 (1993) 1558–1560. doi:10.1126/science.261.5128.1558.

[12] I. Benjamin, Hydrogen Bond Dynamics at Water/Organic Liquid Interfaces, J. Phys. Chem. B. 109 (2005) 13711–13715. doi:10.1021/jp044157f.

[13] P. Jedlovszky, Á. Keresztúri, G. Horvai, Orientational order of the water molecules at the vicinity of the water–benzene interface in a broad range of thermodynamic states, as seen from Monte Carlo simulations, Faraday Discuss. 129 (2005) 35–46. doi:10.1039/B405509H.

[14] C.W. Monroe, M. Urbakh, A.A. Kornyshev, Understanding the anatomy of capacitance at interfaces between two immiscible electrolytic solutions, J. Electroanal. Chem. 582 (2005) 28–40. doi:10.1016/j.jelechem.2005.04.031.

[15] Z. Samec, V. Mareček, D. Homolka, The double layer at the interface between two immiscible electrolyte solutions, J. Electroanal. Chem. Interfacial Electrochem. 187 (1985) 31–51. doi:10.1016/0368-1874(85)85573-8.

[16] Z. Samec, V. Mareček, Study of the Electrical Double Layer at the Interface Between Two Immiscible Electrolyte Solutions by Impedance Measurements, in: V.E. Kazarinov (Ed.), Interface Struct. Electrochem. Process. Bound. Between Two Immiscible Liq., Springer Berlin Heidelberg, Berlin, Heidelberg, 1987: pp. 123–141. doi:10.1007/978-3-642-71881-6_7.

[17] P. Peljo, H.H. Girault, Liquid/Liquid Interfaces, Electrochemistry atUpdate based on the original article by Frédéric Reymond, Hubert H. Girault, Encyclopedia of Analytical Chemistry , © 2000, John Wiley & Sons, Ltd, in: H. Frederic Reymond, H. Girault (Eds.), Encycl. Anal. Chem., John Wiley & Sons, Ltd, Chichester, UK, 2012. doi:10.1002/9780470027318.a5306.pub2.

[18] L.J. Sanchez Vallejo, J.M. Ovejero, R.A. Fernández, S.A. Dassie, Simple Ion Transfer at Liquid|Liquid Interfaces, Int. J. Electrochem. 2012 (2012) 1–34. doi:10.1155/2012/462197.

[19] C. Gavach, A. Savajols, Potentiels biioniques de membranes liquides fortement dissociees, Electrochim. Acta. 19 (1974) 575–581. doi:10.1016/0013-

4686(74)85007-3.

[20] C. Gavach, F. Henry, Chronopotentiometric investigation of the diffusion overvoltage at the interface between two non-miscible solutions, J. Electroanal. Chem. Interfacial Electrochem. 54 (1974) 361–370. doi:10.1016/S0022-0728(74)80409-2.

[21] C. Gavach, P. Seta, F. Henry, A Study of the Ionic Transfer across an Aqueous Solution Liquid Membrane Interface by Chronopotentiometric and Impedance Measurements, Bioelectrochemistry Bioenerg. 1 (1974) 329–342. doi:10.1016/0302-4598(74)80006-1.

[22] J. Koryta, M. Březina, A. Hofmanová, D. Homolka, L.Q. Hung, W. Khalil, V. Mareček, Z. Samec, S.K. Sen, P. Vanýsek, J. Weber, J. Heyrovský, 311 - A new model of membrane transport: electrolysis at the interface of two immiscible electrolyte solutions, Bioelectrochemistry Bioenerg. 7 (1980) 61–68. doi:10.1016/0302-4598(80)87032-2.

[23] J. Koryta, Electrochemical polarization phenomena at the interface of two immiscible electrolyte solutions, Electrochim. Acta. 24 (1979) 293–300. doi:10.1016/0013-4686(79)85048-3.

[24] Z. Samec, V. Mareček, J. Koryta, M.W. Khalil, Investigation of ion transfer across the interface between two immiscible electrolyte solutions by cyclic voltammetry, J. Electroanal. Chem. Interfacial Electrochem. 83 (1977) 393–397. doi:10.1016/S0022-0728(77)80186-1.

[25] F. Scholz, R. Gulaboski, Determining the Gibbs Energy of Ion Transfer Across Water-Organic Liquid Interfaces with Three-Phase Electrodes, ChemPhysChem. 6 (2005) 16–28. doi:10.1002/cphc.200400248.

[26] F. Scholz, U. Schröder, R. Gulaboski, A. Doménech-Carbó, Electrochemistry of Immobilized Particles and Droplets, 2nd Editio, Springer International Publishing, Cham, 2015. doi:10.1007/978-3-319-10843-8.

Chapter 2. Literature review of three-phase electrode ions transfer studies

2.1 Introduction

In this chapter, a literature survey on three-phase ion transfer studies was done. Initially, F. Marken et al. studied TPE ion transfer by using the microdroplets of redox liquids (oily electroactive compounds) as the organic phase [1–9]. Later, Scholz and co-workers replaced the redox liquids with microdroplets of different organic solvents containing electroactive compounds dissolved in them (as the organic phase); and determined the standard Gibbs transfer energies of ions (different anions and cations) in various organic|aqueous systems [1,10,11]. Afterwards, Scholz's microdroplet based TPE method has adopted by many researchers to study the ion transfer. The working principle, experimental setup, and thermodynamic aspects of ions transfer related to the microdroplet TPE method have been explained in the previous chapter. In this chapter, different organic|aqueous systems, redox probes, and ionophores employed in microdroplet based TPE ion transfer studies have been reviewed. Also, other TPE ion transfer methods such as microfluidic, cylindrical metal microelectrode, punctured droplet electrode, and a paper-based device are included. Some applications of TPE ion transfer have been summed up at the end of this chapter.

2.2 Redox liquid as the organic phase

N,N,N',N'-tetraalkylphenylenediamines (TRPDs) (where R = different alkyl groups) are the most used redox liquids for TPE anion transfer studies. Tetramethylphenylenediamine (TMPD) is a solid and water-soluble compound. Except for TMPD, other long alkyl chain TRPDs are liquid, highly lipophilic, and immiscible with water (even in their oxidised radical cationic form). Most importantly, they oxidise before water oxidation occurs in the TPE configuration [1].

TRPDs undergo two one-step, one-electron reversible oxidations; the first step includes the formation of a radical cation (Eq. 2.1) and then to a dication (Eq. 2.2) in the second step [1]. Most TRPDs radical cations are coloured, electron paramagnetic resonance visible, and they show absorption in the visible range. Hence, it is possible to visualise them through the microscope [1,2].

$$TRPD \leftrightharpoons TRPD^{\bullet+} + e^- \qquad 2.1$$

$$TRPD^{\bullet+} \leftrightharpoons TRPD^{2+} + e^- \qquad 2.2$$

The oxidation of TRPD to its radical cation is the most studied reaction for TPE anion transfer from an aqueous to a redox liquid. Initially, Marken et al. [2,3] studied

the one-electron oxidation of oily *N,N,N',N'*-tetrahexylphenylenediamine (THPD) microdroplets deposited on different electrodes and immersed in aqueous electrolytes of different anions. They noticed that the oxidation of THPD was due to the transfer of anions from the aqueous phase to THPD microdroplets (Eq. 2.3). The shape and mid-peak potentials of THPD oxidation depended on the nature of the aqueous anions. In one of their experiments, a yellow coloured THPD microdroplet was deposited on ITO and immersed in a 0.1 M $NaClO_4$ solution to observe the electrochemical process by in situ optical microscopy [2]. After switching to the oxidation potential, the yellow microdroplet turned to blue (the product of $THPD^{\bullet+}$ ClO_4^- is blue). The blue coloured product ($THPD^{\bullet+}$ ClO_4^-) first formed along the edges of the yellow microdroplet, i.e., at the three-phase junction. Upon continuous oxidation, the whole droplet turned to a blue colour [2]. Afterwards, these results had been confirmed by many people as listed in the review by C. E. Banks et al. [4]. The colour change of THPD is the direct evidence that the electron and ion transfer processes happen at the three-phase junction.

$$TRPD_{(org)} + An^-_{(aq)} \leftrightharpoons TRPD^{\bullet+}_{(org)} + An^-_{(org)} + e^- \qquad 2.3$$

Substituted phenylenediamines have been studied for TPE anions transfer reactions [5,6]. F. Marken's work on the effects of the structure of different THPD (para-THPD, meta-THPD, and para-tetrakis(6-methoxyhexyl)phenylenediamine) on anion transfer voltammetry showed that the difference in the interactions between the THPD radical cation and the transferred anion. This different behaviour depends on the chain length of the phenylenediamine and the position of the amine groups [6]. The relation between the measured formal potential and the lipophilicity of the redox liquid (due to increasing alkyl chain in the TRPD) has reported by J. D. Wadhawan et al. [5]. They noticed the positive shift in the mid-peak potential for the given anion transfer, as the number of carbon units in the TRPD alkyl chains increases.

There are a few significant differences between ion transfer studies using redox liquid microdroplet as the organic phase and inert organic microdroplet containing neutral electroactive compound as the organic phase. In the latter case, the electroactive species concentration in the organic droplet is significantly lower than the solvent concentration. Therefore, the interactions among the electroactive species are negligible. Also, the ion transfer driven by the oxidation or reduction of the electroactive species present in the organic solvent does not change the physical and chemical characteristics of the organic droplet. Only the ionic conductivity changes due to the formation of ionic species in the organic droplet [1]. In the comparative study by U. Schröder et al. [7], authors used the pure redox liquid (TRPDs; R = butyl, hexyl, heptyl, octyl, and nonyl) as organic phase and TRPDs dissolved in the NB as the organic phase. Oxidation of the pure redox liquids was accompanied by the transfer of anions (from the aqueous phase) and led to the formation of the ionic liquids. The voltammetric responses showed a narrow first oxidation peak and significant peak separation between the second oxidation and reduction peaks. In the other case, the ion transfer voltammetric response of TRPDs dissolved in the NB was reversible. Regardless of voltammetric shape differences, the

thermodynamics of ions transfer in both cases were the same. This means, the ion transfer was governed by the Gibbs energies of transfer of the anions and not by the ion-pairing interactions [1,7].

The oxidised form of the redox liquid must be highly lipophilic in order to transfer highly hydrophilic anions (like fluoride) or highly charged anions (like sulfate). Marken et al. were the first to show the transfer of sulfate dianion from the aqueous phase to the microdroplet of N,N,N',N'-tetrakis(6-methoxyhexyl)phenylenediamine redox liquid [6]. Later again, Marken et al. showed the transfer of hydrophilic anions such as sulfate, chromate, dichromate, phosphate, and arsenate into a N,N,N',N'-tetraoctylphenylenediamine redox liquid [8,9].

2.3 Electroactive compounds dissolved in water-immiscible solvents as the organic phase

Based on the type of the redox probe dissolved in the water-immiscible organic solvent, anion transfer, cation transfer, or both studies can be performed at the three-phase junction. The comprehensive reviews [10,11] and a book chapter [1] by F. Scholz et al., summed up the experimental studies of determining standard Gibbs energies of ion transfer in different organic|aqueous systems, list of different transferable ions and different redox probes employed for TPE ion transfer studies. These materials were helpful during my studies to understand the fundamentals of TPE ion transfer, design the experiments, and to predict the obtained results.

2.3.1 Solvent systems

The most commonly used organic solvent in the electrochemical ion transfer across organic|aqueous interface is nitrobenzene (NB) because of its low water miscibility, higher dielectric constant (ε_r = 35.6), and good electrolyte dissociation. The aromatic ring and nitrogen parts of the NB, support the solvation/interaction of nonpolar and polar sites of the transferring ions, respectively. Hence, NB is the best solvent for both lipophilic and hydrophilic transferring ions. As mentioned in the reviews by F. Scholz et al. [10,11], TPE configuration with NB|water interface has been used to study the transfer of various inorganic and organic ions (cations and anions), anions of drugs, substituted phenolates, monoanionic amino acids, and different polypeptides. However, NB is highly toxic, and therefore other alternatives are often wanted.

The particular reason for using n-octanol at TPE is the partition coefficients determined in the n-octanol|water system have been used in quantitative structure-activity relationships and in pharmacology to guess drug bioactivity. In n-octanol, the long lipophilic alkyl chain connected to the hydrophilic hydroxyl group look like the lecithin molecules; which are the main constituents of biological membranes. So n-octanol is considered as a perfect organic solvent for mimicking the ion transfer process at the biological membrane [10,11]. Initially, there was a problem using bis(pentamethylcyclopentadienyl)iron(II) (DMFc) redox probe to determine the

standard Gibbs energy of transfer of an anion across n-octanol|water interface; because the standard redox potential of $DMFc^+$/DMFc in n-octanol was unknown. Some attempts (by recording voltammograms) failed to provide accurate data on standard potential due to the high resistance of the n-octanol solvent. Also, TPE configuration could not be used to estimate the standard redox potential of $DMFc^+$/DMFc, since no ion transfer energies data across the n-octanol|water system were known. There are literature data regarding the standard transfer potentials values of several inorganic anions across n-alcohols|water systems (n = 1,2,3,4). These data could be extrapolated by applying a nonlinear regression analysis to get the standard transfer potentials (of Cl^-, I^-, and Br^-) for the n-octanol|water system. Now there are several reports of determining the standard Gibbs energy of transfer of several inorganic anions, organic anions, and drugs in n-octanol|water system [10,11].

2-nitrophenyl octyl ether (NPOE) has been used as an alternative to n-octanol. It shares the structure of both n-octanol and NB. It was found that the lipophilicities of some common inorganic anions determined in NPOE|water system are similar to NB|water system, which means the solvation property of NPOE and NB are similar [11]. Nevertheless, the lipophilicity data determined for the NPOE|water system are not the same as the data of n-octanol|water.

A few experiments have been done to transfer chiral ions across the chiral organic solvent|water interface. Some D- and L-anionic forms of amino acids transfer have performed with the droplets of D- and L-2-octanol having DMFc. In these studies, the Gibbs energy to transfer an L-ion from water to the L-solvent was equal to the transfer of D-ion from water to the D-solvent. Furthermore, Gibbs transfer energies of D-anion to L-solvent and L-anion to D-solvent were higher than the L-ion to the L-solvent and D-ion to the D-solvent [11,12].

2.3.2 The transfer of anions at TPEs

The principal requirement for the TPE anion transfer from aqueous to the organic phase is the reversible oxidation of a neutral lipophilic compound in the organic phase before the water oxidation at the organic|aqueous|electrode three-phase junction. One suitable compound that shows the properties mentioned above is DMFc. It is soluble in several organic solvents, insoluble in water and a non-interactive redox system with the incoming nucleophilic anions such as CN^-, and F^-. Most importantly, DMFc undergoes an electrochemically reversible one-electron redox reaction, is highly stable to molecular oxygen and other factors. This stability mainly arises from the methyl groups around the cyclopentadienyl ring, which are believed to cause more significant steric interference to both specific and nonspecific interactions. Besides, X-ray diffraction studies showed that the methyl groups prevent access of the solvent to the metal center and the cyclopentadienyl ring [1,13]. Therefore, DMFc formal redox potential is solvent independent, and it is commonly used as an internal redox standard in nonaqueous solvents as well as a redox probe for anion transfer studies at the TPE system.

The oxidation of DMFc in the organic phase must be accompanied by the transfer of anion from the aqueous phase to the organic droplet (Eq. 1.13). This approach has been used to find the standard Gibbs energies of transfer of inorganic anions, organic anions of aliphatic and aromatic carboxylic acids, substituted phenols, drugs, amino acids, and peptides. Commonly used organic solvents to study anion transfer with DMFc are DCE, NB, NOP, n-octanol, NPOE, nujol, L- and D-menthol, and room temperature ionic liquids [1,11]. However, M. Opałło and co-workers from our institute studied the TPE anion transfer reactions across the NPOE|water interface using scanning electrochemical microscopy [14]. They detected the expulsion of $DMFc^+$ cation from NPOE to the aqueous phase. This expulsion is more prominent with hydrophilic anions in comparison with hydrophobic anions. Other redox probes such as ferrocene, n-butylferrocene, and tert-butylferrocene were investigated for anion transfer reactions in microfluidic conditions (discussed in section **2.5**). The ion transfer mechanism with them is similar to DMFc, as described in Eq. 1.13.

Tetraphenylporphyrinato (TPP) complexes of Mn, Fe, and Co were used to study the transfer of a series of standard anions (PF_6^-, ClO_4^-, SCN^-, NO_3^-, Br^-, Cl^-, CN^-, and F^-) across the 4-(3-phenylpropyl)-pyridine|aqueous interface [15–17]. Simple anion transfer reaction had seen with weakly coordinating anions (PF_6^-, ClO_4^-, SCN^-, and NO_3^-) (Eq. 1.13). But with nucleophilic anions (CN^- and F^-), Mn and Co-TPP complexes showed coordination interaction in the organic phase [15,16].

2.3.3 The transfer of cations at TPEs

Similar to the anion transfer, the reduction of the neutral lipophilic compound in the organic phase is coupled with the transfer of cation from aqueous to the organic phase (Eq. 1.15). However, the reversible reduction of the compound is essential before the water reduction at the three-phase junction. For cation transfer studies, reduction of iodine [18], iron(III) tetraphenyl porphyrine chloride (Fe(III)TPP-Cl) [19], and tetracyanoquinodimethane (TCNQ) [20] were studied. Additionally, lutetium bis(tetra-tert-butylphthalocyaninato) (LBPC) [21] and 2,2-diphenyl-1-picrylhydrazyl (DPPH) [22] have been used for both cations and anions transfer studies.

The reduction of Fe(III)TPP-Cl, LBPC and TCNQ in the organic phase depend on the nature of the cations present in the aqueous phase; the more lipophilic the cation, the easier is the reduction (according to Eq. 1.24). The Eq. 1.15 describes the overall cation transfer reactions of Fe(III)TPP-Cl, LBPC, and TCNQ. But, TCNQ has studied only alkylammonium cation transfer. In contrast, DPPH at NB|aqueous|graphite interface can be reduced to $DPPH^-$ and oxidised to $DPPH^+$; in this case, the ion transfer from the aqueous phase to NB is due to ion-pair formation in NB [22].

Another way to study the cation transfer is by the electrochemical reduction of iodine in organic droplets immersed in aqueous solutions of different cations. A distinct electrochemical behaviour can be observed when the chloride salts of different cations are present in the aqueous phase. A new reversible process occurs at more positive potentials to the peak of iodide expulsion. This reversible peak shifts 60 mV in the negative direction per decade of increasing chloride concentration; hence, it is attributed

to the reduction of iodine in the NB droplet followed by the expulsion of chloride ions from the NB to water. The reduction mechanism given below is predicted by assuming that the partition of chloride salt between aqueous and NB is mostly driven by the formation of I_2Cl^- ions in the NB [11,18].

$$I_{2(nb)} + Cl^-_{(aq)} + Cat^+_{(aq)} \leftrightharpoons I_2Cl^-_{(nb)} + Cat^+_{(nb)} \quad 2.4$$

$$I_{2(nb)} + 2e^- \leftrightharpoons 2I^-_{(nb)} \quad 2.5$$

$$Cl^-_{(nb)} \leftrightharpoons Cl^-_{(aq)} \quad 2.6$$

But, this method has drawbacks due to the complex reaction mechanism, and iodine is reactive towards many organic compounds [11,18].

2.4 Facilitated ion transfer

In facilitated ion transfer studies, additional compounds called ionophores are added to the organic phase; which can coordinate with the cations present in the aqueous phase, so that the transfer of these cations are facilitated. In other words, ionophores ease the ion transfer by lowering the transfer energy. Different ionophores have been used to transfer the alkali and alkaline earth-metal cations across a variety of organic|aqueous interface by four-electrode ion transfer setup [23–26]. Few ionophores used in TPE ion transfer studies are valinomycin [27,28], dibenzo-18-crown-6 ether and potassium ionophore III (BME-44) [28].

F. Quentel and co-workers [27] studied the transfer of mono and divalent cations at NB|water|pyrolytic graphite three-phase interface; using LBPC as a redox probe and valinomycin as an ionophore. At NB|water interface, the partition of aqueous cations due to the interfacial complexation with valinomycin was observed. This complexation increases the lipophilicity of the cation, and it was clearly seen as the positive shift in the reduction potential of LBPC in the presence of valinomycin. Hence, the cation transfer is controlled by the thermodynamics and kinetics of the interfacial complexation and partition reactions. Recently, M. Podrażka et al. [28] from our group performed the TPE cations transfer studies across 1,2-DCB|water interface; using fullerene C_{60} as a redox probe and facilitated by three different ionophores. They compared the performance of valinomycin, dibenzo-18-crown-6 ether, and potassium ionophore III (BME-44) ionophores with the un-facilitated measurements. The valinomycin showed the most significant positive shift in the transfer potential compared with the un-facilitated experiment.

2.5 Microfluidic TPE ion transfer

S. M. MacDonald and co-workers in the Frank Marken group introduced a TPE microfluidic device to study ion transfer across the NOP|aqueous interface in hydrodynamic condition [29]. It was a rectangular, double channel flow cell with a pair of inlets and outlets. Both NOP and water were in contact with the gold electrode to make the TPE configuration in the microfluidic cell. First, they calibrated the cell by studying the dependency of flow rate on the mass transport controlled current using an aqueous phase of hexaammineruthenium(III) chloride [$Ru(NH_3)_6^{3+}$]. According to the Levich equation for rectangular channel cells; the plot of the mass transport limited current as a function of the cube root of volume flow rate is linear. In the case of $Ru(NH_3)_6^{3+}$ reduction, the cathodic limiting currents were consistent with the Levich equation. Next, they optimised the flow rate of both NOP (having metal complex dye) and the aqueous phase to obtain the constant width of both phases on a gold electrode. Laminar two-phase flow is possible with NOP and water, but the flow rate of one phase affects the width of both phases. Hence, the flow rate of lower viscous liquid should be lower than the more viscous to have the laminar flow. Later they examined the ClO_4^- anions transfer reaction at TPE by dissolving the n-butylferrocene in NOP phase. However, the flow rate effect on the TPE ion transfer limiting current was not consistent with the Levich equation, and oxidation currents were observed to decrease with the increased flow rates. The reason could be that the ion transfer reaction was limited at higher flow rates; which means ions were moved through the channel before they cross the interface. In another work, J. D. Watkins et al. [30] demonstrated the two-phase flow of acetonitrile|aqueous system; acetonitrile is miscible with water but not with a high concentration of salt in the aqueous phase (2 M NaCl). In this work, the microfluidic channel was with a teflon base on which platinum electrodes were sputter-coated. The one-electron reduction of $Ru(NH_3)_6^{3+}$ in the aqueous phase was used to calibrate the cell, and the mass transport controlled limiting current was consistence with the Levich equation. The two-phase flow experiments of oxidation of tert-butylferrocene in acetonitrile in contact with aqueous 2 M NaCl on the platinum WE showed that the currents were independent of volume flow rate.

In the case of NOP|aqueous system, the limiting current decreases with the increased flow rate [29]. However, in the case of acetonitrile|aqueous system, the limiting current was not dependent on the flow rate [30]. D. Kałuza et al. [31] from our group investigated the oxidation of ferrocene at NOP|aqueous|gold electrode three-phase interface to address the strange effect of flow rate with the limiting current. They examined the oxidation of ferrocene over a wide range of flow rates. In lower flow rates, the limiting current decreases with the increasing flow (opposite to the Levich equation), this is due to the diffusion of ions into the NOP phase and developing an extended reaction zone. As the flow rate increases, the diffusion zone becomes thinner, and the current decrease. At higher volume flow rates, the limiting current increases linearly with the cube root of the flow rate (follows Levich equation).

In another study by D. Kałuza et al. [32], they compared anion transfer across NOP|water interface at a droplet-based TPE system and a microfluidic TPE system. They showed that two key factors indicate the anion transfer (i.e., the dependency of voltammetric peak potentials on the ion hydrophobicity and ion concentration) are same in both microfluidic and droplet TPE systems. They also showed that the thermodynamic model of droplet-based TPE ion transfer could be applied to microfluidic TPE systems.

2.6 Other methods of TPE ion transfer

Z. Stojek and co-workers [33,34] proposed a different TPE ion transfer method. A cylindrical metal (platinum or gold) microelectrode was immersed into organic|aqueous interface, such that a microelectrode was in contact with both organic and aqueous solvents (**Fig. 2.1**).

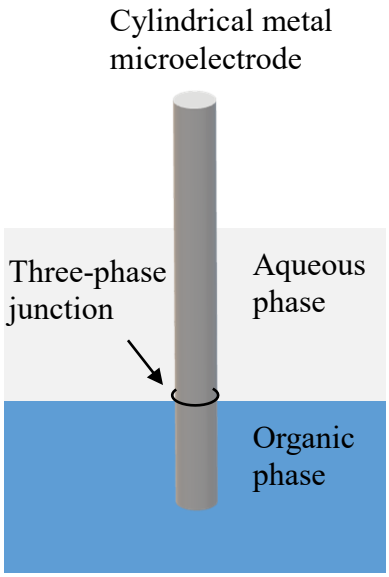

Figure 2.1 Graphical illustration showing the three-phase junction formed on the cylindrical microelectrode (Adapted from [33,34]).

The cylindrical microelectrode method has a few advantages over the microdroplet based TPE configuration. It is difficult to always deposit the same size microdroplets on WE, so the length of the three-phase boundary varies in microdroplet based TPE configuration, and thus the current. But by using cylindrical microelectrodes, a well-defined three-phase boundary can be produced each time. Consequently, the measured currents were reasonably reproducible. Also, the length of the three-phase boundary can be modified easily by just changing the diameter of the metal wire, and measured currents were always proportional to the diameter of the microelectrode. This method has control over the length of the three-phase boundary [33,34]. Another similar method was introduced from the Stojek group; the size-controlled organic droplet was produced out from a capillary to the aqueous phase [35]. The cylindrical microelectrode punctured the droplet in a way that the microelectrode was in contact with both phases. This

approach allowed to attach the stable organic droplet on the metal electrode at any potential. Usually, droplet attached to metal electrode becomes unstable when potential is applied. Three-phase junction created by punctured droplet has similar advantages like cylindrical metal microelectrode. Additionally, change of the droplet and regeneration of the initial electrochemical conditions is possible [35]. The microelectrode concept was later utilised by researchers in our group to create a system with a pencil graphite electrode for TPE studies [28].

Lately, M. Podrażka et al. from our group developed the paper-based method for ion transfer between the NOP|water interface [36]. On the glass slide, a paper soaked in the NOP solvent having redox probe was placed; above this, the working gold mesh electrode was attached. Another paper soaked in the aqueous solution with the counter platinum mesh, and RE was put above the WE. In this work, the authors presented that the paper-based TPE method could be used for ion transfer studies. Furthermore, the obtained results were in good agreement with the previous literature of microdroplet based TPE setups.

2.7 Applications of three-phase ion transfer for deposition at TPE

M. Opallo and co-workers from our institute showed the deposition of gold nanoparticles at three-phase junctions created on ITO WE [37,38]. In one of their works, they deposited gold nanoparticles at ITO|ionic liquid|aqueous three-phase junction; where the ITO WE was running through 1-decyl-3-methylimidazolium bis(trifluoromethylsulfonyl)imide ionic liquid having $HAuCl_4$; which was immiscible with aqueous KPF_6 solution [37]. On ITO, the electrochemical reduction of $AuCl_4^-$ to Au, leads to the expulsion of hydrophilic Cl^- anions from ionic liquid to the aqueous phase. At the same time, Cl^- expulsion was followed by the transfer of PF_6^- anion from the aqueous phase to ionic liquid to balance the charge [37]. A similar kind of Au deposition has done on ITO in contact with toluene|aqueous interface. In that work, tetraoctylammonium tetrachloroaurate was the gold precursor, and the aqueous phase was 0.1 M KPF_6 or $KClO_4$ or KCl [38].

Metalloorganic complex such as copper-tetracyanoquinodimethane (CuTCNQ) was synthesised by Li Huang et al. at the pyrolytic graphite electrode|DCE|aqueous three-phase interface [39]. The electrochemical reduction tetracyanoquinodimethane (TCNQ) in the DCE leads to the transfer of Cu^{2+} ions from an aqueous phase to DCE. Such transfer forms the CuTCNQ complex in the DCE phase.

Z. Stojek et al. deposited the poly(N-vinylcarbazole) polymer at the NB|water| platinum three-phase interface [40]. The NB phase had only N-vinylcarbazole monomer without supporting electrolyte, and it was immiscible with an aqueous electrolyte. A platinum microcylinder electrode was immersed in such a way that it was in contact with both NB and aqueous phases. Upon oxidation (potentiostatic and potentiodynamic), the

poly(N-vinylcarbazole) polymer deposited at the three-phase junction and the thickness was dependent on the deposition time and the kind of aqueous ions.

J. Niedziolka-Jönsson et al. from our institute showed the deposition of the thin silicate sol-gel films at NB|water|electrode interface [41]. The electrode dipped through the upper aqueous phase of Na_2SO_3 and bottom NB phase having the sol-gel precursor. On applying a positive potential to the electrode, protons are produced at the three-phase junction, and they catalyse the sol-gel process. Slowly the electrode was pulled out through NB|water, a thin layer of the silicate film forms on the electrode. An almost similar approach was used again by J. Niedziolka-Jönsson et al. to deposit the nanocomposite silicate on ITO by dispersing carbon nanoparticles in the aqueous phase [42].

2.8 Conclusion

In this chapter, a short literature review of the organic|aqueous solvent systems and different redox probes used in TPE ion transfer reactions has been provided. Also, recently developed TPE ion transfer methods and applications are explained briefly.

Ferrocene derivatives (DMFc, n-butylferrocene, and tert-butylferrocene), different redox liquids (TRPD derivatives), and tetraphenylporphyrinato-metal complexes (Mn and Co) were used to study the anion transfer reactions. The formal oxidation potentials of all of them depend on the lipophilicity of the transferring anion (Eq. 1.23); the oxidation occurs at a more negative potential for the more lipophilic anion. Eq. 1.13 describes the overall anion transfer reaction mechanism with them. Among ferrocene derivatives, DMFc has been widely studied because it is lipophilic and does not interact with incoming nucleophilic anions. Nevertheless, M. Opallo et al. noticed that the DMFc cation could expel to the aqueous phase in the case of hydrophilic chloride anion transfer reaction [14]. Regarding redox liquids, TRPDs having lipophilic alkyl chains could be used to study the highly hydrophilic anion transfer reactions [6,8,9]. Whereas TPP-Co and Mn complexes showed the coordination interactions with the transferred nucleophilic anions (CN^- and F^-) in the organic phase [15,16]. Sofar organometallic complexes of Fe, Lu, Mn, and Co (ferrocene derivatives, LBPC, TPP-Mn, TPP-Fe, and TPP-Co) have used for anion transfer studies. Ru complexes have not been studied due to their higher oxidation potentials; they will not undergo oxidation before the water oxidation event occurs at TPE. I synthesised a Ru^{II} complex having bis(benzimidazolyl)pyridine based ligands, which oxidises before water oxidation at TPE, and the results of anion transfer studies of this complex are discussed in chapter 4.

Fe(III)TPP-Cl, LBPC, TCNQ, and DPPH redox probes were investigated for cation transfer studies at TPE configuration. The Eq. 1.15 describes the overall cation transfer reaction mechanism of Fe(III)TPP-Cl, LBPC, and TCNQ redox probes. Regarding Fe(III)TPP-Cl, authors claim that the reduction of Fe(III) to Fe(II) in NB will not expel Cl^- anions from NB to water, since Fe(III)TPP-Cl does not dissociate in NB

[19]. Using the LBPC redox probe, both cation and anion transfer studies can be performed; however, LBPC is commercially unavailable. S. Wu et al. investigated the TCNQ redox probe for only alkylammonium cations transfer studies [20], they did not study for inorganic cations. In their studies, the reduction potentials of TCNQ were dependent on the lipophilicity of the transferring alkylammonium cations. However, TCNQ derivatives are known to form ion-pair with the supporting electrolytes in the single-phase electrochemistry [43–45]. On the other hand, DPPH reduction (to $DPPH^{-}$) and oxidised (to $DPPH^{+}$) at TPE configuration lead to ion transfer (both anion and cation) due to ion-pair formation [22]. Both TCNQ and DPPH are electroactive organic compounds; they undergo reversible redox reaction. In both compounds, the functional groups obtain the charge when they undergo redox reaction. Hence, to understand more, I studied TCNQ for inorganic and organic cations transfer reactions, and the results are presented in chapter 4.

At TPE configuration, biologically relevant ions transfer (amino acids, peptides, drugs, and other substituted organic ions) studies have done [1,10,11]. But, the redox behaviour of biologically essential compounds is rarely investigated at the TPE setup. Therefore, I investigated a few quinone derivatives at the TPE configuration. The redox behaviour of these quinones influences their biological activities. The results are discussed in chapter 4.

Different methods (cylindrical microelectrode, paper-based, microfluidic, and other methods) have developed to study the three-phase ion transfer studies. Stojek group showed that a reasonably reproducible three-phase boundary could be created with cylindrical microelectrodes, and the measured currents were fairly reproducible [33,34]. Recently, this concept was used by M. Podrażka et al. from our group, created the three-phase junction on the pencil graphite electrode, and studied the facilitated cation transfer [28]. Also, M. Podrażka et al. developed the paper-based TPE device. Ion transfer across the flowing liquid|liquid interface (TPE microfluidic device) is one of the methods studied by Marken and our group [29–31]. In the microfluidic device, the parallel flow of the organic|aqueous interface across the microelectrode creates the three-phase junction. D. Kaluza et al. from our group have made a comparison ion transfer study between a droplet-based TPE system and a microfluidic TPE system [32]. Also, they provided more insight into the strange effect of flow rate with the limiting current in three-phase cyclic voltammetry [31]. An added exciting idea to this is to check voltammetry in the T-junction microfluidic system; where one phase is stationary, and the other is flowing. I attempted the fabrication of T-junction microfluidic systems and performed the anion transfer studies. The obtained results are summarised in chapter 5.

TPE configuration used in the deposition of gold nanoparticles, poly(N-vinylcarbazole), and functionalised/nanocomposite silica films on the electrode. However, the authors did not provide the advantages of using the TPE system for the deposition.

The next chapter in this thesis provides information regarding the chemicals and techniques used in ion transfer studies.

2.9 References

[1] F. Scholz, U. Schröder, R. Gulaboski, A. Doménech-Carbó, Electrochemistry of Immobilized Particles and Droplets, 2nd Editio, Springer International Publishing, Cham, 2015. doi:10.1007/978-3-319-10843-8.

[2] F. Marken, R.D. Webster, S.D. Bull, S.G. Davies, Redox processes in microdroplets studied by voltammetry, microscopy and ESR spectroscopy: oxidation ofN,N,N′,N′-tetrahexylphenylene diamine deposited on solid electrode surfaces and immersed in aqueous electrolyte solution, J. Electroanal. Chem. 437 (1997) 209–218. doi:10.1016/S0022-0728(97)00398-7.

[3] F. Marken, R.G. Compton, C.H. Goeting, J.S. Foord, S.D. Bull, S.G. Davies, Anion Detection by Electro-Insertion into N, N, N′, N′-Tetrahexyl-Phenylenediamine (THPD) Microdroplets Studied by Voltammetry, EQCM, and SEM Techniques, Electroanalysis. 10 (1998) 821–826. doi:10.1002/(SICI)1521-4109(199809)10:12<821::AID-ELAN821>3.3.CO;2-V.

[4] C.E. Banks, T.J. Davies, R.G. Evans, G. Hignett, A.J. Wain, N.S. Lawrence, J.D. Wadhawan, F. Marken, R.G. Compton, Electrochemistry of immobilised redox droplets: Concepts and applications, Phys. Chem. Chem. Phys. 5 (2003) 4053. doi:10.1039/b307326m.

[5] J.D. Wadhawan, A.J. Wain, A.N. Kirkham, D.J. Walton, B. Wood, R.R. France, S.D. Bull, R.G. Compton, Electrocatalytic Reactions Mediated by N , N , N ‘, N ‘-Tetraalkyl-1,4-phenylenediamine Redox Liquid Microdroplet-Modified Electrodes: Chemical and Photochemical Reactions In, and At the Surface of, Femtoliter Droplets, J. Am. Chem. Soc. 125 (2003) 11418–11429. doi:10.1021/ja030315p.

[6] F. Marken, A.N. Blythe, J.D. Wadhawan, R.G. Compton, S.D. Bull, R.T. Aplin, S.G. Davies, Voltammetry of electroactive liquid redox systems: anion insertion and chemical reactions in microdroplets of para -tetrakis(6-methoxyhexyl) phenylenediamine, para - and meta -tetrahexylphenylenediamine, J. Solid State Electrochem. 5 (2001) 17–22. doi:10.1007/s100089900106.

[7] U. Schröder, J. Wadhawan, R.G. Evans, R.G. Compton, B. Wood, D.J. Walton, R.R. France, F. Marken, P.C. Bulman Page, C.M. Hayman, Probing Thermodynamic Aspects of Electrochemically Driven Ion-Transfer Processes Across Liquid|Liquid Interfaces: Pure versus Diluted Redox Liquids, J. Phys. Chem. B. 106 (2002) 8697–8704. doi:10.1021/jp0146059.

[8] F. Marken, C.M. Hayman, P.C. Bulman Page, Chromate and Dichromate Electro-Insertion Processes into a N,N,N′,N′-Tetraoctylphenylenediamine Redox Liquid, Electroanalysis. 14 (2002) 172. doi:10.1002/1521-4109(200202)14:3<172::AID-ELAN172>3.0.CO;2-E.

[9] F. Marken, C.M. Hayman, P.C. Bulman Page, Phosphate and arsenate electro-insertion processes into a N,N,N′,N′-tetraoctylphenylenediamine redox liquid, Electrochem. Commun. 4 (2002) 462–467. doi:10.1016/S1388-2481(02)00345-4.

[10] F. Scholz, Recent advances in the electrochemistry of ion transfer processes at liquid–liquid interfaces, Annu. Rep. Prog. Chem., Sect. C Phys. Chem. 102 (2006) 43–70. doi:10.1039/B417141C.

[11] F. Scholz, R. Gulaboski, Determining the Gibbs Energy of Ion Transfer Across Water-Organic Liquid Interfaces with Three-Phase Electrodes, ChemPhysChem. 6 (2005) 16–28. doi:10.1002/cphc.200400248.

[12] F. Scholz, R. Gulaboski, Gibbs energies of transfer of chiral anions across the interface water|chiral organic solvent determined with the help of three-phase electrodes, Faraday Discuss. 129 (2005) 169. doi:10.1039/b404539d.

[13] I. Noviandri, K. N. Brown, D. S. Fleming, P. T. Gulyas, P. A. Lay, A. F. Masters, L. Phillips, The Decamethylferrocenium/Decamethylferrocene Redox Couple: A Superior Redox Standard to the Ferrocenium/Ferrocene Redox Couple for Studying Solvent Effects on the Thermodynamics of Electron Transfer, J. Phys. Chem. B. 103 (1999) 6713–6722. doi:10.1021/jp991381.

[14] G. Shul, W. Nogala, I. Zakorchemna, J. Niedziolka, M. Opallo, Scanning electrochemical microscopy study of ion transfer process across water/2-nitrophenyloctylether interface supported by hydrophobic carbon ceramic electrode, J. Solid State Electrochem. 12 (2008) 1285–1291. doi:10.1007/s10008-008-0512-8.

[15] M.J. Bonné, C. Reynolds, S. Yates, G. Shul, J. Niedziolka, M. Opallo, F. Marken, The electrochemical ion-transfer reactivity of porphyrinato metal complexes in 4-(3-phenylpropyl)pyridine | water systems, New J. Chem. 30 (2006) 327. doi:10.1039/b514348a.

[16] A.M. Collins, G.J. Blanchard, F. Marken, Spectroelectrochemical Investigation of TPPMn(III/II)-Driven Liquid | Liquid | Electrode Triple Phase Boundary Anion Transfer into 4-(3-Phenylpropyl)-Pyridine: ClO4−, CO3H−, Cl−, and F−, Electroanalysis. 24 (2012) 246–253. doi:10.1002/elan.201100623.

[17] S.M. MacDonald, M. Opallo, A. Klamt, F. Eckert, F. Marken, Probing carboxylate Gibbs transfer energies via liquid|liquid transfer at triple phase boundary electrodes: ion-transfer voltammetry versus COSMO-RS predictions, Phys. Chem. Chem. Phys. 10 (2008) 3925. doi:10.1039/b803582b.

[18] V. Mirčeski, R. Gulaboski, F. Scholz, Determination of the standard Gibbs energies of transfer of cations across the nitrobenzene|water interface utilizing the reduction of iodine in an immobilized nitrobenzene droplet, Electrochem. Commun. 4 (2002) 814–819. doi:10.1016/S1388-2481(02)00456-3.

[19] F. Scholz, R. Gulaboski, K. Caban, The determination of standard Gibbs energies of transfer of cations across the nitrobenzene|water interface using a three-phase electrode, Electrochem. Commun. 5 (2003) 929–934. doi:10.1016/j.elecom.2003.09.005.

[20] S. Wu, B. Su, 7,7′,8,8′-Tetracyanoquinodimethane as a redox probe for studying cation transfer across the water/2-nitrophenyl octyl ether interface at three-phase

junctions supported by carbon ink screen-printed electrodes, J. Electroanal. Chem. 656 (2011) 237–242. doi:10.1016/j.jelechem.2010.11.004.

[21] F. Quentel, V. Mirčeski, M. L'Her, Lutetium Bis(tetra- tert - butylphthalocyaninato): A Superior Redox Probe To Study the Transfer of Anions and Cations Across the Water|Nitrobenzene Interface by Means of Square-Wave Voltammetry at the Three-Phase Electrode, J. Phys. Chem. B. 109 (2005) 1262–1267. doi:10.1021/jp045914c.

[22] K. Dharmaraj, Z. Nasri, H. Kahlert, F. Scholz, The electrochemistry of DPPH in three-phase electrode systems for ion transfer and ion association studies, J. Electroanal. Chem. 823 (2018) 765–772. doi:10.1016/j.jelechem.2018.06.012.

[23] Z. Samec, D. Homolka, V. Mareček, Charge transfer between two immiscible electrolyte solutions part VIII. Transfer of alkali and alkaline earth-metal cations across the water/nitrobenzene interface facilitated by synthetic neutral ion carriers, J. Electroanal. Chem. Interfacial Electrochem. 135 (1982) 265–283. doi:10.1016/0368-1874(82)85125-3.

[24] P. Vanysek, W. Ruth, J. Koryta, Valinomycin mediated transfer of potassium across the water/nitrobenzene interface, J. Electroanal. Chem. Interfacial Electrochem. 148 (1983) 117–121. doi:10.1016/S0022-0728(83)80134-X.

[25] Z. Yoshida, H. Freiser, Mechanism of the carrier-mediated transport of potassium ion across water-nitrobenzene interface by valinomycin, J. Electroanal. Chem. Interfacial Electrochem. 179 (1984) 31–39. doi:10.1016/S0022-0728(84)80272-7.

[26] J. Langmaier, Z. Samec, Voltammetry of Ion Transfer across a Polarized Room-Temperature Ionic Liquid Membrane Facilitated by Valinomycin: Theoretical Aspects and Application, Anal. Chem. 81 (2009) 6382–6389. doi:10.1021/ac9008258.

[27] F. Quentel, V. Mirčeski, M. L'Her, K. Stankoska, Assisted Ion Transfer at Organic Film-Modified Electrodes, J. Phys. Chem. C. 116 (2012) 22885–22892. doi:10.1021/jp3067603.

[28] M. Podrażka, J. Maciejewska, W. Adamiak, E. Witkowska Nery, M. Jönsson-Niedziółka, Facilitated cation transfer at a three-phase junction and its applicability for ionophore evaluation, Electrochim. Acta. 307 (2019) 326–333. doi:10.1016/j.electacta.2019.03.201.

[29] S.M. MacDonald, J.D. Watkins, Y. Gu, K. Yunus, A.C. Fisher, G. Shul, M. Opallo, F. Marken, Electrochemical processes at a flowing organic solvent|aqueous electrolyte phase boundary, Electrochem. Commun. 9 (2007) 2105–2110. doi:10.1016/j.elecom.2007.05.031.

[30] J.D. Watkins, S.M. MacDonald, P.S. Fordred, S.D. Bull, Y. Gu, K. Yunus, A.C. Fisher, P.C. Bulman-Page, F. Marken, High-yield acetonitrile | water triple phase boundary electrolysis at platinised Teflon electrodes, Electrochim. Acta. 54 (2009) 6908–6912. doi:10.1016/j.electacta.2009.06.083.

[31] D. Kaluza, W. Adamiak, T. Kalwarczyk, K. Sozanski, M. Opallo, M. Jönsson-Niedziolka, Anomalous Effect of Flow Rate on the Electrochemical Behavior at a Liquid|Liquid Interface under Microfluidic Conditions, Langmuir. 29 (2013) 16034–16039. doi:10.1021/la403614z.

[32] D. Kaluza, W. Adamiak, M. Opallo, M. Jonsson-Niedziolka, Comparison of Ion Transfer Thermodynamics at Microfluidic and Droplet-Based Three Phase Electrodes, Electrochim. Acta. 132 (2014) 158–164. doi:10.1016/j.electacta.2014.03.105.

[33] E. Bak, M. Donten, Z. Stojek, Three-phase electrochemistry with a cylindrical microelectrode, Electrochem. Commun. 7 (2005) 483–489. doi:10.1016/j.elecom.2005.03.005.

[34] E. Bak, M. Donten, Z. Stojek, Three-phase electrochemistry with cylindrical microelectrode crossing vertically the boundary of two immiscible liquids, J. Electroanal. Chem. 600 (2007) 45–53. doi:10.1016/j.jelechem.2006.02.022.

[35] E. Bak, M. Donten, Z. Stojek, F. Scholz, The punctured droplet electrode – A new three-phase electrode with well defined geometry, Electrochem. Commun. 9 (2007) 386–392. doi:10.1016/j.elecom.2006.09.032.

[36] M. Podrażka, E. Witkowska Nery, A. Pacowska, D.W.M. Arrigan, M. Jönsson-Niedziółka, Paper-Based System for Ion Transfer Across the Liquid–Liquid Interface, Anal. Chem. 90 (2018) 8727–8731. doi:10.1021/acs.analchem.8b02695.

[37] I. Kaminska, J. Niedziolka-Jonsson, A. Roguska, M. Opallo, Electrodeposition of gold nanoparticles at a solid|ionic liquid|aqueous electrolyte three-phase junction, Electrochem. Commun. 12 (2010) 1742–1745. doi:10.1016/j.elecom.2010.10.011.

[38] I. Kaminska, M. Jonsson-Niedziolka, A. Kaminska, M. Pisarek, R. Hołyst, M. Opallo, J. Niedziolka-Jonsson, Electrodeposition of Well-Adhered Multifarious Au Particles at a Solid|Toluene|Aqueous Electrolyte Three-Phase Junction, J. Phys. Chem. C. 116 (2012) 22476–22485. doi:10.1021/jp307674k.

[39] L. Huang, P. Li, N. Pamphile, Z.-Q. Tian, D. Zhan, Electrosynthesis of Copper-Tetracyanoquinodimethane Based on the Coupling Charge Transfer across Water/1,2-Dichloroethane Interface, Electrochim. Acta. 140 (2014) 332–336. doi:10.1016/j.electacta.2014.04.102.

[40] E. Bak, M.L. Donten, M. Donten, Z. Stojek, Electrodeposition of polymer next to the three-phase boundary, Electrochem. Commun. 7 (2005) 1098–1104. doi:10.1016/j.elecom.2005.08.004.

[41] J. Niedziolka-Jonsson, M. Jonsson-Niedziolka, W. Nogala, B. Palys, Electrosynthesis of thin sol–gel films at a three-phase junction, Electrochim. Acta. 56 (2011) 3311–3316. doi:10.1016/j.electacta.2011.01.024.

[42] K. Szot, M. Jönsson-Niedziolka, B. Palys, J. Niedziolka-Jönsson, One-step electrodeposition of carbon–silicate sponge assisted by a three-phase junction for

efficient bioelectrocatalysis, Electrochem. Commun. 13 (2011) 566–569. doi:10.1016/j.elecom.2011.03.011.

[43] S.B. Khoo, J.K. Foley, S. Pons, Electrolyte effects on the cyclic voltammetry of TCNQ and TCNE, J. Electroanal. Chem. Interfacial Electrochem. 215 (1986) 273–285. doi:10.1016/0022-0728(86)87021-8.

[44] S.B. Khoo, J.F. Foley, C. Korzeniewski, S. Pons, C. Marcott, An infrared spectroelectrochemical investigation of the ion pairing reactions of the anions and dianions of TCNE and TCNQ, J. Electroanal. Chem. Interfacial Electrochem. 233 (1987) 223–236. doi:10.1016/0022-0728(87)85018-0.

[45] M. Oyama, R.D. Webster, M. Suárez, F. Marken, R.G. Compton, S. Okazaki, Mechanistic Aspects of the Electrochemical Reduction of 7,7,8,8-Tetracyanoquinodimethane in the Presence of Mg 2+ or Ba 2+, J. Phys. Chem. B. 102 (1998) 6588–6595. doi:10.1021/jp9819846.

Chapter 3. Materials and methodology

This chapter outlines all the chemicals and electrochemical techniques used in the studies of the microdroplet TPE ion transfer. The procedure for the synthesis of bis(tridentate) ruthenium(II) complex having bis(benzimidazolyl)pyridine based ligands $[Ru^{II}(LR)(L)]^0$ is given section **3.2**. I synthesised this complex during my internship visit to Prof. Mas-aaki Haga's laboratory, department of applied chemistry, Chuo University, Tokyo, Japan. Furthermore, the theoretical background of the voltammetric techniques used in the TPE ion transfer studies and the characteristics of ion transfer voltammograms have been described in this chapter.

3.1 Chemicals

All the salts, solvents, and redox probes were used as received without additional purification.

3.1.1 Chemicals used for electrochemistry

Inorganic salts: LiCl (99%, Sigma-Aldrich), NaCl (pure p.a., POCh), KCl (>99.99%, Sigma-Aldrich), RbCl (≥98%, Merck), CsCl (≥98%, Merck), $MgCl_2$ (99%, Sigma-Aldrich), $CaCl_2$ (99%, POCh), $BaCl_2$ (99%, Sigma-Aldrich), $AlCl_3$ (≥98%, ROTH), KPF_6 (98%, Sigma-Aldrich), $NaClO_4$ (>99%, Fluka), NaSCN (purum, Fluka), KNO_3 (99%, POCh), KBr (pure p.a., POCh), KF (>99.99 %, Fluka), Na_2SO_4 (>99.99 %, Fluka).

Organic salts: tetramethylammonium chloride (TMACl) (≥99%, Fluka), tetraethylammonium chloride (TEACl) (≥99%, Fluka), tetrapropylammonium chloride (TPACl) (≥98%, Sigma-Aldrich), tetrabutylammonium chloride (TBACl) (≥98%, Sigma-Aldrich), tetrabutylammonium perchlorate ($TBAClO_4$) (≥98%, Sigma-Aldrich).

Organic solvents: n-octyl-2-pyrrolidone (NOP) (Santa Cruz Biotechnology), acetonitrile (CH_3CN) (99.8 %, Sigma- Aldrich), nitrobenzene (NB) (TCI chemicals), 2-nitrophenyl octyl ether (NPOE) (99.8 %, Sigma- Aldrich), 1,2-dichloroethane (DCE) (99.8 %, Sigma- Aldrich), methonal (CH_3OH) (99.8 %, Sigma- Aldrich).

Aqueous phase: salts were dissolved in ultrapure water to prepare the aqueous phase, which was not saturated with water-immiscible organic solvents.

Redox probes: 1-aminoanthraquinone (AQ) (99.8 %, Sigma- Aldrich), 2,3-dichloro-1,4-naphthoquinone (NQ) (99.8 %, Sigma- Aldrich), 7,7,8,8-tetracyanoquinodimethane (TCNQ) (Sigma-Aldrich), $[Ru^{II}(LR)(L)]^0$ complex (synthesised as described in section 3.2), bis(pentamethylcyclopentadienyl)iron(II) (DMFc), quinizarin green SS.

3.1.2 Chemicals used for the synthesis of $[Ru^{II}(LR)(L)]^0$ complex

µ-Dichloro(*p*-cymene)ruthenium(II)dimer or $[Ru(p\text{-cymene})Cl_2]_2$ (97%, Merk), 2,6-bis(benzimidazol-2-yl)pyridine (LH_2) (97%, Sigma-Aldrich), 2,6-bis(1-(2-octyldodecan)benzimidazol-2-yl)pyridine) (LR) was synthesized by alkylation of 2,6-bis(benzimidazol-2-yl)pyridine with 1-bromo-2-octyl-1-dodecane according to the

literature [1], dimetyloformamid (DMF) (99.8 %, Sigma-Aldrich), tert-butanol (99.8 %, Sigma- Aldrich).

3.2 Synthesis of a neutral bis(tridentate) ruthenium(II) $[Ru^{II}(LR)(L)]^0$ redox probe

Haga and co-workers have synthesised a large number of electroactive organometallic compounds. The tuning of the redox potential by introducing different ligand systems to the metalloorganic complex is one of the Haga's favourite topics of research. He has been working on this topic for approximately more than 30 years. Tuning redox potential is significant for synthesising compounds to use for TPE ion transfer studies; since compounds have to undergo redox reaction at TPE configuration before the water reduction and oxidation events. I used bis(benzimidazolyl)pyridine ligand systems to synthesise Ru complex for TPE anion transfer studies. These types of ligands lower the ruthenium oxidation potential (explained in chapter **4.3**), and they can be made more lipophilic by adding long alkyl chains to the imino nitrogen.

The $[Ru^{II}(LR)(L)]^0$ complex has two tridentate LR and L ligands. LR is 2,6-bis(1-(2-octyldodecyl)benzimidazol-2-yl)pyridine), which was synthesised by the alkylation of 2,6-bis(benzimidazol-2-yl)pyridine (LH_2) with 1-bromo-2-octyl-1-dodecane. The alkylation of LH_2 was carried out by Takumi Watanabe (Haga's student). Another L ligand was obtained after the complexation of LH_2 with Ru metal and deprotonation of LH_2 (leads to L). The synthetic route of a neutral heteroleptic $[Ru^{II}(LR)(L)]^0$ complex involves two steps. In the first step (**Fig. 3.1)**, I synthesised $RuLH_2Cl_3$ complex from $[Ru(p\text{-cymene})Cl_2]_2$ and LH_2 ligand. In the second step (**Fig. 3.2**), $[Ru^{II}(LR)(L)]^0$ complex was synthesised by attaching LR ligand to $RuLH_2Cl_3$ complex, followed by deprotonation (removal of imino N-H protons).

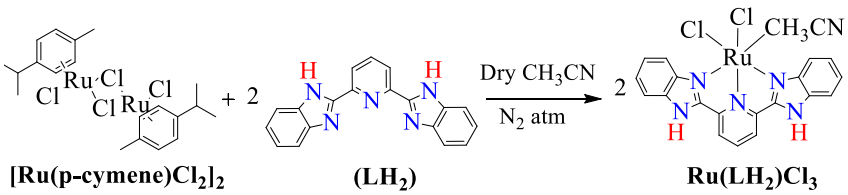

Figure 3.1 Synthetic route to the preparation of $Ru(LH_2)Cl_3$ complex. The imino (N-H) protons are coloured red.

In a nitrogen atmosphere, the ligand LH_2 and $[Ru(p\text{-cymene})Cl_2]_2$ were dissolved in 5 ml dry CH_3CN and refluxed at 70 °C for five hours. The reaction between bis(benzimidazole)pyridine derivatives with Ru complexes take a long time to complete; hence refluxed around 70 to 100 °C to speed up the reactions. While heating, the colour changed from brown to dark brown. After five hours, the resulted solid $RuLH_2Cl_3$ complex was filtered using a 1.0-micron polytetrafluoroethylene filter and dried. **Fig. 3.1** displays the scheme of the reaction.

The obtained solid $RuLH_2Cl_3$ complex was dissolved in 5 ml dry DMF. To this solution, the LR ligand dissolved in 5ml tertiary-butanol was added and refluxed at 100 °C in a nitrogen atmosphere for seven hours. During the reaction, the solution colour turned from dark brown to dark red.

After the completion of the reaction, both DMF and tert-butanol solvents were removed by vacuum distillation. The reaction mixture was dissolved in methanol, and 1 M NaOH was added until the red precipitate of neutral $[Ru^{II}(LR)(L)]^0$ complex forms. To the produced precipitate, 20 ml of water was added, filtered, and vacuum dried. The scheme of the reaction is given in **Fig. 3.2**. The compound was purified by the Sephadex LH 20 column chromatography with acetonitrile-methanol (1: 1v/v) as an eluent. The eluate was recrystallised at 15 °C, obtained $[Ru^{II}(LR)(L)]^0$ crystals were filtered, washed with acetonitrile, and dried for electrochemistry.

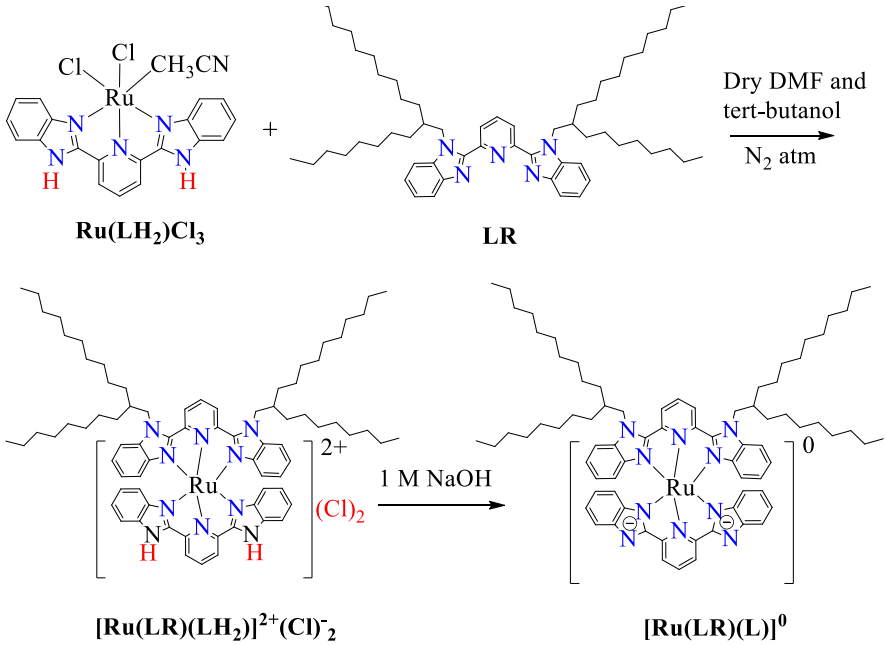

Figure 3.2 Synthesis of neutral bis(tridentate) $[Ru^{II}(LR)(L)]^0$ complex. Upon treatment of $[Ru(LR)(LH_2)]^{2+}(Cl)_2^-$ complex with NaOH; imino protons and chloride (red coloured) were removed to get the neutral $[Ru^{II}(LR)(L)]^0$ complex.

3.3 Equipment and methodology

All voltammetry techniques were performed using a conventional three-electrode cell setup consisting of a working electrode (WE), a reference electrode (RE), and a counter or auxiliary electrode (CE). Before TPE ion transfer studies, electrochemistry of all the redox probes was done in the water-immiscible organic solvents. For these studies, a GC WE, Ag wire quasi-reference or $Ag/AgNO_3$ (0.01 M in CH_3CN) RE, a Pt wire CE were used, and the organic solvents were deoxygenated by purging argon gas for 30 min. For

the TPE ion transfer, a three-electrode cell setup with glassy carbon (GC) WE (3 mm radius), Ag/AgCl (3.5 M KCl) RE, and a Pt wire CE were used.

Before electrochemical measurements, the GC WEs were polished on the fabric polishing pad using water-alumina slurry (Al_2O_3 of size 1, 0.3 and 0.05 µm) and followed by sonication in ultrapure water and ethanol. The preparation of WE for microdroplet TPE ion transfer studies has already discussed in chapter 1. All voltammetry techniques were performed using the Biologic SP-300, an ALS/CH model 660A, or a Palmsens4 potentiostat.

3.3.1 Voltammetric techniques and their theoretical aspects

Voltammetry involves a set of electroanalytical techniques, where the interfacial charge transfer processes are driven by applying a controlled time-dependent external potential to the electrochemical cell and measure the resulting current as a function of the applied potential. Voltammetric measurements give information about the redox reaction happens at the WE|electrolyte interface, i.e., regarding the kinetics and thermodynamics of the interfacial charge transfer reactions and adsorption phenomena [2,3].

The three-electrode cell setup is the generally used configuration to record voltammograms. We apply the controlled potential to the WE, to change its potential concerning the fixed potential of the RE and measure the current that flows between the WE and CE. The plot of the resulting current versus the applied potential is called a voltammogram. The potentiostat controls the electrical potential difference between the WE|electrolyte interface, which is the driving force for the electrochemical reaction. The electrolyte potential is equivalent to the potential of the metallic phase of the RE. The potential difference between the WE|electrolyte interface is identical to that between WE and RE. The potentiostat sets the voltage between WE and CE to have the aspired potential difference between the WE|electrolyte interface, which is equal to the RE [2,3].

The WE can be made from various materials like carbon, metal, and semiconductors. The qualities of the perfect WE are low resistance, reproducible surface, a broad potential range, capable of delivering a high signal-to-noise response, must be constructed from a material that is inert to the solvents and analytes throughout the potential window. The carbon-based solid electrodes exhibit the characters mentioned above. GC is one of them, a rod of GC is sealed into an inert plastic electrode body such that a micro disc of the GC material is open to be exposed to the solution [4].

The role of the RE is to keep its potential constant and serve as a clear and stable reference point to control the potential of the WE by the potentiostat. During the measurements, the chemical composition of the RE should not change, because the composition controls its constant electrical potential. In the case of measuring minimal current that does not alter the potential of the RE, a two-electrode setup of WE and RE can be used. Few commonly used REs in aqueous media are saturated calomel electrode (SCE) and the Ag/AgCl electrodes. For three-phase electrochemistry, I used Ag/AgCl (3.5 M KCl) RE. The controlling redox process in Ag/AgCl RE is [4]:

$$AgCl + e^- \leftrightharpoons Ag^+ + Cl^- \quad (3.1)$$

To perform electrochemistry in nonaqueous media, I used silver/silver cation RE with the filing CH_3CN solution containing $AgNO_3$ (0.01 M) and $TBAClO_4$ (0.1 M). The controlling redox reaction is:

$$Ag^+ + e^- \leftrightharpoons Ag \quad (3.2)$$

The CE offers the surface area for a redox reaction to balance the reaction that occurs at the WE. The surface area of the CE should be more than the surface area of the WE. Almost all potentiostats use the feedback circuit that applies such a potential between the CE and WE so that the WE potential matches precisely to the value it should have [2]. The CE used in both single-phase and three-phase experiments was a platinum wire.

Voltammetry can be categorised into three types; potential sweep, potential step, and constant potential methods. In the potential sweep methods (e.g., cyclic voltammetry), the potential of the WE is linearly scanned. In the case of a potential step method (e.g., square wave voltammetry), the potential is stepped, which allows eliminating the capacitive current. In the constant potential methods (e.g., bulk electrolysis), a constant potential is applied for a particular time period. Cyclic voltammetry and square wave voltammetry techniques were mainly used in TPE ion transfer studies.

3.3.1.1 Cyclic voltammetry

Cyclic voltammetry is the most commonly used potential sweep technique to get the qualitative and quantitative information of the redox reactions. It provides substantial information about the thermodynamics of the redox process and the kinetics of the heterogeneous electron transfer reactions. Cyclic voltammetry involves the linear sweep of the WE potential by triangular potential waveform (shown in **Fig. 3.3)** and measuring the current as a function of the applied linear potential [5].

The voltage is swept from E_1 to E_2 in the forward scan and swept back from E_2 to E_1 in the reverse scan; the rate at which scan is done (slope of V vs t) is the voltammetric scan rate. The obtained current is plotted against the applied voltage is called the cyclic voltammogram (CV). There are different conventions to plot the voltammetric data. I followed the IUPAC convention; where the positive/oxidation potentials are plotted in the positive "x" direction, and the anodic currents (oxidation currents) are positive.

A typical CV obtained for the oxidation of DMFc (Eq. 3.3) is given in **Fig. 3.4**. Where E_{pa} and E_{pc} are anodic and cathodic peak potentials; I_{pa} and I_{pc} are the anodic and cathodic peak currents, respectively. The term $E^{0\prime}$ refers to the formal potential of the redox couple $DMFc/DMFc^+$. CV curve involves the process of the electron transfer reaction between WE|electrolyte interface (interfacial redox reaction) and the movement of electroactive material to the WE (mass transfer phenomenon, e.g., diffusion).

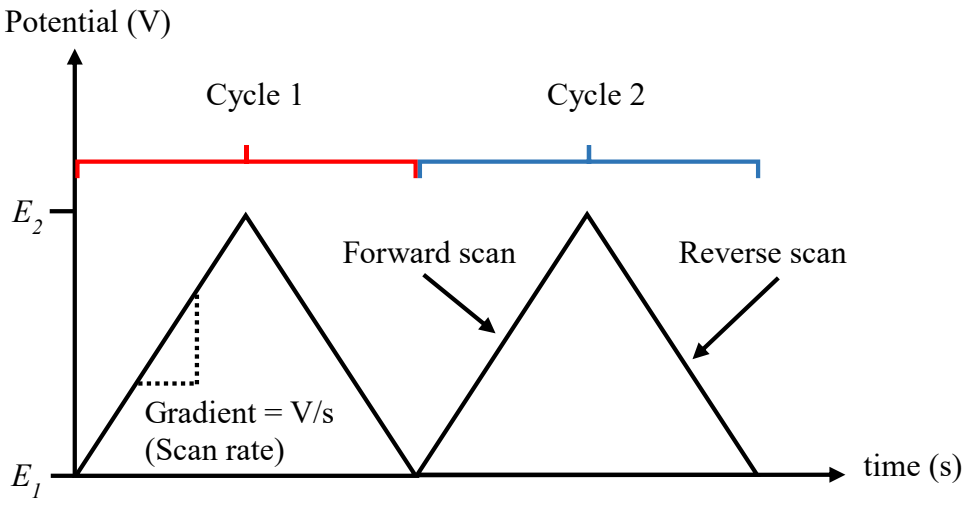

Figure 3.3 Potential vs time profile used to do the cyclic voltammetry. Adapted from page 36 of [5] and [6].

$$DMFc \leftrightharpoons DMFc^{+} + e^{-} \qquad 3.3$$

The redox reaction (Eq. 3.3) is an interfacial heterogeneous electron transfer process which takes place at the WE|electrolyte interface only. Which means that both DMFc and $DMFc^{+}$ exist in the same phase (electrolyte solution), but electrons are from a different phase (WE), and they are exchanged at WE|electrolyte interface between the electrode and the redox species. Therefore, altering the electrical potential of the WE allows the shifting of the redox equilibrium of Eq. 3.3 in a required direction, i.e., to the right-hand side of DMFc oxidation or the left-hand side of the $DMFc^{+}$reduction.

Before the start of cyclic voltammetry (**Fig 3.4**), only DMFc species were present in the solution (no $DMFc^{+}$ species) and homogeneously distributed at a bulk concentration. When the potential of the WE scanned from lower to the higher value; accordingly, oxidation of DMFc to $DMFc^{+}$ at the WE making the current to flow and decreasing DMFc concentration near the vicinity of the WE. The concentration gradient produced at the proximity of the WE results in the mass transfer called diffusion. Diffusion is the primary and slow way of moving reactants to the WE when the solution is in unstirred condition, and diffusion resupplies the DMFc from the bulk. The current increases as the oxidation of DMFc continue, at some point (E_{pa}), current starts to decrease as the scan continues because the diffusion layer has developed adequately above the WE so that the rate of diffusion of DMFc from the bulk to the surface of the WE is slower and cannot maintain the steady-state concentration near the WE. When the scan is reversed, the electrode reaction in Eq. 3.3 is drifted on the left-hand side (reduction of $DMFc^{+}$). The reduction reaction happens in the opposite sense to the oxidation sweep with a similar kind of mass transport process [3,7].

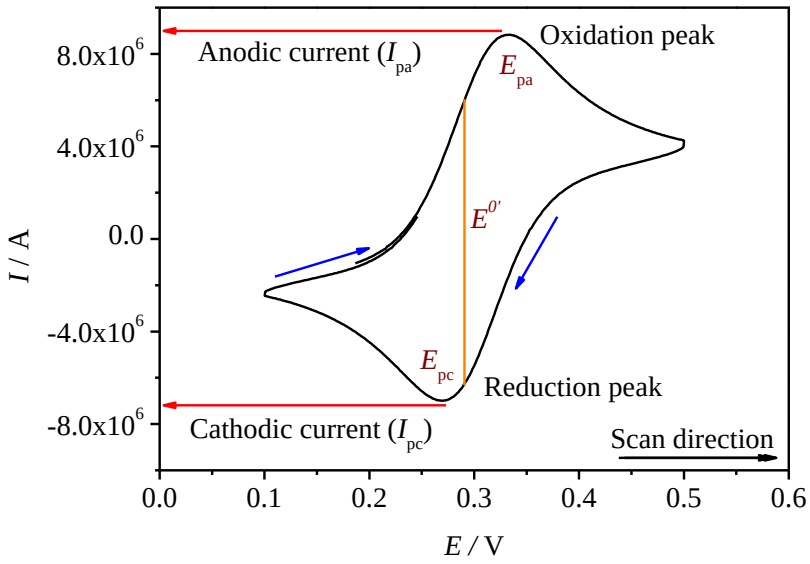

Figure 3.4 CV of 1 mM DMFc in acetonitrile with 0.1 M TBACl supporting electrolyte at a scan rate of 40 mV s^{-1}.

The overall WE reaction can be limited by the rate of mass transport (υ_{mt}) (i.e., mainly the transport of reactants to the WE), and the rate of charge transfer (υ_{ct}) at the WE|electrolyte interface. When the υ_{ct} is faster than the υ_{mt}, a rapid equilibrium establishes between the oxidised and reduced forms of the electroactive compounds at the WE interface. Then the ratio of surface activities $\left(\frac{a_{Ox}}{a_{Red}}\right)$ at the interface for the electrode potential (E) is given by the Nernst equation (Eq. 3.4) [2].

$$E = E^0 + \frac{RT}{nF} ln \left(\frac{a_{Ox}}{a_{Red}}\right) \qquad 3.4$$

In the above equation, E^0 is the standard potential, R indicates the universal gas constant, T denotes the temperature, n is the number of electrons, and F indicates Faraday's constant. The system where $\left(\frac{a_{Ox}}{a_{Red}}\right)$ agrees with the potential given by the Nernst equation is called the reversible system [2]. In another case, where the υ_{mt} is faster than the υ_{ct}, the equilibrium does not establish with the adequate rate; the ratio of surface activities for the potential deviates from the ratio provided by the Nernst equation. This electrochemical system is called irreversible [2].

The formal potential ($E^{0\prime}$) for a reversible system is at the midpoint between E_{pa} and E_{pc}, which is given by [6].

$$E^{0\prime} = \frac{E_{pa} + E_{pc}}{2} \qquad 3.5$$

For reversible couples, the number of electrons (n) involved in the reaction can be determined by the peak-to-peak separation (ΔE_p) [6].

$$\Delta E_{\mathrm{p}} = E_{\mathrm{pa}} - E_{\mathrm{pc}} \cong \frac{0.059\ \mathrm{V}}{n} \qquad 3.6$$

One electron process has ΔE_{p} of 0.059 V. If the process is irreversible, peak-to-peak separation increases.

For the electrochemically reversible system comprising diffusion, the peak current is described by the Randles−Sevcik equation [8]. According to this equation, the peak current (I_{p}) rises linearly with the square root of the scan rate (υ).

$$I_{\mathrm{p}} = 0.446nFA\mathrm{C}^{0}\left(\frac{nF\upsilon \mathrm{D}_{0}}{RT}\right)^{1/2} \qquad 3.7$$

Where n indicates the number of electrons transferred during the redox event, A denotes the electrode surface area, D_0 signifies the diffusion coefficient of the analyte, and C^0 is the bulk concentration of the analyte.

The value of I_{pa} and I_{pc} should be identical for the electrochemically reversible couple [6].

$$\frac{I_{\mathrm{pa}}}{I_{\mathrm{pc}}} = 1 \qquad 3.8$$

3.3.1.2 Square wave voltammetry

The interfacial charge transfer processes happen at the electrode (redox reactions) are termed as faradaic processes, and the current obtained due to faradaic processes in voltammetry is called faradaic current (I_{f}). Other interfacial phenomenon named as non-faradaic processes, which mainly involve the formation of the electric double layer at the WE|electrolyte interface giving current is designated as non-faradaic or charging current (I_{c}). This microscopic electric double layer formed because of the additional charge at the WE and the arrangement of the counter charged ions of the electrolyte (**Fig. 3.5**). Besides, polar solvent molecules can also arrange at the interface according to the electrode charge. The electrical double layer behaves as a capacitor with very low capacitance. General current obtained in the CV has both constituents of I_{f} and I_{c}, but I_{c} will be higher than I_{f} if the concentration of the electroactive species is deficient [3].

Applying a small potential step or increment (a few mV) results in a formation of an electrical double layer in few milliseconds, I_{c} decays more quickly than I_{f} (as shown in the inset of **Fig. 3.5**). In a square wave voltammetric technique, the sensitivity of voltammetry is enhanced by reducing the contribution of the I_{c}, which is succeeded by using a waveform having a square wave superimposed on the staircase potential–time function (**Fig. 3.6**). The potential variation step is presented in **Fig. 3.6**, every single potential step is an impose of two oppositely positioned potential pulses called forward and reverse pulses. In **Fig. 3.6**, the ΔE is the scan increment, and τ is the duration of a single potential step. Hence, the scan rate (υ) is the ratio of ΔE and τ ($\upsilon = \Delta E / \tau$). The

duration of the two pulses is $t_p = \tau / 2$, and the height of the single pulse is the square-wave amplitude (E_{sw}).

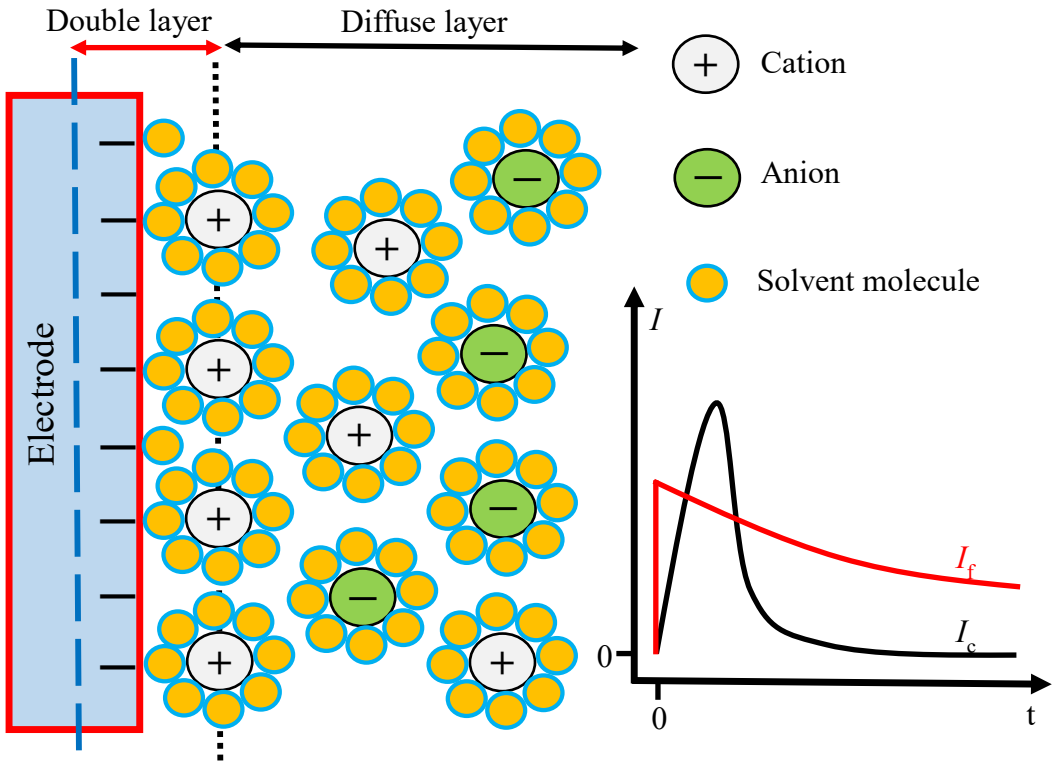

Figure 3.5 A simple drawing of the electric double obtained at the WE|electrolyte interface and an inset showing the expected variation of the charging (I_c) and faradaic current (I_f) with time. Adapted from [3] and page 60 of [5].

The essential parameters in the square wave voltammetric technique are ΔE, t_p, and E_{sw} [3]. The reason to have imposed pulses is to drive the reaction in both anodic and cathodic direction; this process is repeated for each potential step. The current measured at the end of each (forward and reverse) pulses give the forward (I_{for}) and reverse components (I_{rev}) of square wave voltammogram (SWV), respectively. For every potential step, both the components are measured, and the difference between I_{for} and I_{rev} components is the net current (I_{net}) ($I_{net} = I_{for} - I_{rev}$), which is more significant than both components. The general shape of the forward and reverse components look like linear sweep voltammetry. The I_{net} component in the SWV is the well-defined peak; the peak height and position are significant in the analytical point of view. The reason to measure the current at the end of the pulses is the reduce the charging current.

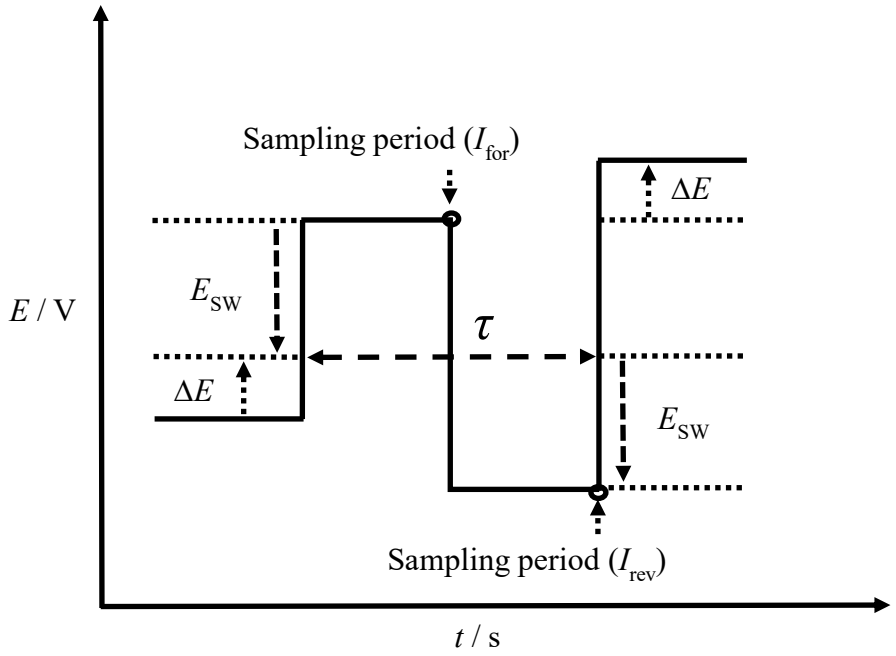

Figure 3.6 Square wave voltammetry potential-time waveform. Adapted from [3].

3.3.1.3 TPE ion transfer cyclic and square wave voltammograms

For ion transfer studies at the TPE setup, subsequent CV cycles are scanned. **Fig. 3.7** depicts the continuous CV cycles of DMFc oxidation (to $DMFc^+$) at the three-phase junction, which is accompanied by the transfer of Cl^- anions from water to NOP (Eq. 3.9).

$$DMFc_{(NOP)} + Cl^-_{(aq)} \leftrightharpoons DMFc^+_{(NOP)} + Cl^-_{(org)} + e^- \qquad 3.9$$

The current magnitude in the three-phase CV cycles confirms whether Cl^- anions transferred from water to NOP or the $DMFc^+$ species expelled from NOP to the water. The stable current during the continuous CV cycles (**Fig. 3.7**) specifies that Cl^- anions transfer to the NOP droplet (Eq. 3.9). In the event of $DMFc^+$ species expulsion from the droplet, the current should decrease rapidly since the droplet volume is substantially less related to the volume of the aqueous phase [9,10]. Surely $DMFc^+$ ejection can be witnessed when the aqueous phase comprises anions of very high standard Gibbs energies of transfer.

The scan rate studies of the reversible couple for the TPE anion transfer reaction shows the linear dependency of I_{pa} with $\sqrt{\upsilon}$, and almost identical values of I_{pa} and I_{pc}. However, ΔE_p varies with increasing the scan rate due to the increase in the ohmic drop inside the droplet. Furthermore, the formal oxidation potential depends on the lipophilicity and concentration of the transferring anion (Eq. 1.23), which is usually studied by performing three-phase SWVs.

Similar to the anion transfer CV cycles, cation transfer CVs also show stable current during cycling [11], the ration of I_{pa} over I_{pc} should be identical, and the redox process should be a diffusional (follow a Randles-Sevick equation). Also, the formal reduction potential varies with the lipophilicity and concentration of the aqueous cation (Eq. 1.24).

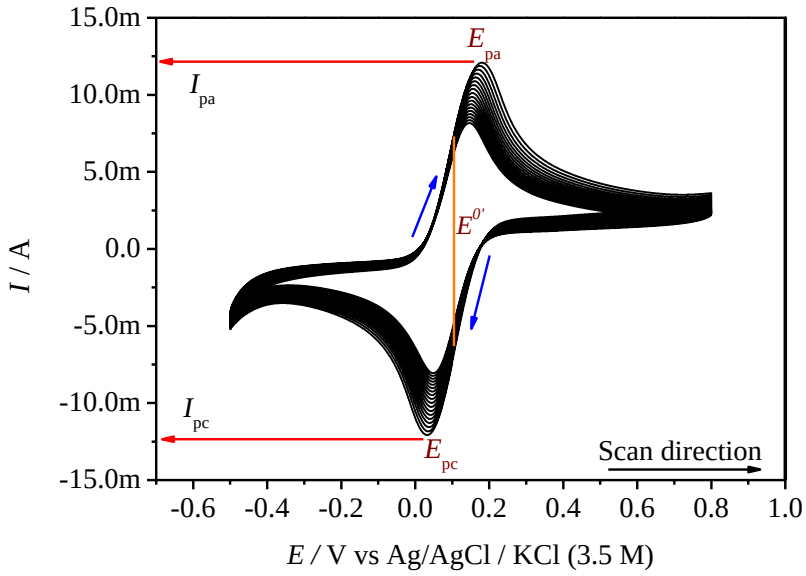

Figure 3.7 CV cycles (at 40 mV s^{-1}) performed at TPE configuration, a droplet of NOP (having 10 mM DMFc) deposited on the GC electrode, and submerged in 0.1 M KCl.

The SWV components for the TPE anion transfer (Eq. 3.9) are displayed in **Fig. 3.8**, which looks almost identical to a typical single-phase SWV. The characteristics of ion transfer SWV are; the I_{net} should increase during the successive scans of the same droplet because of the increase in the ion concentration inside the droplet. In different scan rates, SWV peak potentials should be unaffected.

As mentioned earlier, the confirmation of ion transfer reaction is the dependency of the formal oxidation potential on the lipophilicity of aqueous ion and its concentration; which is examined by conducting SWV experiments in the aqueous phase of different ions and different concentrations. For anion transfer reaction, the SWV oxidation peak potentials are lower for more lipophilic anions. For the set of standard anions (PF_6^-, ClO_4^-, SCN^-, NO_3^-, Br^-, Cl^-, CN^-, and F^-), the oxidation potential of the SWVs vary as $PF_6^- < ClO_4^- < SCN^- < NO_3^- < Br^- < Cl^- < F^-$. Besides, as the anion concentration increases in the aqueous phase, the oxidation peak potential of SWV shifts negatively [12].

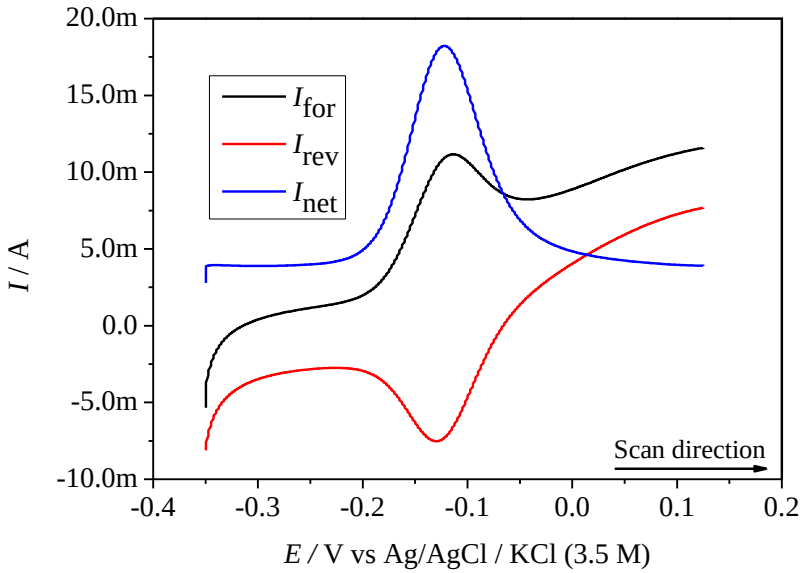

Figure 3.8 SWV of TPE configuration, a droplet of NOP (having 10 mM DMFc) deposited on the GC electrode, and submerged in 0.1 M KCl.

In the case of a cation transfer reaction, the reduction potential of the SWVs is more negative for the more hydrophilic cations [11,13]. Additionally, as the concentration of the aqueous cation decreases, the reduction potentials of the SWVs continuously shift to negative potentials.

In the next chapters, I discussed TPE ion transfer CVs and SWVs in detail, along with the obtained results.

3.4 References

[1] M. a. Haga, N. Kato, H. Monjushiro, K. Wang, M.D. Hossain, Metal coordination to amphiphilic Ru complexes at the air-water interface, Supramol. Sci. 5 (1998) 337–342. doi:10.1016/S0968-5677(98)00028-5.

[2] F. Scholz, Voltammetric techniques of analysis: the essentials, ChemTexts. 1 (2015) 17. doi:10.1007/s40828-015-0016-y.

[3] V. Mirceski, S. Skrzypek, L. Stojanov, Square-wave voltammetry, ChemTexts. 4 (2018) 17. doi:10.1007/s40828-018-0073-0.

[4] Cynthia G. Zoski, Handbook of Electrochemistry, First edit, Elsevier, 2007. doi:10.1016/B978-0-444-51958-0.X5000-9.

[5] D.A.C. Brownson, C.E. Banks, The Handbook of Graphene Electrochemistry, Springer London, London, 2014. doi:10.1007/978-1-4471-6428-9.

[6] P.T. Kissinger, W.R. Heineman, Cyclic voltammetry, J. Chem. Educ. 60 (1983) 702. doi:10.1021/ed060p702.

[7] G.A. Mabbott, An introduction to cyclic voltammetry, J. Chem. Educ. 60 (1983)

697. doi:10.1021/ed060p697.

[8] N. Elgrishi, K.J. Rountree, B.D. McCarthy, E.S. Rountree, T.T. Eisenhart, J.L. Dempsey, A Practical Beginner's Guide to Cyclic Voltammetry, J. Chem. Educ. 95 (2018) 197–206. doi:10.1021/acs.jchemed.7b00361.

[9] F. Scholz, Š. Komorsky-Lovrić, M. Lovrić, A new access to Gibbs energies of transfer of ions across liquid|liquid interfaces and a new method to study electrochemical processes at well-defined three-phase junctions, Electrochem. Commun. 2 (2000) 112–118. doi:10.1016/S1388-2481(99)00156-3.

[10] F. Scholz, Recent advances in the electrochemistry of ion transfer processes at liquid–liquid interfaces, Annu. Rep. Prog. Chem., Sect. C Phys. Chem. 102 (2006) 43–70. doi:10.1039/B417141C.

[11] F. Scholz, R. Gulaboski, K. Caban, The determination of standard Gibbs energies of transfer of cations across the nitrobenzene|water interface using a three-phase electrode, Electrochem. Commun. 5 (2003) 929–934. doi:10.1016/j.elecom.2003.09.005.

[12] D. Kaluza, W. Adamiak, M. Opallo, M. Jonsson-Niedziolka, Comparison of Ion Transfer Thermodynamics at Microfluidic and Droplet-Based Three Phase Electrodes, Electrochim. Acta. 132 (2014) 158–164. doi:10.1016/j.electacta.2014.03.105.

[13] F. Quentel, V. Mirčeski, M. L'Her, Lutetium Bis(tetra- tert - butylphthalocyaninato): A Superior Redox Probe To Study the Transfer of Anions and Cations Across the Water|Nitrobenzene Interface by Means of Square-Wave Voltammetry at the Three-Phase Electrode, J. Phys. Chem. B. 109 (2005) 1262–1267. doi:10.1021/jp045914c.

Chapter 4. Results and Discussion

This chapter is divided into three subchapters. The first subchapter **4.1** describes the redox behaviour of AQ and NQ in NOP solvent and at the three-phase junction. In the second subchapter **4.2**, findings concerning the suitability of TCNQ as a redox probe for cation transfer studies at the TPE configuration are discussed. The last subchapter **4.3** contains electrochemical investigations of the $[Ru^{II}(LR)(L)]^0$ complex in NB and at TPE configuration for anion transfer studies.

4.1 Three-phase electrochemistry of important quinones at GC|n-octyl pyrrolidone|aqueous interface

In this subsection, a brief introduction is provided to the redox behaviour associated bioactivities of quinone derivatives (AQ and NQ) and quinone electrochemistry in different media. I highlight the challenges and reasons to select the quinones for three-phase electrochemistry. I discuss all the results obtained from the electrochemical behaviour of AQ and NQ in NOP solvent and at TPE configuration for cation transfer reaction.

4.1.1 Introduction to the significance of quinones electrochemistry

The electrochemistry of the quinone derivatives is under continuous study due to their significance in both chemical and biological viewpoints. From the chemical point of view; quinones are modern energy storage materials for aqueous flow batteries [1,2], used as a sensitiser in solar cells [3], reductive photoredox catalysts [4] and other applications [5]. Also, quinones are the vital functional groups in various biomolecules, and their redox behaviour has a significant impact on the biochemical processes happening in living systems (photosynthesis and cellular respiration) [6–10]. Examples for such quinones are anthraquinone and naphthoquinone derivatives, and their biological activities are influenced mainly by the electrochemical properties.

Anthracycline chemotherapy drugs belong to a class of anthraquinones. They have a planar anthraquinone chromophore that can be introduced between adjacent base pairs of DNA to treat various forms of human cancer [9,11]. The healing efficiency and toxicity of anthracyclines are associated with their redox behaviour [9,12–14]. A one-electron reduced semiquinone radical moiety (in the anthracycline drug) contributes significantly to determine the toxicity [9,15,16]. Vitamin K formulations and ubiquinone-10 (coenzyme Q) belong to the class of naphthoquinones; ubiquinone plays an essential task in the respiratory chain of mitochondria. It is a redox component responsible for the generation of pH gradients across the membrane in mitochondria (Q cycle) [16,17]. Thus, studying quinone electrochemistry is necessary to understand the reaction pathways and redox behaviour in the biological and chemical environments.

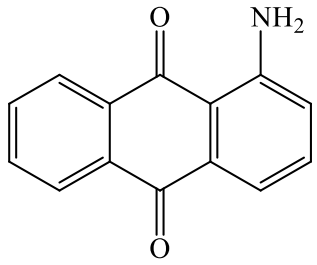

1-aminoanthraquinone (**AQ**)

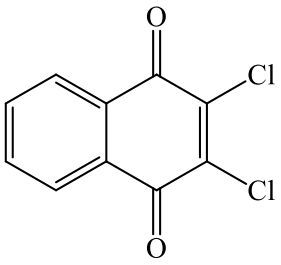

2,3-dichloro-1,4-naphthoquinone (**NQ**)

Figure 4.1 Structure of the studied quinone derivatives; AQ and NQ.

Electrochemistry of quinones has been studied in several conditions such as in different pH, solvents of different polarity and different supporting electrolytes. These studies gave us more insight into the ion-pair formation of reduced quinones with supporting electrolytes, effects of hydrogen bond on quinones redox behaviour, and stability of reduced quinones [9]. In this work, I investigated the three-phase electrochemistry of AQ and NQ (**Fig. 4.1**) at GC|NOP|aqueous three-phase interface. The motives for these studies are: (1) The lipophilic|hydrophilic (NOP|water) interface existing at TPE configuration is one of the simplest models to represent the complex biological membrane. Hence it is necessary to understand quinones redox behaviour in this condition. (2) Reduction of quinones at TPE configuration to study the cation transfer from aqueous to the organic phase. I wanted to examine the mechanism when cation transfer is driven by the reduction of carbonyl functional groups in quinones.

However, not all the lipophilic quinones can be used to study the cation transfer reaction at the TPE configuration because quinones have to reduce at the three-phase junction (to obtain the cation transfer) before the water reduction event happens at the WE|water interface. I performed the initial studies with different quinones such as benzophenones, halogen-substituted benzophenones, acenaphthenequinone, 1,8-naphthalic anhydrides, 3,5-dibenzyloxyacetophenone, quinizarin green SS, AQ, and NQ derivatives. However, quinones with two carbonyl groups on the opposite sides of the anthracene and naphthalene ring structures (AQ, NQ, and quinizarin green SS) have shown reduction at the three-phase junction. However, quinizarin green SS was not stable at the three-phase junction; it escaped to the aqueous phase. The reduction of halogen-substituted benzophenones and 3,5-dibenzyloxyacetophenone happened in NOP solvent but did not happen at TPE configuration (before the water reduction). This is the main reason that most lipophilic electroactive compounds can not be used to study cation transfer at the three-phase junction.

4.1.2 Electrochemistry of quinones

In aqueous buffer solutions, quinones (Q) exhibit a reversible single step two-electron reduction, and the reduction potentials change with pH in a Nernstian manner. At acidic pH, quinones undergo a reversible single step two-electron two-proton reduction process (Eq. 4.1). At alkaline pH, quinones show a single step two-electron reduction in which protons are not involved (Eq. 4.2). While in a neutral pH, the reduction is either a single step two-electron one-proton or the single step two-electron without the contribution of protons [9,18].

$$Q + 2H^{+} + 2e^{-} \leftrightharpoons QH_2 \qquad 4.1$$

$$Q + 2e^{-} \leftrightharpoons Q^{2-} \qquad 4.2$$

In a dry neutral aprotic media or non-polar solvents, typically quinones undergo two-step reduction; the first step corresponds to the generation of semiquinone radical anion ($Q^{\bullet-}$) and the second step to the quinone dianion (Q^{2-}). In CVs, quinones reduction display two distinct cathodic waves; in which the first reduction wave (Q to $Q^{\bullet-}$) is reversible, and the second wave (Q to Q^{2-}) is quasi-reversible in some scan rates [9,19]. Both reductions are diffusion-controlled; the reduction potentials depend on the polarity of the solvent and the type of supporting electrolytes used [19]. During the reduction event, the cations of the supporting electrolyte form the ion pairs with the $Q^{\bullet-}$ and Q^{2-}. Hence, reduction potentials depend on the nature of the cation present; the degree of the potential shift is influenced by the ionic potential of the cation (Φ_{eff}) and cations concentration [9]. Φ_{eff} is given by [9]:

$$\Phi_{eff} = Z/(r + \delta) \qquad 4.3$$

Where Z represents the charge of the cation, r indicates the Pauling radius of cation, and **δ** signifies the Latimer type correction factor. Therefore, the more substantial positive shift in the reduction potential can be seen for the cation with the higher charge and smaller size.

4.1.3 Electrochemistry of 1-aminoanthraquinone dissolved in NOP

CV measurement of AQ in the NOP solvent is shown in **Fig. 4.2**. AQ showed two reductions at potentials around -0.77 V and -1.3 V vs Ag, which are attributed to the AQ radical anion ($AQ^{\bullet-}$) and AQ dianion (AQ^{2-}) correspondingly. NOP is a viscous non-polar aprotic solvent; generally, in a neutral aprotic media, quinones undergo two-step reductions corresponding to $Q^{\bullet-}$ and Q^{2-} respectively [9].

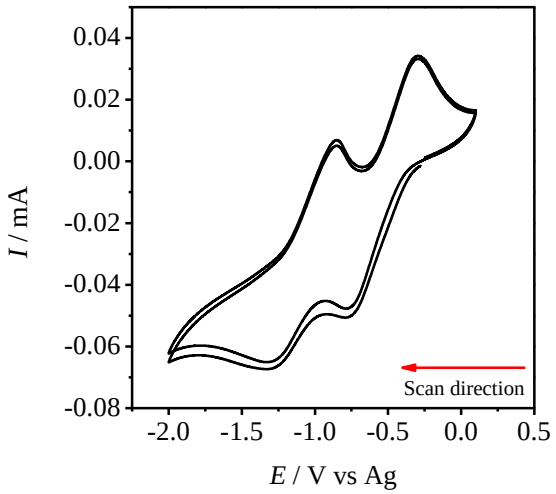

Figure 4.2 CVs at 20 mV s^{-1} of 10 mM AQ dissolved in NOP solvent with 0.1 M TBACl as the supporting electrolyte.

4.1.4 Electrochemistry of 1-aminoanthraquinone at GC|NOP|aqueous three-phase interface

Fig. 4.3a displays the CV cycles of 10 mM AQ at TPE configuration with 0.1 M TBACl solution. Continual CV cycles are stable; AQ exhibited a pair of redox peaks with a slight decrease in the peak current over multiple cycles. Quinones in an aqueous environment undergo a single-step two-electron reduction (i.e., from Q to Q^{2-}) [9,20,21]. Due to the presence of water at TPE configuration, AQ showed a single-step two-electron reduction to AQ^{2-} (**Fig. 4.3a**).

In three-phase junction CVs, the peak current remarkably depends on whether the reduced probe is escaped from organic to water or the counter ions transferred from aqueous to the organic phase. In the first case, current decreases with the continuous scan; in the latter instance, the current is stable with subsequent scans or enhances due to the migration of ions inside the droplet [22]. The stability of the peak current in CVs of **Fig 4.3a** shows that the reduced AQ^{2-} species do not escape to the aqueous phase; instead, it promotes the transfer of cation ions from water to NOP to maintain the electroneutrality in the NOP droplet. In these CV measurements, after the first cycle, the cathodic peak shifts in the direction of less negative potential and stabilises quickly. A similar kind of an initial peak shift has seen by F. Scholz et al. while oxidising DMFc at TPE configuration with 0.1 M KNO_3; the reason for this effect is unknown [22]. Nevertheless, it may be due to the decrease in the resistance of the organic droplet [23].

Subsequent SWVs of AQ at TPE configuration is presented in **Fig. 4.3b**. The peak potentials are unaffected, and the increase in peak current is mainly due to the increase in the concentration of TBA^+ ions inside the droplet. On the other hand, the preliminary peak shift witnessed in CV cycles did not affect the SWV peak potential.

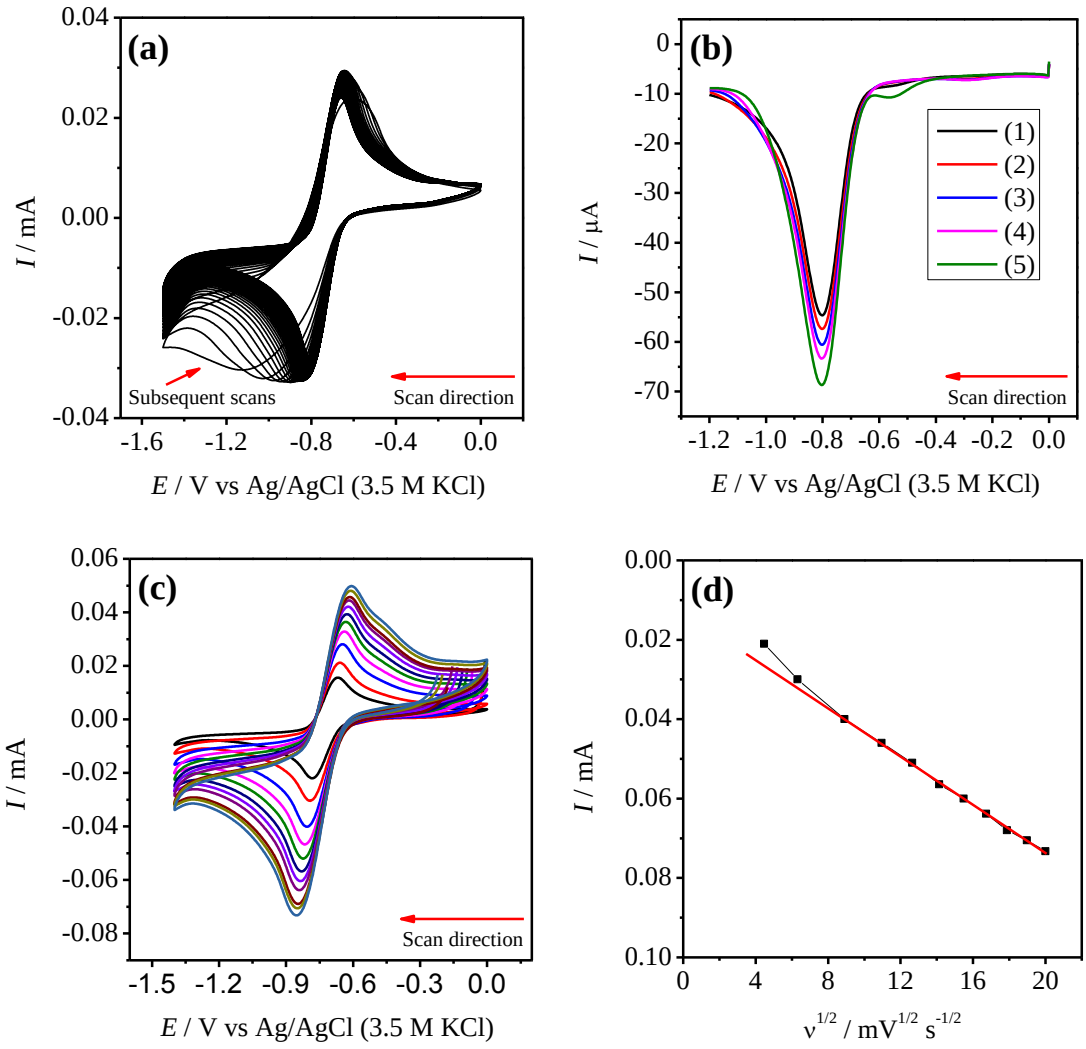

Figure 4.3 All measurements were performed at TPE configuration; the droplet of NOP containing 10 mM AQ was deposited on GC WE and dipped in 0.1 M TBACl. **(a)** Subsequent CVs (50 cycles) at 20 mV s^{-1}. **(b)** Successive SWVs. **(c)** CVs at different scan rates (20, 40, 80, 120, 160, 180, 240, 280, 320, 360, 400 mV s^{-1}). **(d)** The plot of cathodic peak current as a function of the square root of scan rates.

Fig. 4.3c shows the CVs of AQ measured at different scan rates (20 to 400 mV $s^{-1/2}$). As the scan rate increases, ΔE_p changes from 117 to 242 mV, and the ratio of cathodic to anodic peak areas are nearly one. The increase in the ΔE_p is probably because of the increase in ohmic drop [24].

Fig. 4.3d displays the plot of the cathodic peak current against the square root of scan rate. AQ derivatives are recognised to absorb on the electrode surfaces of GC and pyrolytic graphite [9,25–27]. However, the peak current is linear with the square root of a scan rate in **Fig. 4.3d**; which specifies that the AQ reduction is controlled by diffusion

of the AQ towards the three-phase junction. At low scan rates, the deviation from linearity is by the thinness of the organic phase; the large diffusion zone is obtained, and the droplet acts like a thin cell. Hence, shows a linear dependence of the scan rate (like adsorbed species) [28].

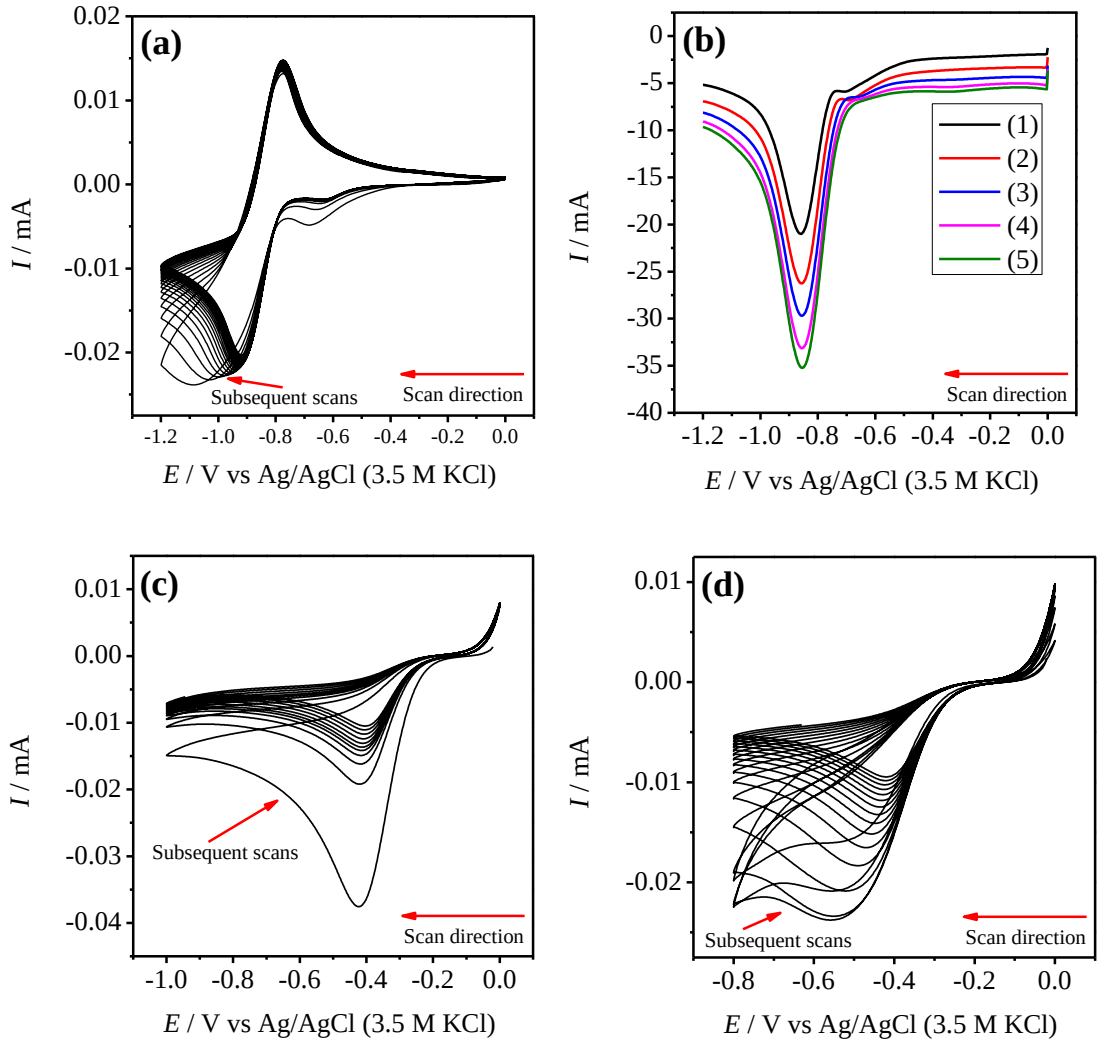

Figure 4.4 (a) Succeeding CVs (30 cycles at 20 mV s^{-1}) and **(b)** SWVs of NOP droplet containing 10 mM AQ is attached on GC and submerged in 0.1 M KCl solution. Consequent three-phase CV cycles (at 20 mV s^{-1}) of 10 mM AQ dissolved NOP droplet on GC in 0.1 M HCl **(c)** and 0.1 M TBACl in 0.1 M HCl **(d)**.

Fig. 4.4a and **4.4b** present the three-phase measurements of AQ containing NOP droplet on GC in 0.1 M KCl; to check the redox behaviour of AQ in an inorganic aqueous phase. The obtained results are similar to the case with TBACl (**Fig 4.3a** and **4.3b**). Nevertheless, when HCl is used as the aqueous solution, the CVs are entirely irreversible, and the current decreases rapidly with each successive scan (**Fig 4.4c**). Similar behaviour is seen with 0.1 M TBACl in 0.1 M HCl aqueous phase (**Fig 4.4d**). The cause for this is the fast hydrogenation of the O^{-} groups of the AQ and expulsion

to the aqueous solution. AQ is soluble in acidic aqueous solutions and polymerises at positive potentials [29].

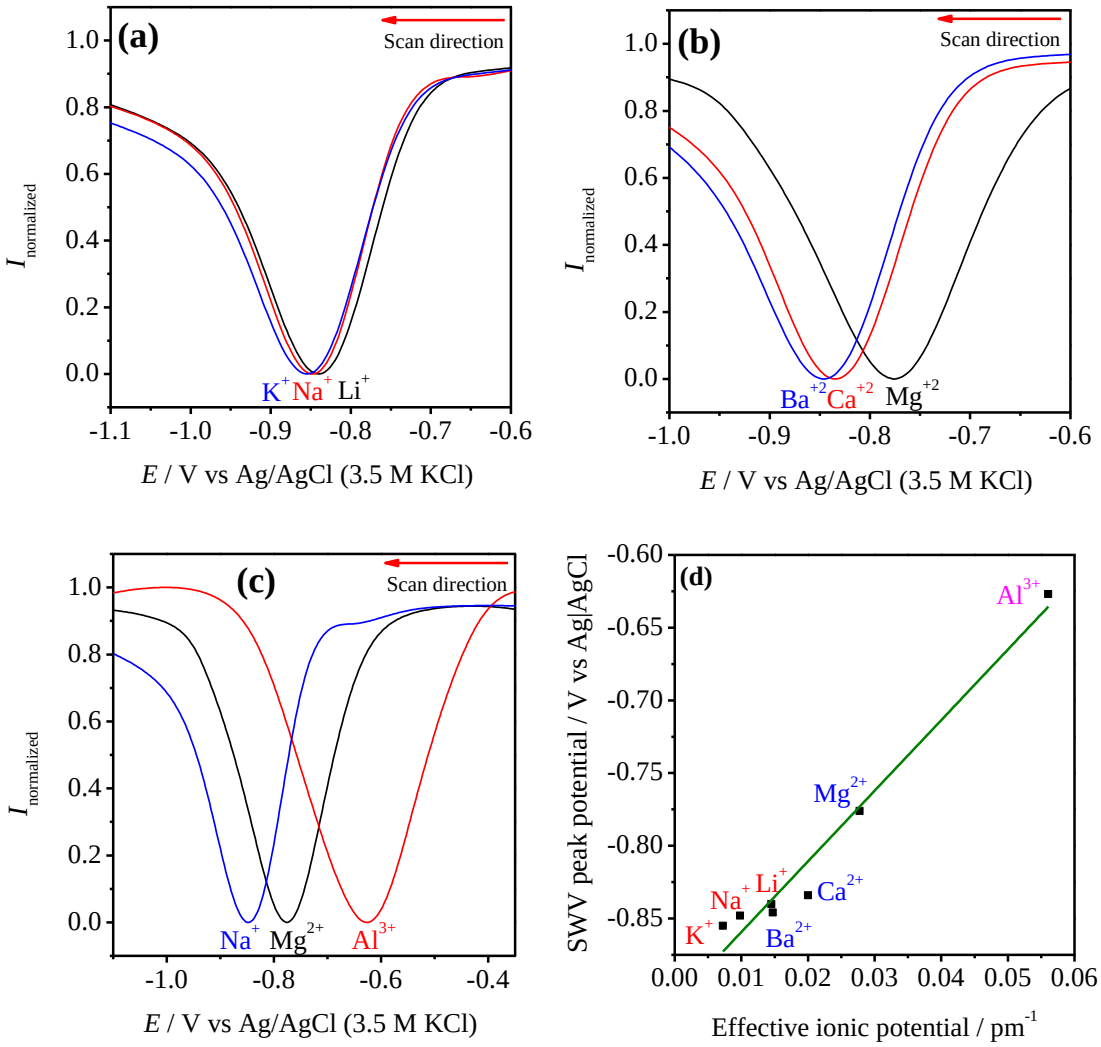

Figure 4.5 Normalized SWVs of 10 mM AQ dissolved in NOP droplets, attached on GC WE and submerged in different salt solutions; **(a)** cations of +1 charge, **(b)** cations of +2 charge, **(c)** comparison of mono-, di- and trivalent cations. **(d)** The plot of peak potential against the effective ionic potential.

In the case of cation transfer, the SWV peaks potentials are dependent on the lipophilicity of the cation and its concentration [24,30–32]. **Fig 4.5a–c** present the series of SWV measurements performed by immersing AQ containing NOP droplets in the inorganic salt solutions of different cations. The peak potential shift for monovalent cations are relatively small and the sequence vary as $K^+ > Na^+ > Li^+$ (**Fig. 4.5a**). For divalent cations, the potential shifts are noticeable in the order $Ba^{2+} > Ca^{2+} > Mg^{2+}$ as shown in **Fig. 4.5b**. The peak potential for trivalent Al^{3+} is even less negative compared to the Na^+ and Mg^{2+} ions (**Fig. 4.5c**). In these SWVs (**Fig 4.5 a–c**), the trend of AQ

reduction potentials do not follow the order of lipophilicity (Hofmeister series) (potential shift is not according to Eq. 1.24). Lipophilicity based cation transfer has seen with Fe(III)TPP-Cl, iodine, and LBPC redox probes [24,31,33]; where the transfer potential increase with the inverse of the ionic radius (as per the Born rule) [34].

In the case of AQ (**Fig 4.5 a−c**), the order of SWV peak shift shows a good dependency on the size and the charge of the aqueous cations; that is the ionic potential of the cations (Φ_{eff}). As discussed earlier, reduced quinones form ion pairs with the cations of the supporting electrolyte, hence the reduction potential depends on the supporting electrolyte [9]. In the case of alkali and alkaline earth ions, quinone reduction potential depends on the association constant between the quinone and the cation in pairing [35–37]. Hence the possible explanation for the peak shift in **Fig 4.5 a−c** is that AQ^{2-} forms an ion pair with the transferred cation in NOP droplet. Which is further evident by an excellent linear relationship between the ionic potential and the SWV reduction potential, as shown in **Fig. 4.5d**. Thus, the positive shift in the AQ reduction potential is seen for the cations with larger charge and smaller size in **Fig 4.5a−c**. The ion-pair formation has a significant impact on the transfer potential than the solvation of cation in the organic phase.

4.1.5 Electrochemistry of 2,3-dichloro-1,4-naphthoquinone in NOP

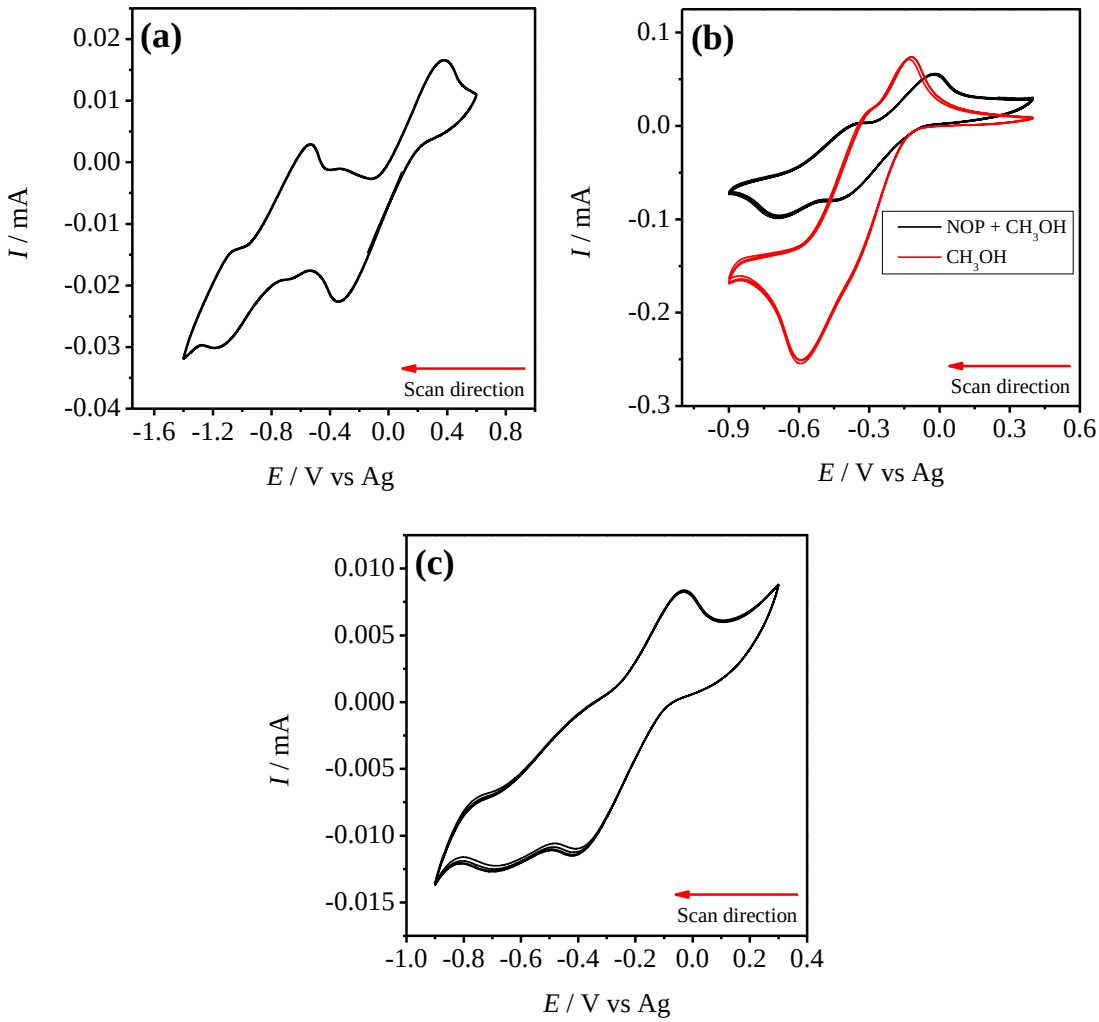

Figure 4.6 (a) CVs at 20 mV s^{-1} of 10 mM NQ in NOP with 0.1 M TBACl as supporting electrolyte. **(b)** CVs (at 20 mV s^{-1}) of 10 mM NQ in 50% NOP + 50% CH_3OH solution (black CVs) and in CH_3OH solution (red CVs); both contains 0.1 M TBACl supporting electrolyte. **(c)** CVs at 20 mV s^{-1} of 10 mM NQ in water-saturated NOP with 0.1 M TBACl supporting electrolyte.

CV of NQ in NOP (**Fig. 4.6a**) shows mainly two reduction steps; the first step is attributed to the formation of NQ radical anion ($NQ^{\bullet-}$) and the second step to the NQ dianion (NQ^{2-}). As presented in **Fig 4.6b** black CVs, even in the presence of a protonating agent (CH_3OH) in NOP or if NOP is saturated with water (**Fig 4.6 c**); still, NQ undergoes two-step two-electron reduction mechanism. The one-step two-electron reduction mechanism dominates only in pure CH_3OH solution (red CVs in **Fig 4.6 b**). Nevertheless, AQ shifts from two-step one-electron to one-step two-electron mechanism when a little MeOH is added to the NOP solvent.

4.1.6 Electrochemistry of 2,3-dichloro-1,4-naphthoquinone at GC|NOP|aqueous three-phase interface

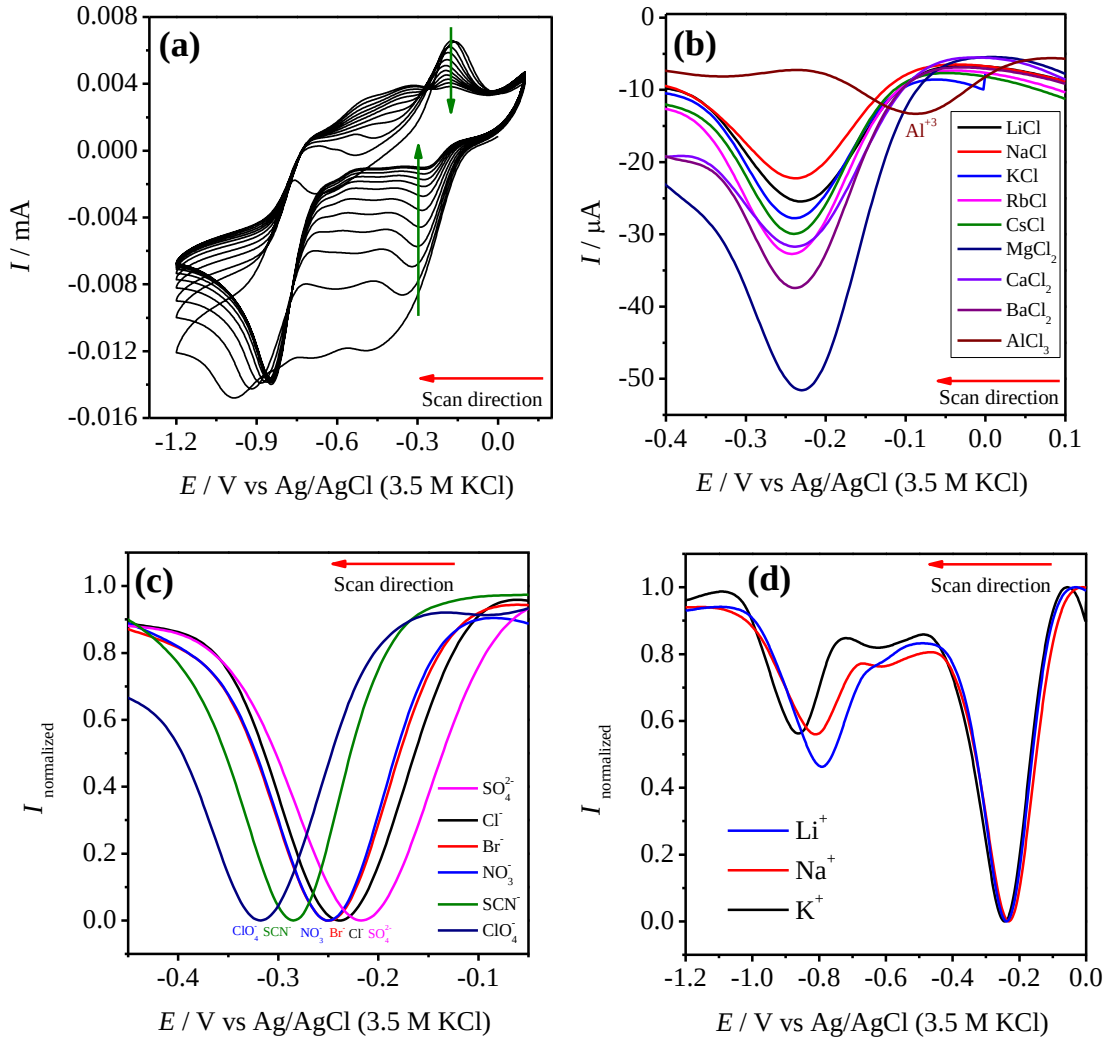

Figure 4.7 All measurements were performed at TPE configuration; 10 mM NQ was dissolved in the droplet of NOP, deposited on GC WE, and immersed in different electrolytes. **(a)** CVs at 20 mV s^{-1} of NQ droplet dipped in 0.1 M TBACl. **(b)** SWVs of NQ droplets in different cationic solutions. **(c)** Normalized SWVs of NQ droplets dipped in different anionic solutions. **(d)** SWVs of NQ at TPE configuration showing two reduction steps.

Three-phase subsequent CV cycles of NQ in 0.1 M TBACl (**Fig. 4.7a**) showed two pairs of redox peaks; in which the first set of peaks around -0.5 to -0.2 V vs Ag/AgCl are unstable, current decreases continuously and peaks vanish upon scanning. Whereas the second pair of redox peaks (around -0.85 V) become stable with continuous cycling. The first reduction is assigned to the formation of $NQ^{\bullet-}$ and the second reduction to the formation of NQ^{2-}. As discussed earlier, the decrease in the current of the three-phase CVs indicates the redox probe expulsion from organic to the aqueous phase. In **Fig. 4.7a**,

the steady decrease in the current of the first set of redox peaks (marked with green arrows in **Fig. 4.7a**) illustrates that $NQ^{\bullet-}$ is expelled from the NOP to the aqueous phase. But the stability of the second redox peaks specifies that NQ^{2-} is stable in the droplet. The ejection of $NQ^{\bullet-}$ should contribute to the decrease in the peak current of the second redox step (i.e., $NQ^{\bullet-} \rightarrow NQ^{2-}$). Hence, the stable second redox step is possibly due to the slow change of the two-step one-electron reduction mechanism to the one-step two-electron mechanism. This could be due to the increasing water content of NOP over time, feasibly by the formation of microemulsion at TPE configuration [38–40]. To explore this further, SWVs studies of both reductions were performed in electrolytes of different anions and cations.

Fig. 4.7b presentations the SWVs (showing only the first reduction peak) of NQ in the different cationic aqueous phase. Here the peak potential did not vary for the different cations (except for Al^{3+}), indicating NQ reduction is not dependent on aqueous cations. Instead, as shown in **Fig. 4.7c**, there is a clear dependence of the first reduction potential on the hydrophilicity of the aqueous anion. The peak potential shifts in the negative direction as the hydrophilicity of the anion decreases; the potential shift varies as $SO_4^{2-} < Cl^- < Br^- < NO_3^- < SCN^- < ClO_4^-$. This may be due to the salting out of the $NQ^{\bullet-}$ when it is expelled to the aqueous phases. Salting out phenomenon is well known for several molecules, which is similar to the salting out of proteins [41,42].

As stated earlier, $NQ^{\bullet-}$ species expulsion from NOP to water should decrease the current of the second reduction peak in three-phase junction CVs (**Fig. 4.7a**). Hence, $NQ^{\bullet-}$ species could be adsorbed at the NOP|aqueous interface [22], or locked in a micro-emulsion formed at the TPE configuration [38–40].

Fig. 4.7d displays the SWVs of both reductions of NQ in electrolytes of different cations with same anions (LiCl, NaCl, and KCl). The first reduction of all SWVs is at the same potential (-0.25 V vs Ag/AgCl) because anions are the same. While the second reduction potentials shift negatively based on the size of the cations in the order of $K^+ > Na^+ > Li^+$. All the results from **Fig. 4.7 a–d** specify that, during the first reduction, $NQ^{\bullet-}$ species escape from NOP droplet to aqueous phase and also adsorb at the NOP|water interface. In the second reduction, the NQ^{2-} forms a pair with the incoming cation in the NOP droplet.

However, to understand more about the $NQ^{\bullet-}$ expulsion at TPE, chronoamperometry (CA) was carried out at -0.5 V vs Ag/AgCl for 6 hours using Au wire WE running through the equal volumes of both the phases. The photograph of the cell after CA is given in **Fig. 4.8a**, where the aqueous phase is turbid. **Fig. 4.8b** shows the precipitation at the NOP|water interface.

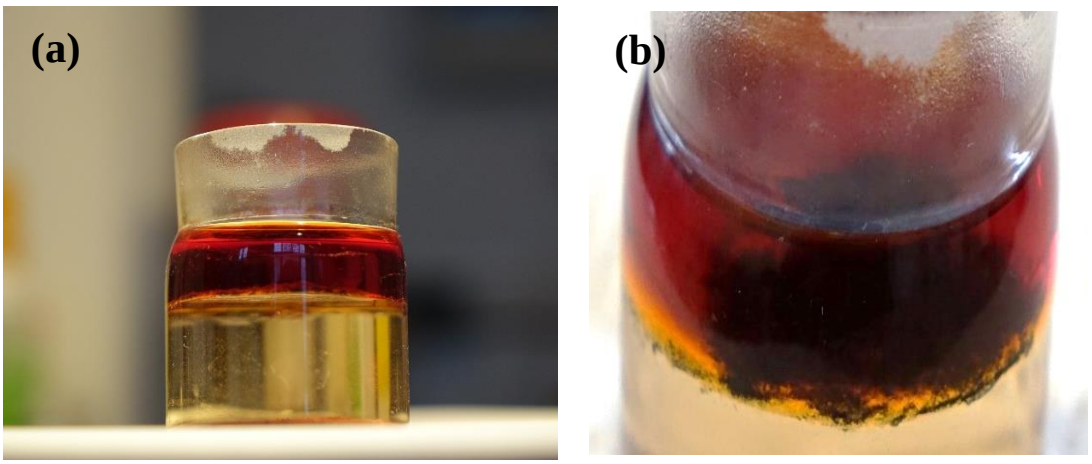

Figure 4.8 Photographs of the cell after CA measurement was performed at -0.5 V vs Ag/AgCl (3.5 M KCl) for 6 hours.

4.1.7 Conclusion

I investigated the electrochemistry AQ and NQ in NOP solvent and at GC|NOP|aqueous TPE configuration. Both quinones exhibited consecutive two-step one-electron reductions in NOP solvent. Due to the presence of the aqueous phase at TPE configuration, quinones reduction mechanism has changed from two-step one-electron to one-step two-electron. However, this change with AQ is immediate; for NQ, it is gradual. Hence, both behaved differently at the three-phase, which is presented in **Fig. 4.9**.

AQ showed a single-step two-electron reduction, which is accompanied by the cation transfer from water. During the reduction-driven cation transfer, AQ^{2-} stays stable in the NOP droplet. The cation transfer potential did not depend on the lipophilicity of the cation (not according to Eq. 1.24). Instead, it was determined by the ionic potential due to ion-pair formation between AQ^{2-} Cat^{2+} in the droplet.

NQ exhibited two reductions at TPE configuration; during the first reduction, $NQ^{\bullet-}$ species escape to the aqueous phase and also adsorb on the NOP|aqueous interface or collected in an emulsion. In the second reduction, NQ^{2-} species stay in the NOP droplet and is associated with the cations transfer from water to NOP.

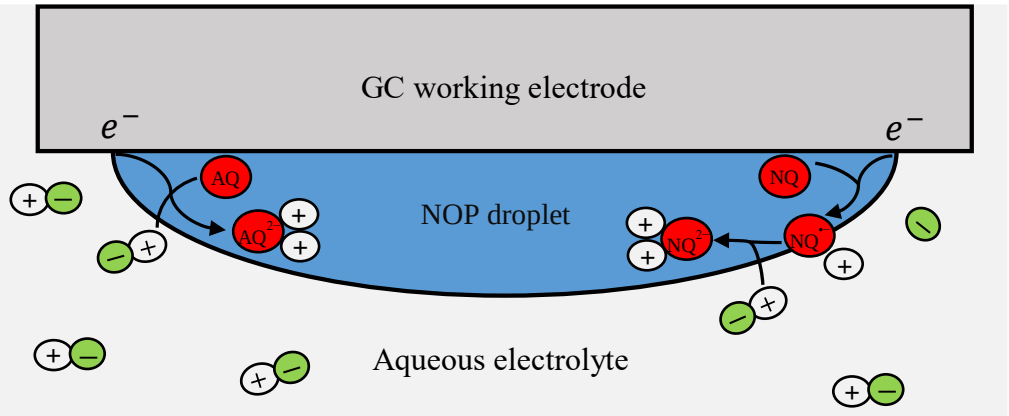

Figure 4.9 Redox behaviour of AQ and NQ at TPE configuration.

4.2 Three-phase electrochemistry of 7,7,8,8-tetracyanoquinodimethane at GC|n-octyl pyrrolidone|aqueous interface

In this work, I examined the use of TCNQ for cation transfer studies at the TPE configuration. TCNQ is a well-known organic redox probe, used in the investigations of heterogeneous electron and cation transfer across the immiscible organic|aqueous interfaces. In 2011, S. Wu and B. Su showed that TCNQ could be used for the alkylammonium cations transfer studies at carbon ink screen-printed electrode|NPOE|aqueous three-phase interface [43]. Hence, I wanted to investigate TCNQ for inorganic cation transfer at GC|NOP|water three-phase interface.

4.2.1 Introduction and importance of TCNQ electrochemistry

TCNQ is an organic electroactive molecule insoluble in water. In polar solvents such as CH_3CN and DCE, it shows a reversible one-electron two-step reductions to form the radical anion ($TCNQ^{\bullet-}$) initially and then to the dianion ($TCNQ^{2-}$) (**Fig. 4.10)** [43–49].

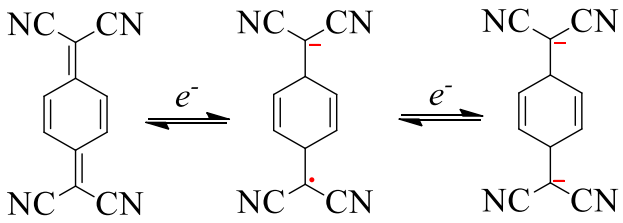

Figure 4.10 Molecular structures of TCNQ, $TCNQ^{\bullet-}$ and $TCNQ^{2-}$ respectively.

Electrochemical reduction of TCNQ in organic solvents with different transition metal electrolytes is the conventional method to synthesis metal-TCNQ complexes [49,50]. Both $TCNQ^{\bullet-}$ and $TCNQ^{2-}$ are excellent ligands for the synthesis of metal-TCNQ based semiconducting coordination polymers and metalorganic complexes [51]. These highly conductive charge-transfer complexes found applications in catalysis, data storage, sensing, photocatalytic degradation of organic dyes, and electron transfer reactions [51,52].

In CH_3CN, TCNQ undergoes a diffusion-controlled two-step one-electron reduction; the diffusion coefficients of $TCNQ^{\bullet-}$ and $TCNQ^{2-}$ are 1.7 and 1.2 $cm^2\ s^{-1}$, respectively [47]. $TCNQ^{2-}$ is not stable in the presence of oxygen; it decomposes to form dicyano-p-toluoylcyanide [47,53,54]; however, $TCNQ^{\bullet-}$ is relatively stable under ambient condition [51]. In the case of electrochemical reduction of 2,3,5,6-tetrafluoro-7,7,8,8-tetracyanoquinodimethane ($TCNQF_4$) in CH_3CN, it is feasible to have an air-stable $TCNQF_4^{2-}$ dianion [55].

The effect of acid on the electrochemical reduction of TCNQ, the stability of both $TCNQ^{\bullet-}$ and $TCNQ^{2-}$ in acidic conditions, and the kinetics protonation of $TCNQ^{\bullet-}$ to $HTCNQ^{\bullet}$ are well examined in many solvent systems by Yamagishi and co-workers [56–

58]. Regardless of aerial oxidation of $TCNQ^{2-}$, the protonation of $TCNQ^{2-}$ is possible in the presence of appropriate metal cations to get the air-stable H_2TCNQ [59,60].

In CH_3CN and DMSO, the ion formation between electrochemically generated $TCNQ^{2-}$ with different cations (mono- and divalent) are well studied [61–63]. It appeared that divalent cations (Ba^{2+} and Mg^{2+}) presented stronger interactions than monovalent cations such as Na^{+}[63].

Electron transfer rates across the organic|aqueous interface have measured by using TCNQ in the organic phase with aqueous ferrocene or tris(2,2-bipyridyl)-dichlororuthenium (III) [64,65]. It was found that the electron transfer was accompanied by the transfer of anions from the aqueous phase in the DCE|water system. In NB|water system, electron transfer was accompanied by the expulsion of the $TCNQ^{\bullet-}$ [65].

4.2.2 Electrochemistry of TCNQ in NOP solvent

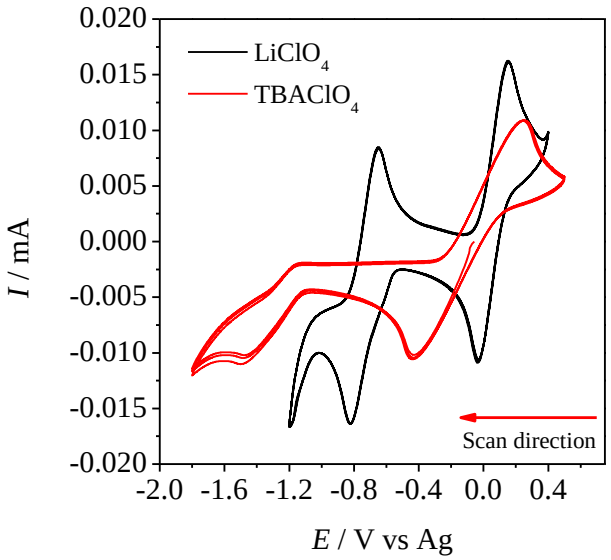

Figure 4.11 CV cycles (at 50 mV s^{-1}) of 10 mM TCNQ in NOP with 0.1 M $TBAClO_4$ (red) or $LiClO_4$ (black) as supporting electrolyte.

The CV measurements of TCNQ in NOP with different supporting electrolytes are shown in **Fig. 4.11**. Two subsequent one-electron reductions of TCNQ corresponding to the $TCNQ^{\bullet-}$ and $TCNQ^{2-}$ were observed. These results are in consistence with the previous reports, where the CVs were measured in DCE [46], NPOE [43] and CH_3CN [43–49]. However, TCNQ successive reductions in DCE and CH_3CN are electrochemically reversible and diffusion-controlled. In the case of NOP, which is viscus and non-polar solvent, the redox behaviour is affected by the supporting electrolyte (**Fig. 4.11**). Both reductions with $LiClO_4$ (black CVs) are reversible; whereas,

with $TBAClO_4$ (red CVs), the second reduction peak is not well-developed. This may be due to weak ion-pair interaction between $TCNQ^{2-}$ and TBA^+ in viscous NOP.

4.2.3 Electrochemistry of TCNQ at GC|NOP|aqueous interface

Fig. 4.12a−e show the results of successive CV cycles (of different potential range) of TCNQ dissolved NOP droplets in different electrolytes. In these CVs, the electrochemical reduction of TCNQ disturbs the charge neutrality of the NOP droplet; which leads to either the transfer of the cations from water to NOP or the ejection of reduced TCNQ anions from NOP to the aqueous phase.

Fig. 4.12a and **b** display the first two consecutive reductions of TCNQ at TPE configuration with 0.1 M KNO_3 (hydrophilic K^+ cation) and TBACl (hydrophobic TBA^+ cation) respectively. The two reductions correspond to TCNQ → $TCNQ^{\bullet-}$ and $TCNQ^{\bullet-}$ → $TCNQ^{2-}$ are seen. The remarkable decrease in the peak currents (indicated by red arrows) in both CVs specifies the ejection of the reduced probe during CV cycles (Eq. 4.4). This could be the result of an increase in the solubility of TCNQ due to the salt formation between reduced TCNQ anions and aqueous cations at the three-phase junction. When CVs measured at 2 mVs^{-1} (**Fig. 4.12c**), the faster decrease in peak currents was seen because ions have more time to diffuse away from the three-phase junction to the aqueous phase. Also, when CVs performed until the first reduction (**Fig. 4.12d**), the escape of $TCNQ^{\bullet-}$ is seen.

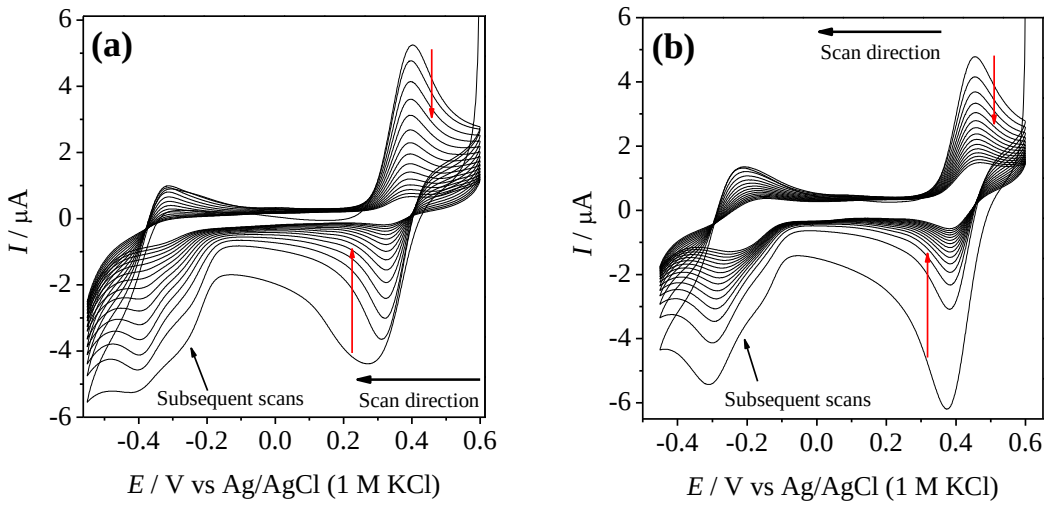

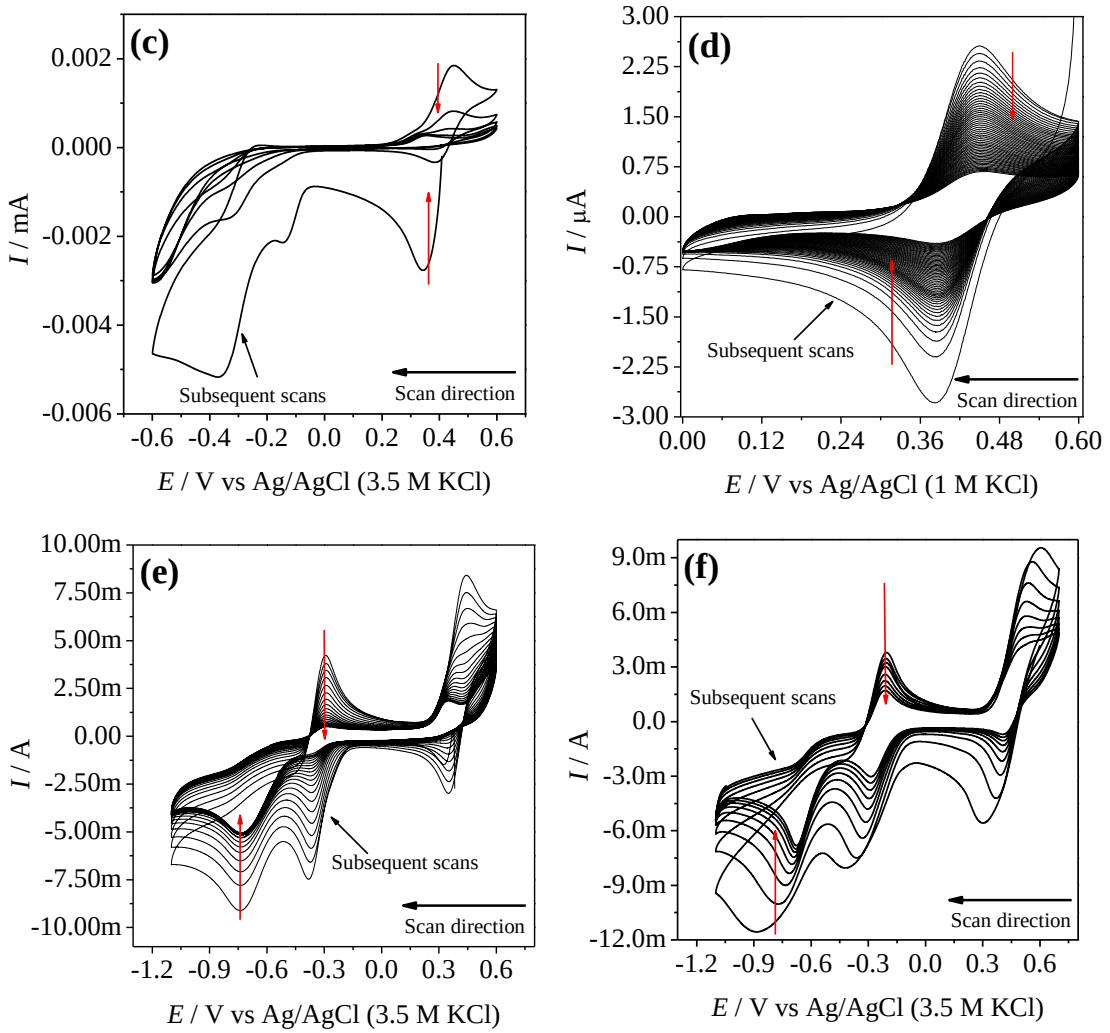

Figure 4.12 Consecutive CVs performed at TPE configuration; 10 mM TCNQ was dissolved in NOP dropplets, deposited on GC and immersed in different electrolytes. **(a)** CVs (20 mVs^{-1}) in 0.1 M KNO_3, (**b)** CVs (20 mVs^{-1}) in 0.1 M TBACl, **(c)** CVs (2 mVs^{-1}) in 0.1 M TBACl, and **(d)** CVs (20 mVs^{-1}) showing only first reduction in 0.1 M TBACl. CVs (20 mVs^{-1}) showing all three reductions in 0.1 M KNO_3 **(e)** and 0.1 M TBACl **(f)**.

$$TCNQ_{(org)} + Cat^{+}_{(aq)} + e^{-} \leftrightharpoons TCNQ^{-}_{(aq)} + An^{-}_{(aq)} \qquad 4.4$$

Fig. 4.12e and **f** show the three-phase CVs of TCNQ scanned to the more negative potential in electrolytes of hydrophilic (K^+) and hydrophobic (TBA^+) cations. Both CVs show the third irreversible reduction peak, while the first two reductions are for the reduction of TCNQ to $TCNQ^{\bullet-}$ and $TCNQ^{2-}$ accordingly. The third reduction could be the reduction of dicyano-p-toluoylcyanide. Because of the presence of oxygen and water at the three-phase junction, $TCNQ^{2-}$ could decompose to form dicyano-p-toluoylcyanide [53,54].

Another possibility of the third reduction may be the reduction of the protonated TCNQ (HTCNQ$^-$ and H_2TCNQ), but this is doubtful. The protonation of TCNQ^{2-} will lead to either electrochemically active HTCNQ$^-$ or the electro inactive H_2TCNQ. However, protonation is challenging to happen at the three-phase condition before TCNQ^{2-} decomposes to dicyano-p-toluoylcyanide. Only in dry box condition, TCNQ^{2-} protonation happens, which leads to the electroactive HTCNQ$^-$. But, the reduction potential of HTCNQ$^-$ is at more positive; means HTCNQ$^-$ reduction happens before the reduction of TCNQ^{2-} [47].

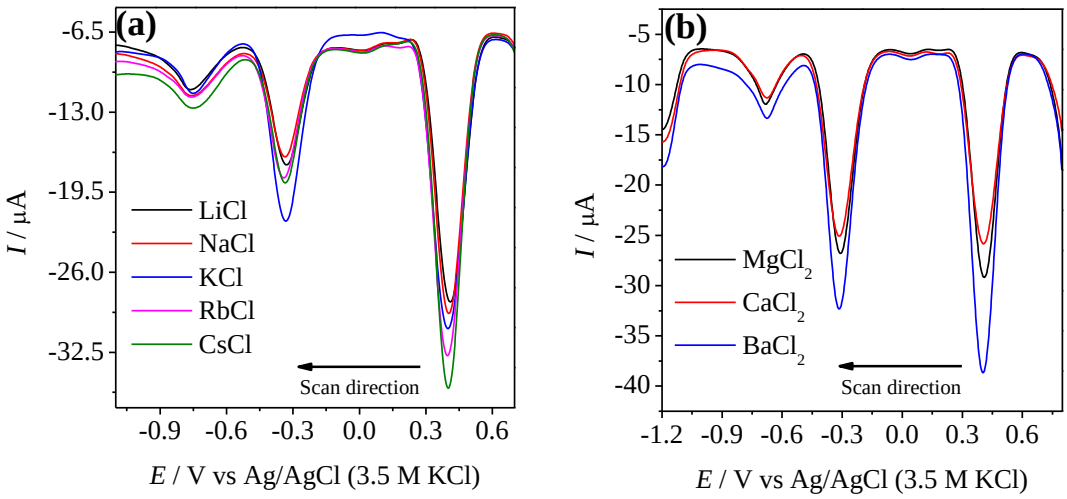

Figure 4.13 Three-phase junction SWVs of 10 mM TCNQ dissolved in NOP droplets, attached to GC and dipped in 0.1 M electrolytes of different inorganic cations.

Fig. 4.13a and **b** show the TPE SWVs of TCNQ in inorganic salt solution of different cations. Neither of the three reduction potentials did change significantly for the cation of +1 (**Fig. 4.13a)** and +2 charge (**Fig. 4.13b)**. If the TCNQ reduction is associated with cation transfer, then SWV peak potentials should shift more negative for hydrophilic cations ($Li^+ > Na^+ > K^+$) [24,31].

Moreover, TCNQ reduction in CH_3CN leads to the ion-pair formation of TCNQ^{2-} with cations of supporting electrolytes (Ba^{2+} and Mg^{2+}) [63]. As explained previously with the AQ, TPE reduction of AQ is associated with the transfer of cation from water to NOP due to the ion-pair formation between the reduced AQ and aqueous cation in NOP. In such ion transfer, the SWV reduction potentials vary with the ionic potentials of the cations instead of their hydrophilicity. In the instance of TCNQ, this behaviour is absent, as shown in **Fig. 4.13b**, which specifies no cation transfer to NOP.

On the contrary, the peak potentials (first reduction) shift negatively with the increase in the hydrophobicity of the aqueous anion **(Fig. 4.14a)**; in the order of SO_4^{2-} < Cl^- < Br^- < NO_3^- < SCN^- < ClO_4^- < PF_6^-. This is because of the salting-out effect during TCNQ$^{\bullet-}$ escape from NOP to water. This result is similar to the salting-out effect of NQ$^{\bullet-}$ at TPE configuration (previously explained). Additionally, salts of TCNQ$^{\bullet-}$ with tetraalkylammonium ions, alkali, and alkaline earth metals can form effortlessly at room

temperature when $TCNQ^{\bullet-}$ interacts with certain metals or metal iodides and alkyl-substituted ammonium [66,67].

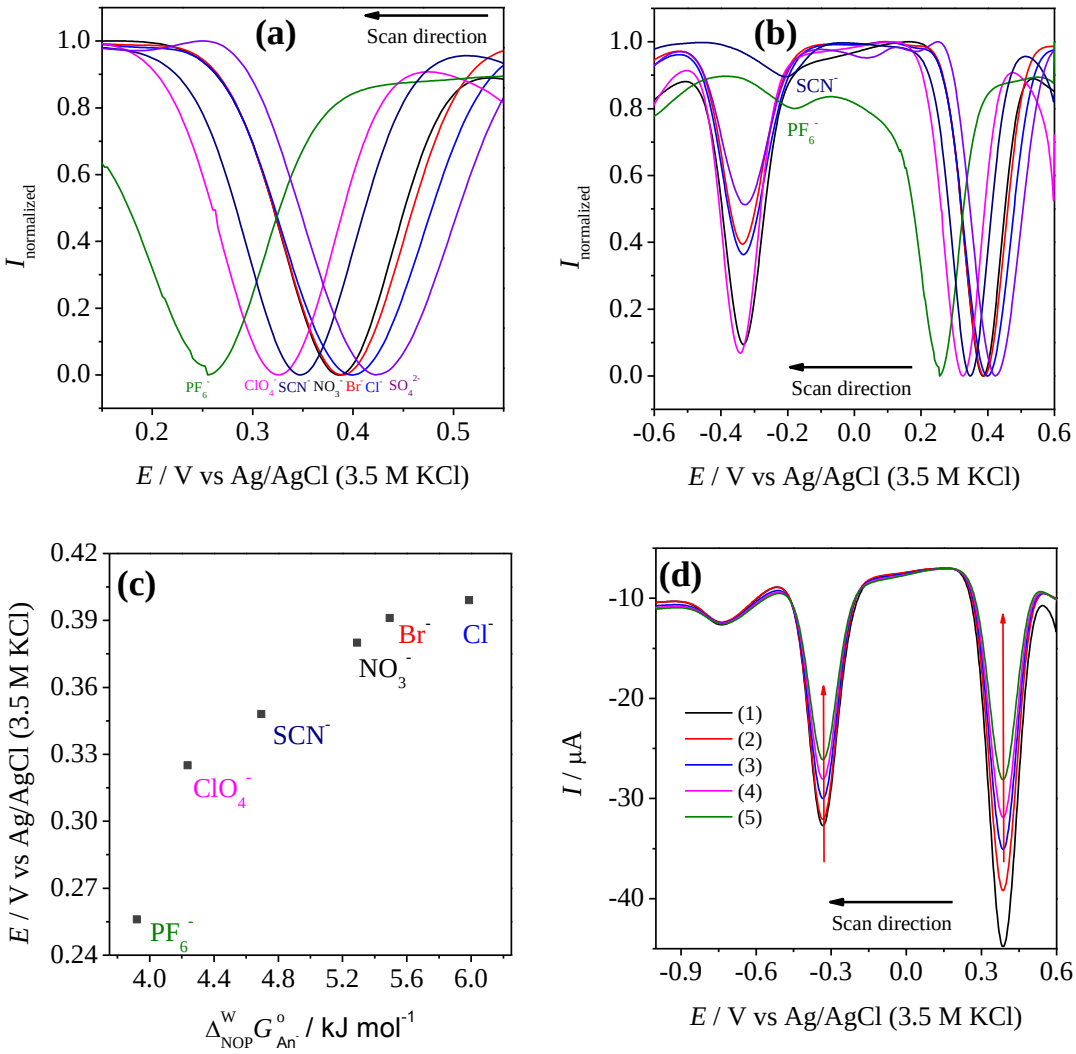

Figure 4.14 TPE SWVs TCNQ in electrolytes of different anions − **(a)** showing only the first reduction and **(b)** showing the first two consecutive reductions. **(c)** Gibbs energy of transfer between water and NOP vs the TCNQ reduction peak potentials. **(d)** Successive SWVs of TCNQ in 0.1 M KNO_3.

The second reduction potential is not affected by the type of aqueous anion **(Fig. 4.14b)**. Because in the first reduction, $TCNQ^{\bullet-}$ has already transferred to the aqueous phase; further reduction happens in water, and hence is not accompanied by ion transfer. With the large PF_6^- and SCN^- anions, the second reduction happens at less negative potential compared with other anions; the reason for this behaviour is not apparent.

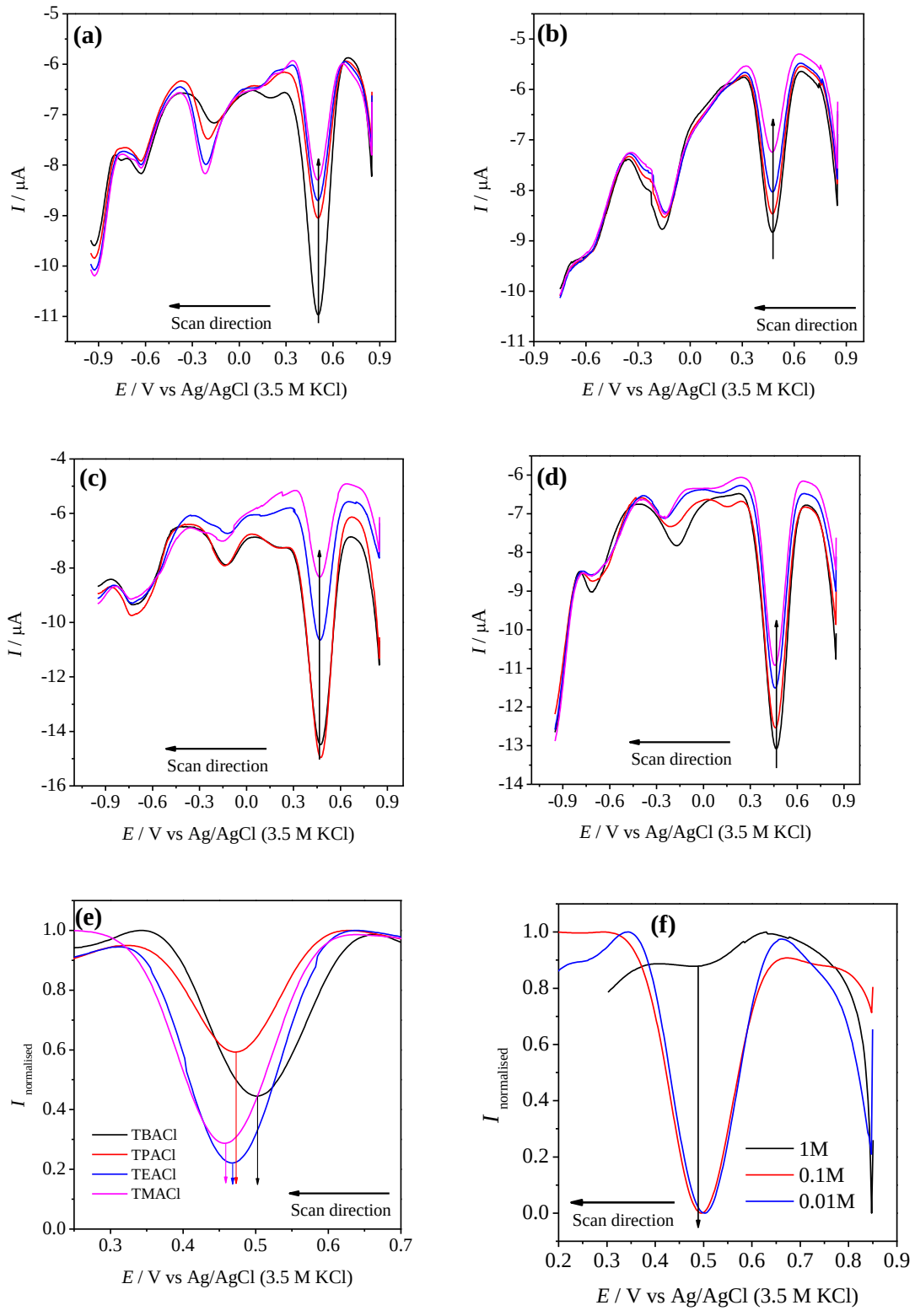

Figure 4.15 Consecutive SWVs of the NOP droplets (contain 10 mM TCNQ) attached to GC and immersed in 0.01 M TBACl **(a)**, TPACl **(b)**, TEACl **(c)**, and TMACl **(d)** solutions. **(e)** Comparison of TPE SWVs of first reduction potentials. **(f)** Concentration studies; SWVs of 10 mM TCNQ containing NOP droplets on GC in 0.01 M TBACl (blue), 0.1 M TBACl (red) and 1 M TBACl (black).

Even though the first reduction potential shift follows the hydrophobicity of the anion (according to the Eq. 1.23); there is no linear relationship between reduction potential vs Gibbs energy of transfer between water and NOP (**Fig. 4.14c**). A set of successive SWVs recorded for the same droplet is given in **Fig. 4.14d**; the peak current decrease (marked with red arrows) during each continual scans specifies the expulsion of reduced TCNQ anions.

Fig. 4.15a−d show the successive SWVs of TCNQ containing NOP droplets on GC in solutions of different tetralkylammonium cations. In all the cases, the peak potential of the first reduction did not change, but the peak current decrease with each subsequent scan. These results are similar in comparison to inorganic cations. However, the peak potential of the second reduction is not stable during successive scans; the reason for this behaviour is unknown. **Fig. 4.15e** shows the comparison SWVs of the first reduction with different tetralkylammonium salts; the peak shift is insignificant and varies according to the lipophilicity of cations (TBA^+ < TPA^+ < TEA^+ < TMA^+). Nevertheless, peak potentials (first reduction) are independent on the concentration of the TBA cation (**Fig. 4.15f**); which supports the postulate of $TCNQ^{\bullet-}$ anion expulsion over the cation transfer. The effect of concentration on the second and third reduction potentials is non-linear.

All the results discussed so far were from the measurements performed using NOP as an organic phase in three-phase experiments. S. Wu et al. showed the transfer of alkylammonium cations by using TCNQ at carbon ink screen-printed electrode|NPOE|aqueous three-phase interface [43]; in this work, they used the NPOE organic phase. Hence I too investigated TCNQ electrochemistry using NPOE as the organic phase at GC|NPOE|aqueous interface, and results are shown in **Fig. 4.16** and **4.17**. At GC|NPOE|aqueous interface, TCNQ showed two reductions; where the second reduction is irreversible and current decreases with each cycle (**Fig. 4.16a)**. The current decrease is still observable even for the CV cycles of the shortened potential range (**Fig. 4.16b**), which specifies the escape of the reduced $TCNQ^{\bullet-}$ from NPOE droplet to water during scans. Besides, the decrease in peak current was seen in the subsequent SWVs measurements of TCNQ droplet in 0.1 M TBACl (**Fig. 4.17a**). Furthermore, I performed the SWVs of TCNQ in the aqueous solution of different alkylammonium cations (**Fig. 4.17b**). I did not observe the distinct peak shift for TMA^+, TEA^+, and TPA^+ cations; however, TBA^+ showed a slight positive shift in the TCNQ reduction potential.

My results are in contrast to the results published by S. Wu et al. [43]. The reason may be that the use of the screen-printed electrode in their measurements can stop the expulsion of $TCNQ^{\bullet-}$. However, TCNQ is not sufficiently lipophilic for TPE cation transfer studies using GC electrode.

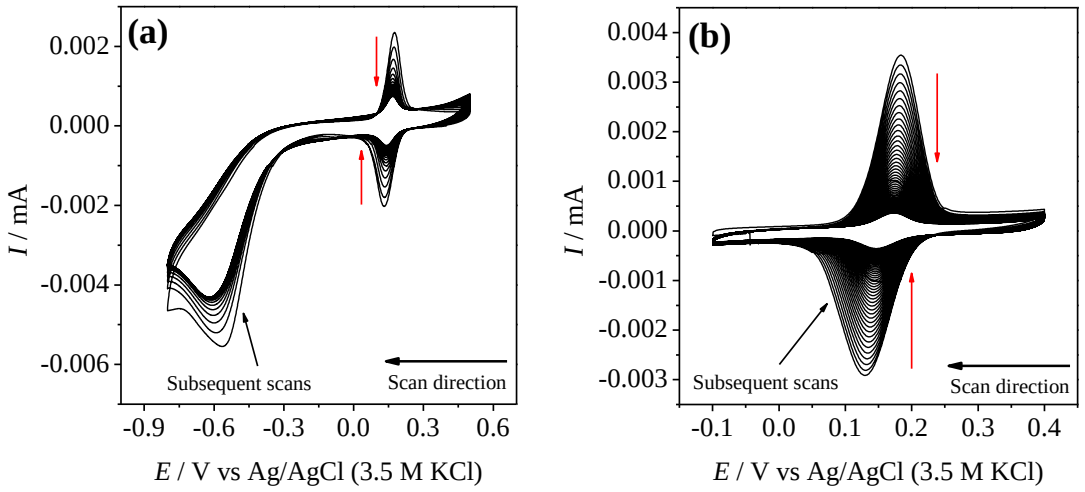

Figure 4.16 Successive CV cycles (at 20 mVs^{-1}) of 10 mM TCNQ dissolved in NPOE droplet, attached to GC, and submerged in 0.1 M TBACl. **(a)** Showing both reductions of TCNQ. **(b)** Showing only the first reduction.

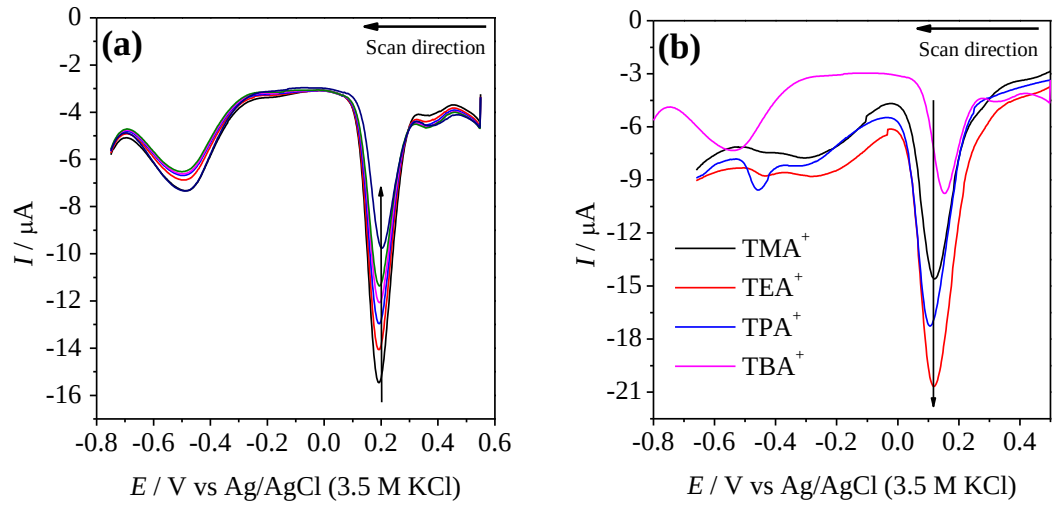

Figure 4.17 (a) Successive SWVs of 10 mM TCNQ dissolved in NPOE droplet, attached to GC, and submerged in 0.1 M TBACl. **(b)** TPE SWVs TCNQ in electrolytes of different alkylammonium cations.

4.2.4 Conclusions

Cation transfer studies at TPE configuration is mainly limited by the lack of sufficiently lipophilic redox probe; hence, a few molecules such as [Fe(III)TPP-Cl] [24], LBPC [31] and 2,2-diphenyl-1-picrylhydrazyl [68] have been used so far.

Due to the promising results published by Wu and Su [43], I investigated the cation transfer studies at GC|NOP|aqueous and GC|NPOE|aqueous configurations. My results clearly show that the reduced TCNQ anions ($TCNQ^{\bullet -}$ and $TCNQ^{2-}$) do not stay in the organic phase (**Fig. 4.18)**, because in all the three-phase CVs and SWVs, the current decreases with each consecutive scan. Also, the SWV reduction potential did not vary with cations but shown dependency on the anion hydrophobicity; which further confirms the escape of $TCNQ^{\bullet -}$ species. In the case of organic cations transfer; SWV reduction potential showed inconsiderable dependency on the concentration and lipophilicity. In conclusion, TCNQ is not a reliable redox probe for three-phase junction cation transfer experiments.

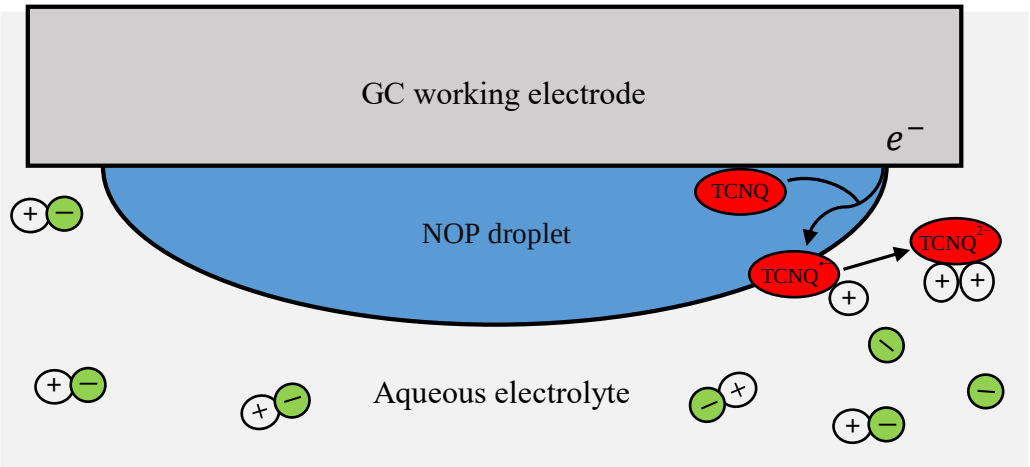

Figure 4.18 Redox behaviour of TCNQ at GC|NOP|aqueous TPE configuration.

4.3 Three-phase electrochemistry of a lipophilic neutral heteroleptic bis(tridentate) ruthenium(II) complex $[Ru^{II}(LR)(L)]^0$ at GC|NB|aqueous interface

As explained in the previous chapters, the essential properties of the redox probe used for TPE anion transfer studies are; 1) the compound has to be neutral and sufficiently lipophilic to avoid the expulsion of the oxidised redox probe from the organic phase to water; 2) compound has to oxidise at the three-phase junction (lower oxidation potential) before the water oxidation takes place at the WE|aqueous interface. Most of the highly lipophilic electroactive compounds don not qualify the second requirement; hence, a few compounds such as DMFc [22,69,70] and TPP-metal complexes (Mn, Fe, and Co) are used for anion transfer studies [71]. However, Opałło and co-workers from our institute showed that the oxidised DMFc expulsion to water is possible with hydrophilic Cl^- anions [72]. In the case of TPP-metal complexes; transferred nucleophilic anions (F^- and SCN^-) can coordinate to the TPP-metal complexes in the organic phase [71,73]. Hence, a new, highly lipophilic non-interacting redox probe is required.

In collaboration with Prof. Masa-aki Haga (department of applied chemistry, Chuo University, Japan), we synthesised a mononuclear ruthenium(II) complex $[Ru^{II}(LR)(L)]^0$ with two tridentate ligands of 2,6-bis(1-(2-octyldodecan)benzimidazol-2-yl)pyridine (LR) and 2,6-bis(benzimidazol-2-yl)pyridine (L). This complex was characterised by using nuclear magnetic resonance spectroscopy, electrospray ionisation and matrix-assisted laser desorption mass spectrometry, UV-VIS spectroscopy and X-ray photoelectron spectroscopy. All the molecular characterisations and structural elucidation were done by M. Haga and group. I did the synthesis and electrochemistry of this complex in NB (single-phase) and at GC|NB|aqueous three-phase interface for anion transfer studies.

4.3.1 Electrochemistry of $[Ru^{II}(LR)(L)]^0$ complex dissolved in NB

CVs of $[Ru^{II}(LR)(L)]^0$ complex in NB are shown in **Fig. 4.19a**; the black CV cycles were scanned to anodic direction from -0.95 V vs $Ag/AgNO_3$ to +0.6 V, and the red ones were scanned to higher potential, i.e., up to 0.95 V vs $Ag/AgNO_3$. In short-range CVs (black CVs), a reversible metal-based $Ru^{II/III}$ redox peak was witnessed at a mid-peak potential of -0.095 V vs $Ag/AgNO_3$. The ratio of I_{pa} to I_{pc} is close to 1, and ΔE_p is 90 mV. This complex exhibited oxidation at lower potential (-0.095 V vs $Ag/AgNO_3$) compared to $[Ru(LR)(LH_2)]^{2+}$ type, due to the deprotonation at N-H sites of L ligand, since metal-based $Ru^{II/III}$ redox potential can be modified by the use of different auxiliary ligands [74]. In the case of $[Ru^{II}(LR)(L)]^0$ complex, the benzimidazolyl based tridentate ligand (L) has π-donor imidazole nitrogen and π-acceptor pyridine nitrogen. Ru coordination to the benzimidazole unit increases the acidity of imino N-H protons and easy to deprotonate. This kind of deprotonation has a considerable effect on the redox behaviour of Ru [75,76]. Haga and co-workers synthesised such deprotonated Ru complexes and studied their electrochemical properties [77]. CVs scanned to a higher potential (red CVs in **Fig. 4.19a)** exhibited an irreversible second redox peak with the

gradual diminishing of the first redox peak ($Ru^{II/III}$). This could be the irreversible oxidation of the tridentate ligand.

The scan rate studies and the plot of peak current as a function of the square root of the scan rate are presented in **Fig. 4.19b** and **4.19c**, respectively. The linear relationship of the peak currents to the square root of the scan rates shows that the $Ru^{II/III}$ redox reaction is diffusion-controlled; follows the Randles-Sevcik equation, and this complex does not adsorb on the GC surface.

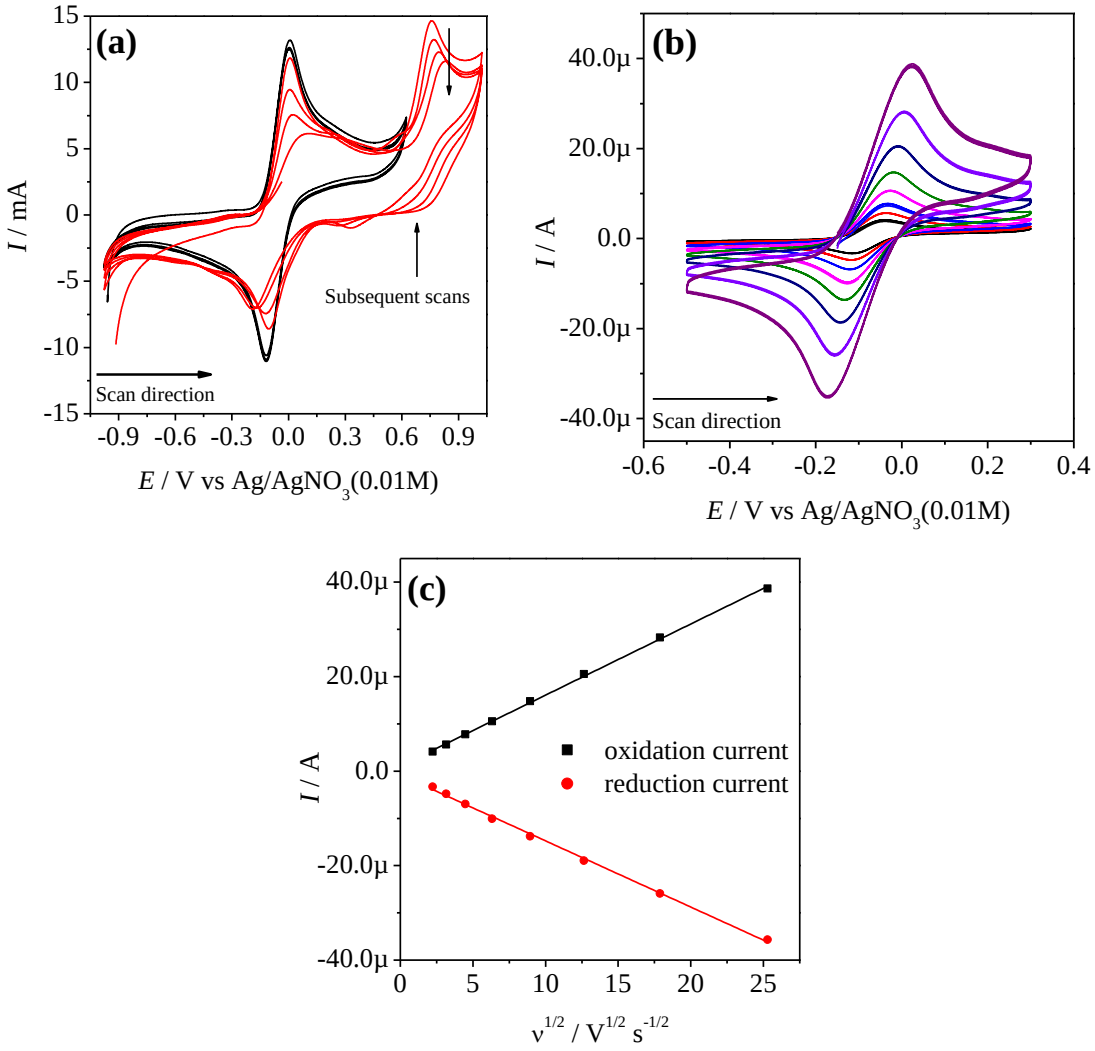

Figure 4.19 (a) CV cycles (at 50 mV s^{-1}) and **(b)** scan rate studies (5, 10, 20, 40, 80, 160, 320 and 640 mVs^{-1}) of 10 mM $[Ru^{II}(LR)(L)]^0$ complex dissolved in NB with 0.1 M TBACl supporting electrolyte. **(c)** The plot of peak current versus the square root of the scan rate (both red and black lines are the linear fit of the data).

4.3.2 Three-phase electrochemistry of $[Ru^{II}(LR)(L)]^0$ at GC|NB|aqueous interface

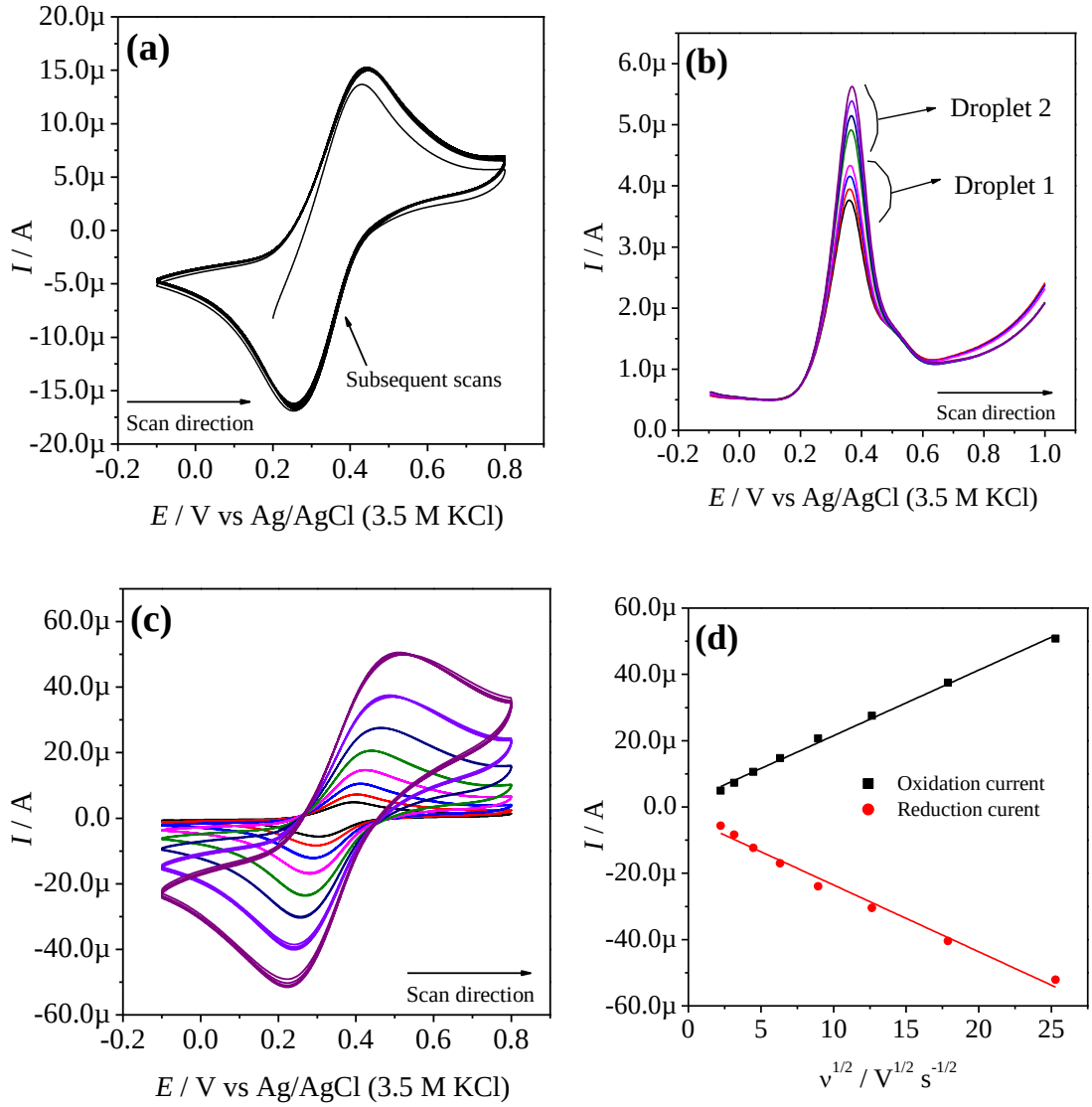

Figure 4.20 Three-phase junction electrochemistry of 10 mM $[Ru^{II}(LR)(L)]^0$ complex dissolved in NB droplet (2 µL), deposited on GC electrode and immersed in 0.1 M KNO_3 solution. **(a)** Consecutive CV cycles at 50 mVs^{-1}). **(b)** Successive SWVs. **(c)** Scan rate studies at 5, 10, 20, 40, 80, 160, 320 and 640 mVs^{-1}. **(d)** Plot for the peak current versus the square root of the scan rate (the red and black lines are the linear fit of the data).

The three-phase junction multiple CV cycles of 10 mM $[Ru^{II}(LR)(L)]^0$ complex is shown in **Fig. 4.20a**. The complex displayed stable and reversible $Ru^{II/III}$ redox process. CV cycles are completely reproducible with almost equal areas of anodic and cathodic peaks. The peak current and potentials are unaffected even after 50 consecutive CV cycles; specifying the excellent stability of the $[Ru^{II}(LR)(L)]^0$ complex and no escape of oxidised $[Ru^{III}(LR)(L)]^+$ species from the NB to the aqueous solution.

Two sets of successive SWVs recorded using two different droplets (**Fig. 4.20b)** show that the peak potentials are unaffected (0.362V vs Ag/AgCl). Besides, peak current increase with subsequent scans and potentials are unaffected with the increasing rest time of NB droplet in the aqueous phase. This indicates that the concentration of aqueous anion increases in NB droplet during scans, and the droplet becomes more conductive.

Fig. 4.20c shows the CVs at different scan rates ranging from 5 to 640 mVs^{-1}; as the scan rate increases, ΔE_p increases from 90 to 270 mV due to the increase in the ohmic drop in the droplet. The plot for peak current versus the square root of the scan rate is presented in **Fig. 4.20d**. Both I_{pa} and I_{pc} depend linearly on the square root of the scan rate; indicating that the redox process is under semi-infinite diffusion control (follows the Randles-Sevick equation).

In the NB microdroplet, oxidation of $[Ru^{II}(LR)(L)]^0$ to $[Ru^{III}(LR)(L)]^+$ drives the transport of an anion from the aqueous phase to NB to maintain the charge neutrality in the NB (Eq. 4.5). Another possibility is the expulsion of $[Ru^{III}(LR)(L)]^+$ form NB to water; however, the stable three-phase CVs (**Fig. 4.20a**) indicates the stability of $[Ru^{III}(LR)(L)]^+$ in NB droplet.

$$[Ru^{II}(LR)(L)]^0_{(NB)} + An^-_{(W)} \leftrightarrow [Ru^{III}(LR)(L)]^+_{(NB)} + An^-_{(NB)} + e^- \qquad 4.5$$

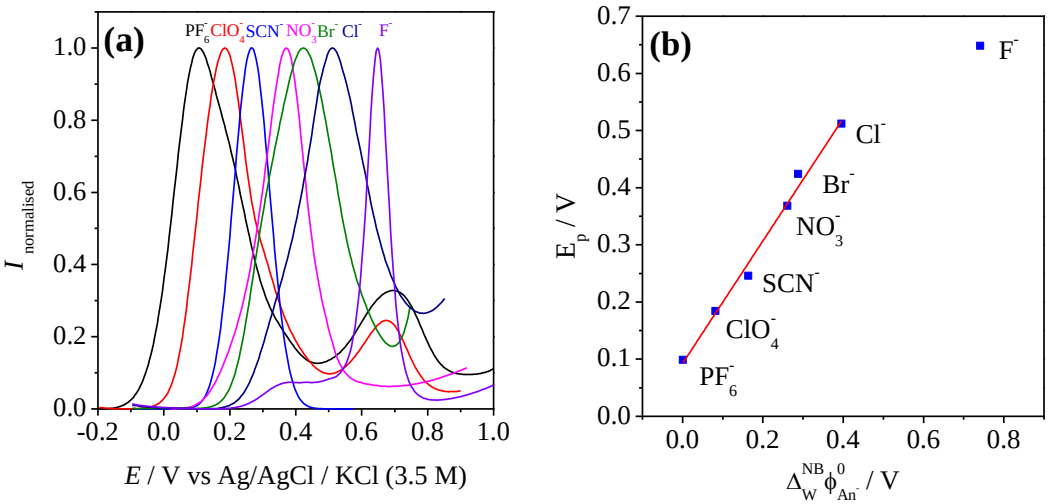

Figure 4.21 (a) Normalised SWVs recorded at TPE configuration by depositing the 2 µL droplet of NB containing 10 mM $[Ru^{II}(LR)(L)]^0$ complex on GC WE and submerged in 0.1 M aqueous solution of different anions. **(b)** The plot of SWV peak positions versus the standard transfer potential ($\Delta\phi^{(NB)\ominus}_{(aq),An^-}$); the red line is a linear fit with a slope of 1.07 and the R^2 value of 0.99.

The proof for anion transfer reaction is the dependency of the formal oxidation potential of $[Ru^{II}(LR)(L)]$ complex on the hydrophilicity of aqueous anion and its concentration (Eq. 1.23). This behaviour was examined by performing SWVs of the $[Ru^{II}(LR)(L)]^0$ complex containing NB droplets dipped in 0.1 M aqueous electrolytes of different anions (KF, KCl, KBr, KNO_3, $NaClO_4$, NaSCN, and KPF_6) and different concentrations of KNO_3 solutions.

Fig. 4.21a reveals that the SWV peak ($[Ru^{II}(LR)(L)]^0$ oxidation) potential shifts to higher potential when the anion of the aqueous electrolyte is more hydrophilic. The potential measured for PF_6^-, ClO_4^-, SCN^-, NO_3^-, Br^-, Cl^- and F^- is 0.104, 0.184, 0.268, 0.371, 0.423, 0.511 and 0.648 V respectively. The peak potentials are higher for more hydrophilic anions and follow the Hofmeister series; $PF_6^- < ClO_4^- < SCN^- < NO_3^- < Br^- < Cl^- < F^-$. **Fig. 4.21b** is a plot of peak potentials against the standard transfer potential. All the standard transfer potentials (except PF_6^- and F^-) are collected from [34], PF_6^- was determined from the Born equation [34] using the ionic radius (0.255 nm) provided in [78] and F^- from [79]. In the plot (**Fig. 4.21b)**, all data points are on the line (except for F^-) with a slope close to one. The data point of hydrophilic F^- ion is away from the line but much above the Cl^- indicating the large possibility of F^-transfer over the oxidised $[Ru^{II}(LR)(L)]^+$ ion expulsion.

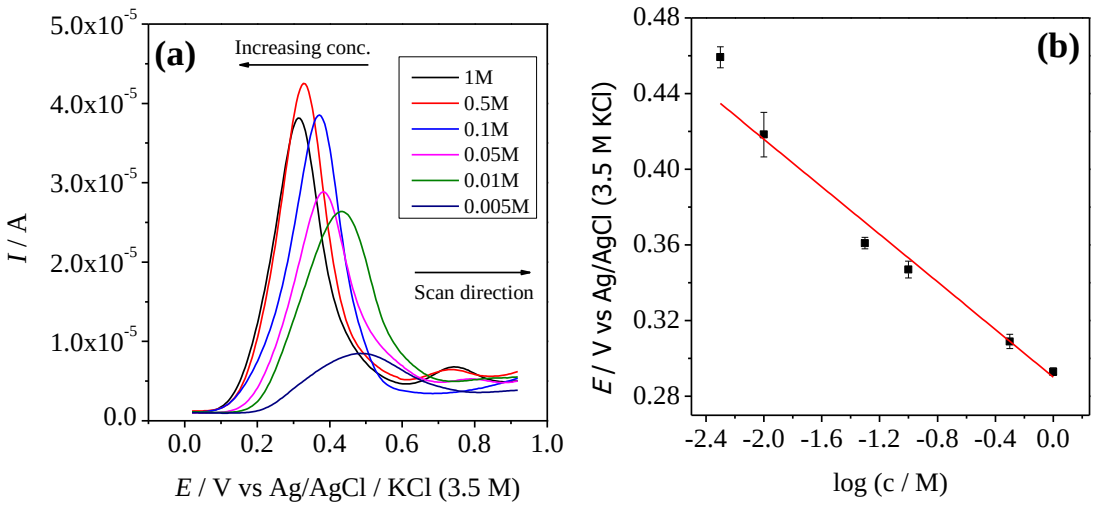

Figure 4.22 (a) SWVs performed at the three-phase junction; NB droplets containing 10 mM $[Ru^{II}(LR)(L)]^0$ complex are attached to GC WE and immersed in KNO_3 solutions of different concentrations (1, 0.5, 0.1, 0.05, 0.01, and 0.005 M). **(b)** The dependency of SWV peak potential on the logarithm of aqueous anion concentration. The slope of the fitted line is 63 ± 6 mV/decade, and R^2 is 0.95806.

As shown in **Fig. 4.22a**, the concentration dependency was examined by measuring TPE SWVs in different concentrations of KNO_3 solutions. The oxidation potential continuously shifts negatively as the concentration increases from 0.005 to 1 M. Which resulted in the dependency of peak potential by the magnitude of 63 ± 6 mV

per decade change on the concentration of KNO_3 (**Fig. 4.22b**); in comparison with the expected 59 mV per decade according to Eq. 1.23.

4.3.3 Three-phase electrochemistry with PF_6^-, ClO_4^- and SCN^- anions

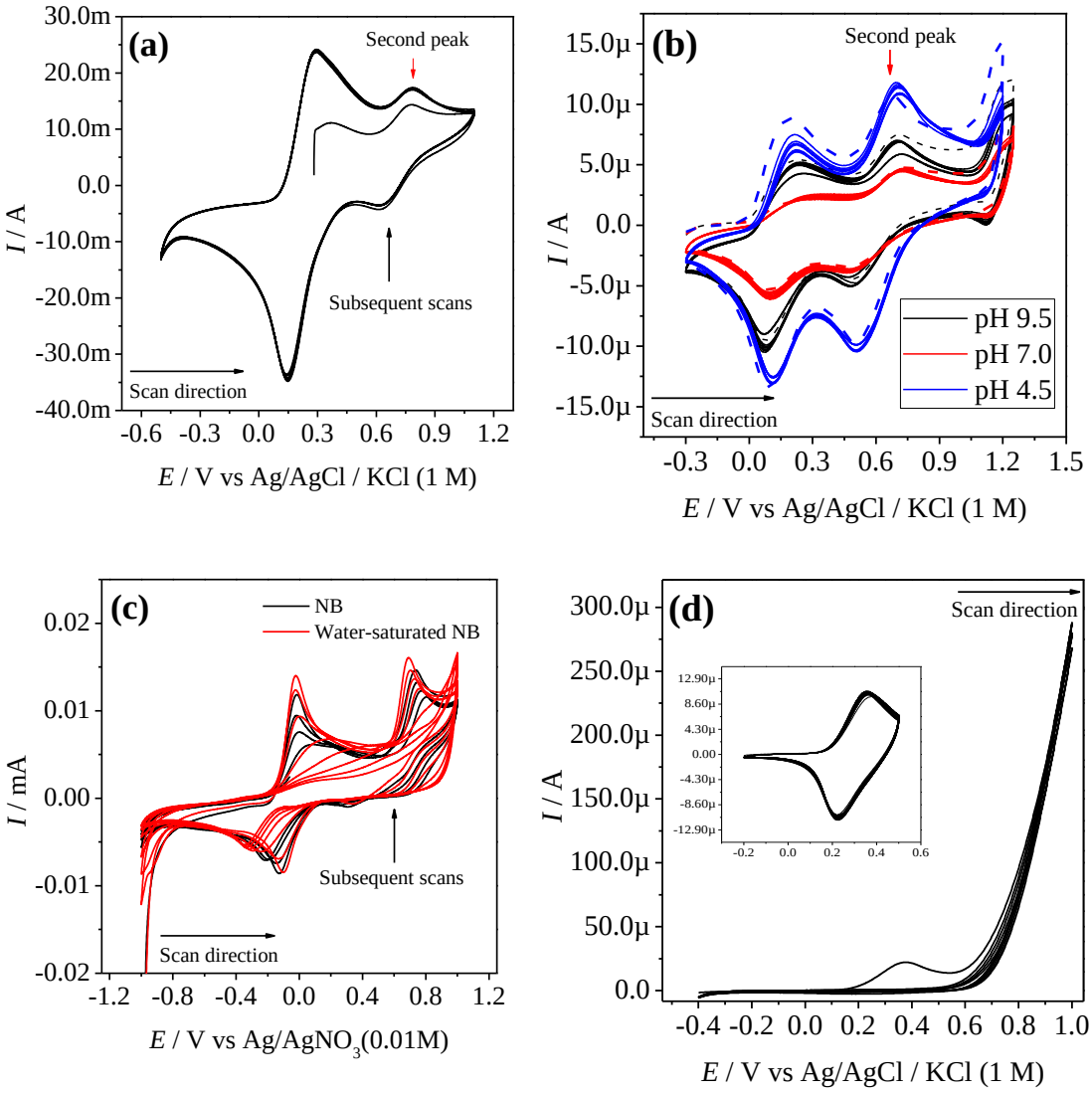

Figure 4.23 Three-phase CV cycles, where, GC WE was modified with 2 µL droplet of NB having 10 mM $[Ru^{II}(LR)(L)]^0$ complex and submerged in **(a)** 0.1 M $KClO_4$ solution and **(b)** 0.1 M KPF_6 of different pH. **(c)** CVs 10 mM $[Ru^{II}(LR)(L)]^0$ complex in NB and water-saturated NB. **(d)** Three-phase CVs 10 mM $[Ru^{II}(LR)(L)]^0$ in 0.1 M NaSCN solution and the inset shows the CVs of the short scan.

As presented in **Fig. 4.23a** and **b**, the additional second peak shows up around 0.7 V vs Ag/AgCl with lipophilic PF_6^- and ClO_4^- anions (also in **4.21a**). The causes of these peaks are not fully understood due to the following reasons:

1) Ru^{III} to Ru^{IV} oxidation is not anticipated at such low potential [76] and is not observed in the CVs of $[Ru^{II}(LR)(L)]^0$ in NB solvent (**Fig. 4.19a)**.
2) Another hypothesis is that these peaks are due to the proton assisted transfer. But in the CVs **Fig. 4.23a** and **b**, the second peak is reversible, and its potential is independent of pH between 4.5 and 9.5, as shown in **Fig. 4.23b**.
3) The third possibility may be the hydrogen bond interaction between the (benzimidazolate)pyridine ligands and water at the three-phase junction. Such interactions affect the potential of Ru oxidation [80,81]. Nevertheless, CVs of $[Ru^{II}(LR)(L)]^0$ oxidation in water-saturated NB did not show such shift and look similar to the CVs in NB (**Fig. 4.23c**).
4) The last possibility may be due to the ion-pair formation of $[Ru^{II}(LR)(L)]^0$ complex with incoming anions (PF_6^- and ClO_4^-). Haga and co-workers have seen the redox potential shift of similar Ru-complex at the higher acid condition by the addition of $HClO_4$, but this shift did not happen with the addition of HCl [82].

Some studies exposed that the chemical reversibility of the redox probe is incomplete if a metal ion reacts with nucleophiles [83]. Similarly, the three-phase electrochemistry is affected if the incoming anion reacts with the metal centre in the organic droplet. More nucleophilic anions such as CN^- and F^- coordinate with the metal centres of TPP-metal complexes of Mn and Co during three-phase junction experiments [71,73]. **Fig. 4.23d** displays, the CV scans of 10 mM $[Ru^{II}(LR)(L)]^0$ complex in NB droplet on GC in 0.1 M NaSCN solution; current increases intensely and the $Ru^{II/III}$ oxidation peak fades in the second scan. CVs scanned to the shorter window (0.5 V Ag/AgCl) were stable and reproducible, as shown in the inset of **Fig. 4.23d**. Hence, with SCN^-, $[Ru^{II}(LR)(L)]^0$ complex loss its redox activity due to the coordinating interaction, moreover SCN^- is recognised to form complexes with Ru metal centre [84,85]. Besides, $SCN^-$is an ambidentate ligand, which can interact to the metal centre through N or S and forms the stable complex with different metals.

4.3.4 Three-phase electrochemistry of $[Ru^{II}(LR)(L)]^0$ at different pH of the aqueous phase

As already stated, the deprotonated benzimidazole nitrogen sites of L ligand in $[Ru^{II}(LR)(L)]^0$ complex can easily be protonated at moderate pH. Water is almost completely insoluble in NB (around 0.2% water by volume at room temperature), but at the TPE configuration, the NB droplet is in contact with the large volume of water; hence it can be quickly saturated with water [86].

The CVs of Cl^- ion transfer at different pH are shown in **Fig. 4.24.** The pH of 0.1 M KCl is 6.95; it was changed (to 6.0, 4.0, and 2.5) by the addition of HCl and KOH (to pH 9.8). At pH 9.8, 6.95 and 6.0, only one peak corresponding to the oxidation of $[Ru^{II}(LR)(L)]^0$ to $[Ru^{III}(LR)(L)]^+$ is seen. However, at pH 4 and 2.5, a new peak appears in the CVs around 0.9 to 1.0 V vs Ag/AgCl; this could be the $Ru^{II/III}$ oxidation of the complex having protonated ligands.

Upon protonation of $[Ru^{II}(LR)(L)]^0$ types of complex, a positive shift of the $Ru^{II/III}$ oxidation potential is reported by Haga and collaborators [82]. In acetonitrile/buffer media, a ruthenium(II) complex of tridentate 2,6-bis(benzimidazol-2-yl)pyridine ligands showed the pH dependency for the proton-coupled electron-transfer reactions [82]. The formal $Ru^{(III/II)}$ potential was progressively shifted in the negative direction as the solution pH increases; due to the deprotonation of imino proton of the tridentate 2,6-bis(benzimidazol-2-yl)pyridine ligand.

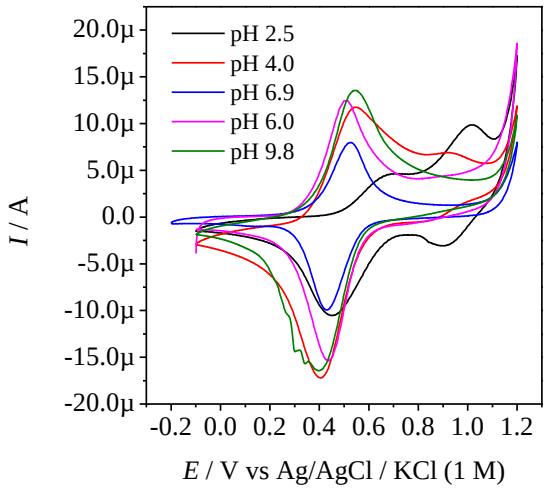

Figure 4.24 TPE configuration CVs of 10 mM $[Ru^{II}(LR)(L)]^0$ complex containing NB droplets deposited on GC and immersed in 0.1 M KCl solutions of different pH.

4.3.5 Conclusions

In collaboration with M. Haga and group, we synthesised a neutral heteroleptic bis(tridentate) ruthenium(II) complex $[Ru^{II}(LR)(L)]^0$ and characterised. The presence of 2-octyldodecyl chains on the LR ligand makes it highly lipophilic. The deprotonation of benzimidazole nitrogen sites of L ligand fulfilled the prime requirements of three-phase ion transfer studies; which includes the isolation of $[Ru^{II}(LR)(L)]^0$ as a neutral complex without counter anions and considerably lower $Ru^{II/III}$ oxidation potential.

This complex is stable at the three-phase junction, oxidation of $[Ru^{II}(LR)(L)]^0$ to $[Ru^{III}(LR)(L)]^+$ in NB is coupled with the transfer of anion from the aqueous phase to NB. This was confirmed by studying the dependence of SWV oxidation potential on the hydrophobicity of aqueous anion and its concentration. Oxidation of $[Ru^{II}(LR)(L)]^0$ with lipophilic PF_6^- and ClO_4^- anions showed an unknown additional reversible peak, with SCN^-we anticipate the coordinating interaction.

4.3.6 References

[1] B. Huskinson, M.P. Marshak, C. Suh, S. Er, M.R. Gerhardt, C.J. Galvin, X. Chen, A. Aspuru-Guzik, R.G. Gordon, M.J. Aziz, A metal-free organic–inorganic aqueous flow battery, Nature. 505 (2014) 195–198. doi:10.1038/nature12909.

[2] M.R. Gerhardt, L. Tong, R. Gómez-Bombarelli, Q. Chen, M.P. Marshak, C.J. Galvin, A. Aspuru-Guzik, R.G. Gordon, M.J. Aziz, Anthraquinone Derivatives in Aqueous Flow Batteries, Adv. Energy Mater. 7 (2017) 1601488. doi:10.1002/aenm.201601488.

[3] C. Li, X. Yang, R. Chen, J. Pan, H. Tian, H. Zhu, X. Wang, A. Hagfeldt, L. Sun, Anthraquinone dyes as photosensitizers for dye-sensitized solar cells, Sol. Energy Mater. Sol. Cells. 91 (2007) 1863–1871. doi:10.1016/j.solmat.2007.07.002.

[4] J.I. Bardagi, I. Ghosh, M. Schmalzbauer, T. Ghosh, B. König, Anthraquinones as Photoredox Catalysts for the Reductive Activation of Aryl Halides, European J. Org. Chem. 2018 (2018) 34–40. doi:10.1002/ejoc.201701461.

[5] J.R. Tobias Johnsson Wass, E. Ahlberg, I. Panas, D.J. Schiffrin, Quantum chemical modeling of the reduction of quinones, J. Phys. Chem. A. 110 (2006) 2005–2020. doi:10.1021/jp055414z.

[6] F.L. Crane, M.D. Henninger, Function of Quinones in Photosynthesis, in: Vitam. Horm., 1967: pp. 489–517. doi:10.1016/S0083-6729(08)60218-6.

[7] M. Uchimiya, A.T. Stone, Reversible redox chemistry of quinones: Impact on biogeochemical cycles, Chemosphere. 77 (2009) 451–458. doi:10.1016/j.chemosphere.2009.07.025.

[8] E.A. Hillard, F.C. de Abreu, D.C.M. Ferreira, G. Jaouen, M.O.F. Goulart, C. Amatore, Electrochemical parameters and techniques in drug development, with an emphasis on quinones and related compounds, Chem. Commun. (2008) 2612. doi:10.1039/b718116g.

[9] P.S. Guin, S. Das, P.C. Mandal, Electrochemical Reduction of Quinones in Different Media: A Review, Int. J. Electrochem. 2011 (2011) 1–22. doi:10.4061/2011/816202.

[10] P. Mitchell, The protonmotive Q cycle: A general formulation, FEBS Lett. 59 (1975) 137–139. doi:10.1016/0014-5793(75)80359-0.

[11] J. V. McGowan, R. Chung, A. Maulik, I. Piotrowska, J.M. Walker, D.M. Yellon, Anthracycline Chemotherapy and Cardiotoxicity, Cardiovasc. Drugs Ther. 31 (2017) 63–75. doi:10.1007/s10557-016-6711-0.

[12] D. Barasch, O. Zipori, I. Ringel, I. Ginsburg, A. Samuni, J. Katzhendler, Novel anthraquinone derivatives with redox-active functional groups capable of producing free radicals by metabolism: are free radicals essential for cytotoxicity?, Eur. J. Med. Chem. 34 (1999) 597–615. doi:10.1016/S0223-5234(00)80029-X.

[13] Y. Kawakami, A.J. Hopfinger, Prediction of initial reduction potentials of compounds related to anthracyclines and implications for estimating cardiotoxicity, Chem. Res. Toxicol. 3 (1990) 244–247. doi:10.1021/tx00015a009.

[14] J. William Lown, H.-H. Chen, J.A. Plambeck, E.M. Acton, Further studies on the generation of reactive oxygen species from activated anthracyclines and the relationship to cytotoxic action and cardiotoxic effects, Biochem. Pharmacol. 31 (1982) 575–581. doi:10.1016/0006-2952(82)90162-9.

[15] A. Kumbhar, S. Padhye, D. Ross, Cytotoxic properties of iron-hydroxynaphthoquinone complexes in rat hepatocytes, BioMetals. 9 (1996) 235–240. doi:10.1007/BF00817921.

[16] B. Kalyanaraman, P.I. Premovic, R.C. Sealy, Semiquinone anion radicals from addition of amino acids, peptides, and proteins to quinones derived from oxidation of catechols and catecholamines. An ESR spin stabilization study., J. Biol. Chem. 262 (1987) 11080–7.

[17] Y. Wang, S. Hekimi, Understanding Ubiquinone, Trends Cell Biol. 26 (2016) 367–378. doi:10.1016/j.tcb.2015.12.007.

[18] J.Q. Chambers, Electrochemistry of quinones, in: Quinonoid Compd. Vol. 1, John Wiley & Sons, Inc., Chichester, UK, 2010: pp. 719–757. doi:10.1002/9780470772119.ch12.

[19] N. Gupta, H. Linschitz, Hydrogen-Bonding and Protonation Effects in Electrochemistry of Quinones in Aprotic Solvents, J. Am. Chem. Soc. 119 (1997) 6384–6391. doi:10.1021/ja970028j.

[20] P.S. Guin, S. Das, P.C. Mandal, Electrochemical reduction of sodium 1,4-dihydroxy-9,10- anthraquinone-2-sulphonate in aqueous and aqueous dimethyl formamide mixed solvent: A cyclic voltammetric study, Int. J. Electrochem. Sci. 3 (2008) 1016–1028.

[21] N.H. Furman, K.G. Stone, A Polarographic Study of Certain Anthraquinones 1, J. Am. Chem. Soc. 70 (1948) 3055–3061. doi:10.1021/ja01189a064.

[22] F. Scholz, Š. Komorsky-Lovrić, M. Lovrić, A new access to Gibbs energies of transfer of ions across liquid|liquid interfaces and a new method to study electrochemical processes at well-defined three-phase junctions, Electrochem. Commun. 2 (2000) 112–118. doi:10.1016/S1388-2481(99)00156-3.

[23] V. Mirčeski, R. Gulaboski, F. Scholz, Square-wave thin-film voltammetry: influence of uncompensated resistance and charge transfer kinetics, J. Electroanal. Chem. 566 (2004) 351–360. doi:10.1016/j.jelechem.2003.11.046.

[24] F. Scholz, R. Gulaboski, K. Caban, The determination of standard Gibbs energies of transfer of cations across the nitrobenzene|water interface using a three-phase electrode, Electrochem. Commun. 5 (2003) 929–934. doi:10.1016/j.elecom.2003.09.005.

[25] K. Shi, K.-K. Shiu, Adsorption of some quinone derivatives at electrochemically activated glassy carbon electrodes, J. Electroanal. Chem. 574 (2004) 63–70. doi:10.1016/j.jelechem.2004.07.027.

[26] J. Xu, Q. Chen, G.M. Swain, Anthraquinonedisulfonate Electrochemistry: A Comparison of Glassy Carbon, Hydrogenated Glassy Carbon, Highly Oriented Pyrolytic Graphite, and Diamond Electrodes, Anal. Chem. 70 (1998) 3146–3154. doi:10.1021/ac9800661.

[27] S.W. Han, S.W. Joo, T.H. Ha, Y. Kim, K. Kim, Adsorption Characteristics of Anthraquinone-2-carboxylic Acid on Gold, J. Phys. Chem. B. 104 (2000) 11987–11995. doi:10.1021/jp002630t.

[28] A. Bard, L. Faulkner, Electrochemical Methods: fundamentals and applications. -2nd ed., 1944. doi:10.1016/B978-0-12-381373-2.00056-9.

[29] W.A. Badawy, K.M. Ismail, S.S. Medany, Optimization of the electropolymerization of 1-amino-9,10-anthraquinone conducting films from aqueous media, Electrochim. Acta. 51 (2006) 6353–6360. doi:10.1016/j.electacta.2006.04.021.

[30] R. Gulaboski, The determination of the standard Gibbs energies of ion transfer between water and heavy water by using the three-phase electrode approach, Electrochem. Commun. 6 (2004) 215–218. doi:10.1016/j.elecom.2003.12.001.

[31] F. Quentel, V. Mirčeski, M. L'Her, Lutetium Bis(tetra- tert - butylphthalocyaninato): A Superior Redox Probe To Study the Transfer of Anions and Cations Across the Water|Nitrobenzene Interface by Means of Square-Wave Voltammetry at the Three-Phase Electrode, J. Phys. Chem. B. 109 (2005) 1262–1267. doi:10.1021/jp045914c.

[32] F. Scholz, R. Gulaboski, Determining the Gibbs Energy of Ion Transfer Across Water-Organic Liquid Interfaces with Three-Phase Electrodes, ChemPhysChem. 6 (2005) 16–28. doi:10.1002/cphc.200400248.

[33] V. Mirčeski, R. Gulaboski, F. Scholz, Determination of the standard Gibbs energies of transfer of cations across the nitrobenzene|water interface utilizing the reduction of iodine in an immobilized nitrobenzene droplet, Electrochem. Commun. 4 (2002) 814–819. doi:10.1016/S1388-2481(02)00456-3.

[34] A.G. Volkov, Liquid Interfaces in Chemical, Biological and Pharmaceutical Applications, 1st ed., Marcel Dekker, New York, 2001.

[35] J.S. Jaworski, M.K. Kalinowski, Electrochemical studies of ion pairs and triplets formed by alkali metal cations with 1,2-naphthosemiquinone and 1,2-naphthoquinone dianion, J. Electroanal. Chem. Interfacial Electrochem. 76 (1977) 301–314. doi:10.1016/S0022-0728(77)80482-8.

[36] J.S. Jaworski, Solvent and ion pairing effects on the reaction entropy for the electroreduction of aromatic molecules, J. Electroanal. Chem. 219 (1987) 209–219. doi:10.1016/0022-0728(87)85041-6.

[37] K. Miyoshi, M. Oyama, S. Okazaki, Electrochemical Analysis of Ion-Pair Formation Reactions Involving Organic Dianions Using Differential Pulse Voltammetry, Electroanalysis. 13 (2001) 917–922. doi:10.1002/1521-4109(200107)13:11<917::AID-ELAN917>3.0.CO;2-D.

[38] D. Kaluza, W. Adamiak, M. Opallo, M. Jonsson-Niedziolka, Comparison of Ion Transfer Thermodynamics at Microfluidic and Droplet-Based Three Phase Electrodes, Electrochim. Acta. 132 (2014) 158–164. doi:10.1016/j.electacta.2014.03.105.

[39] I. Kaminska, M. Jonsson-Niedziolka, A. Kaminska, M. Pisarek, R. Hołyst, M. Opallo, J. Niedziolka-Jonsson, Electrodeposition of Well-Adhered Multifarious Au Particles at a Solid|Toluene|Aqueous Electrolyte Three-Phase Junction, J. Phys. Chem. C. 116 (2012) 22476–22485. doi:10.1021/jp307674k.

[40] K. Aoki, M. Li, J. Chen, T. Nishiumi, Spontaneous emulsification at oil–water interface by tetraalkylammonium chloride, Electrochem. Commun. 11 (2009) 239–241. doi:10.1016/j.elecom.2008.11.012.

[41] P.M. Gross, The "Salting out" of Non-electrolytes from Aqueous Solutions., Chem. Rev. 13 (1933) 91–101. doi:10.1021/cr60044a007.

[42] D.F. McCain, O.E. Allgood, J.T. Cox, A.E. Falconi, M.J. Kim, W.-Y. Shih, A Colorful Laboratory Investigation of Hydrophobic Interactions, the Partition Coefficient, Gibbs Energy of Transfer, and the Effect of Hofmeister Salts, J. Chem. Educ. 89 (2012) 1074–1077. doi:10.1021/ed300017a.

[43] S. Wu, B. Su, 7,7′,8,8′-Tetracyanoquinodimethane as a redox probe for studying cation transfer across the water/2-nitrophenyl octyl ether interface at three-phase junctions supported by carbon ink screen-printed electrodes, J. Electroanal. Chem. 656 (2011) 237–242. doi:10.1016/j.jelechem.2010.11.004.

[44] A.M. Bond, S. Fletcher, F. Marken, S.J. Shaw, P.G. Symons, Electrochemical and X-ray diffraction study of the redox cycling of nanocrystals of 7,7,8,8-tetracyanoquinodimethane. Observation of a solid–solid phase transformation controlled by nucleation and growth, J. Chem. Soc., Faraday Trans. 92 (1996) 3925–3933. doi:10.1039/FT9969203925.

[45] G.N. Kamau, J.F. Rusling, Microelectrode voltammetry of TCNQ in aprotic solvent at low concentrations of non-reducing and reducing salts, J. Electroanal. Chem. Interfacial Electrochem. 292 (1990) 187–198. doi:10.1016/0022-0728(90)87335-H.

[46] L. Huang, P. Li, N. Pamphile, Z.-Q. Tian, D. Zhan, Electrosynthesis of Copper-Tetracyanoquinodimethane Based on the Coupling Charge Transfer across Water/1,2-Dichloroethane Interface, Electrochim. Acta. 140 (2014) 332–336. doi:10.1016/j.electacta.2014.04.102.

[47] T.H. Le, A. Nafady, X. Qu, A.M. Bond, L.L. Martin, Redox and Acid–Base Chemistry of 7,7,8,8-Tetracyanoquinodimethane, 7,7,8,8-Tetracyanoquinodimethane Radical Anion, 7,7,8,8-Tetracyanoquinodimethane

Dianion, and Dihydro-7,7,8,8-Tetracyanoquinodimethane in Acetonitrile, Anal. Chem. 84 (2012) 2343–2350. doi:10.1021/ac2030514.

[48] Y. Kanzaki, S. Mitani, D. Shiomi, Y. Morita, T. Takui, K. Sato, Microscopic Behavior of Active Materials Inside a TCNQ-Based Lithium-Ion Rechargeable Battery by in Situ 2D ESR Measurements, ACS Appl. Mater. Interfaces. 10 (2018) 43631–43640. doi:10.1021/acsami.8b14967.

[49] A.R. Harris, A.K. Neufeld, A.P. O'Mullane, A.M. Bond, R.J.S.S. Morrison, A.P. O'Mullane, A.M. Bond, R.J.S.S. Morrison, Voltammetric, EQCM, Spectroscopic, and Microscopic Studies on the Electrocrystallization of Semiconducting, Phase I, CuTCNQ on Carbon, Gold, and Platinum Electrodes by a Nucleation-Growth Process, J. Electrochem. Soc. 152 (2005) C577. doi:10.1149/1.1955047.

[50] A. Nafady, A.M. Bond, A. Bilyk, A.R. Harris, A.I. Bhatt, A.P. O'Mullane, R. De Marco, Tuning the Electrocrystallization Parameters of Semiconducting Co[TCNQ] 2 -Based Materials To Yield either Single Nanowires or Crystalline Thin Films, J. Am. Chem. Soc. 129 (2007) 2369–2382. doi:10.1021/ja067219j.

[51] A. Nafady, A.P. O'Mullane, A.M. Bond, Electrochemical and photochemical routes to semiconducting transition metal-tetracyanoquinodimethane coordination polymers, Coord. Chem. Rev. 268 (2014) 101–142. doi:10.1016/j.ccr.2014.01.017.

[52] M. Mohammadtaheri, R. Ramanathan, V. Bansal, Emerging applications of metal-TCNQ based organic semiconductor charge transfer complexes for catalysis, Catal. Today. 278 (2016) 319–329. doi:10.1016/j.cattod.2015.11.017.

[53] M.C. Grossel, A.J. Duke, D.B. Hibbert, I.K. Lewis, E.A. Seddon, P.N. Horton, S.C. Weston, An Investigation of the Factors that Influence the Decomposition of 7,7',8,8'-Tetracyanoquinodimethane (TCNQ) and Its Salts to, and Structural Characterization of, the α,α-Dicyano- p -toluoylcyanide Anion, Chem. Mater. 12 (2000) 2319–2323. doi:10.1021/cm991160g.

[54] M.R. Suchanski, R.P. Van Duyne, Resonance Raman spectroelectrochemistry. IV. The oxygen decay chemistry of the tetracyanoquinodimethane dianion, J. Am. Chem. Soc. 98 (1976) 250–252. doi:10.1021/ja00417a049.

[55] T.H. Le, A. Nafady, X. Qu, L.L. Martin, A.M. Bond, Detailed Electrochemical Analysis of the Redox Chemistry of Tetrafluorotetracyanoquinodimethane TCNQF 4 , the Radical Anion [TCNQF 4] •– , and the Dianion [TCNQF 4] 2– in the Presence of Trifluoroacetic Acid, Anal. Chem. 83 (2011) 6731–6737. doi:10.1021/ac201373d.

[56] A. Yamagishi, M. Sakamoto, The Protonation of the TCNQ Anion Radical by Hydrogen Chloride, Bull. Chem. Soc. Jpn. 47 (1974) 2152–2157. doi:10.1246/bcsj.47.2152.

[57] A. Yamagishi, M. Yamada, Effects of Quinones on the Protonation Reaction of TCNQ Anion Radical; The Role of a Protonated Quinone as a Strong Electron

Acceptor, Bull. Chem. Soc. Jpn. 49 (1976) 371–374. doi:10.1246/bcsj.49.371.

[58] A. Yamagishi, Rate of Protonation of TCNQ Anion Radical in Water, Bull. Chem. Soc. Jpn. 49 (1976) 1417–1418. doi:10.1246/bcsj.49.1417.

[59] T.A. Hudson, R. Robson, A New Class of TCNQ Derivatives Easily Generated from TCNQH 2 Containing Discrete TCNQ 2− Anions and Noncoordinating Cations, Cryst. Growth Des. 9 (2009) 1658–1662. doi:10.1021/cg801400j.

[60] B.F. Abrahams, R.W. Elliott, T.A. Hudson, R. Robson, A new type of 3D [(M II) 2 (TCNQ −II) 3] 2 − coordination network with spacious channels of hexagonal cross-section generated from TCNQH 2, CrystEngComm. 14 (2012) 351–354. doi:10.1039/C1CE06104F.

[61] S.B. Khoo, J.K. Foley, S. Pons, Electrolyte effects on the cyclic voltammetry of TCNQ and TCNE, J. Electroanal. Chem. Interfacial Electrochem. 215 (1986) 273–285. doi:10.1016/0022-0728(86)87021-8.

[62] S.B. Khoo, J.F. Foley, C. Korzeniewski, S. Pons, C. Marcott, An infrared spectroelectrochemical investigation of the ion pairing reactions of the anions and dianions of TCNE and TCNQ, J. Electroanal. Chem. Interfacial Electrochem. 233 (1987) 223–236. doi:10.1016/0022-0728(87)85018-0.

[63] M. Oyama, R.D. Webster, M. Suárez, F. Marken, R.G. Compton, S. Okazaki, Mechanistic Aspects of the Electrochemical Reduction of 7,7,8,8-Tetracyanoquinodimethane in the Presence of Mg 2+ or Ba 2+, J. Phys. Chem. B. 102 (1998) 6588–6595. doi:10.1021/jp9819846.

[64] F. Li, A.L. Whitworth, P.R. Unwin, Measurement of rapid electron transfer across a liquid/liquid interface from 7,7,8,8-tetracyanoquinodimethane radical anion in 1,2-dichloroethane to aqueous tris(2,2-bipyridyl)-ruthenium (III), J. Electroanal. Chem. 602 (2007) 70–76. doi:10.1016/j.jelechem.2006.12.002.

[65] J. Zhang, P.R. Unwin, Microelectrochemical measurements of electron transfer rates at the interface between two immiscible electrolyte solutions: Potential dependence of the ferro/ferricyanide-7,7,8,8-tetracyanoquinodimethane (TCNQ)/TCNQ˙– system, Phys. Chem. Chem. Phys. 4 (2002) 3820–3827. doi:10.1039/b108882c.

[66] L.R. Melby, R.J. Harder, W.R. Hertler, W. Mahler, R.E. Benson, W.E. Mochel, Substituted Quinodimethans. II. Anion-radical Derivatives and Complexes of 7,7,8,8-Tetracyanoquinodimethan, J. Am. Chem. Soc. 84 (1962) 3374–3387. doi:10.1021/ja00876a029.

[67] H. Kubota, Y. Takahashi, H. Hasegawa, T. Shimada, J. Harada, T. Inabe, Charge Carrier Doping into the Peierls Insulator of the TCNQ Anion Radical Salt (TCNQ = 7,7,8,8-Tetracyanoquinodimethane), J. Phys. Chem. C. 120 (2016) 11545–11551. doi:10.1021/acs.jpcc.6b02665.

[68] K. Dharmaraj, Z. Nasri, H. Kahlert, F. Scholz, The electrochemistry of DPPH in three-phase electrode systems for ion transfer and ion association studies, J. Electroanal. Chem. 823 (2018) 765–772. doi:10.1016/j.jelechem.2018.06.012.

[69] R. Gulaboski, K. Riedl, F. Scholz, Standard Gibbs energies of transfer of halogenate and pseudohalogenate ions, halogen substituted acetates, and cycloalkyl carboxylate anions at the water|nitrobenzene interface, Phys. Chem. Chem. Phys. 5 (2003) 1284–1289. doi:10.1039/b210356g.

[70] Š. Komorsky-Lovrić, K. Riedl, R. Gulaboski, V. Mirčeski, F. Scholz, Determination of Standard Gibbs Energies of Transfer of Organic Anions across the Water/Nitrobenzene Interface, Langmuir. 18 (2002) 8000–8005. doi:10.1021/la020285o.

[71] M.J. Bonné, C. Reynolds, S. Yates, G. Shul, J. Niedziolka, M. Opallo, F. Marken, The electrochemical ion-transfer reactivity of porphyrinato metal complexes in 4-(3-phenylpropyl)pyridine | water systems, New J. Chem. 30 (2006) 327. doi:10.1039/b514348a.

[72] G. Shul, W. Nogala, I. Zakorchemna, J. Niedziolka, M. Opallo, Scanning electrochemical microscopy study of ion transfer process across water/2-nitrophenyloctylether interface supported by hydrophobic carbon ceramic electrode, J. Solid State Electrochem. 12 (2008) 1285–1291. doi:10.1007/s10008-008-0512-8.

[73] A.M. Collins, G.J. Blanchard, F. Marken, Spectroelectrochemical Investigation of TPPMn(III/II)-Driven Liquid | Liquid | Electrode Triple Phase Boundary Anion Transfer into 4-(3-Phenylpropyl)-Pyridine: ClO4−, CO3H−, Cl−, and F−, Electroanalysis. 24 (2012) 246–253. doi:10.1002/elan.201100623.

[74] W. Yang, Y. Zhong, S. Yoshikawa, J. Shao, S. Masaoka, K. Sakai, J. Yao, M. Haga, Tuning of Redox Potentials by Introducing a Cyclometalated Bond to Bis-tridentate Ruthenium(II) Complexes Bearing Bis(N -methylbenzimidazolyl)benzene or -pyridine Ligands, Inorg. Chem. 51 (2012) 890–899. doi:10.1021/ic2016885.

[75] A. Singh, B. Chetia, S.M. Mobin, G. Das, P.K. Iyer, B. Mondal, Ruthenium monoterpyridine complexes with 2,6-bis(benzimidazol-2-yl)pyridine: Synthesis, spectral properties and structure, Polyhedron. 27 (2008) 1983–1988. doi:10.1016/j.poly.2008.03.008.

[76] X. Xiaoming, M. Haga, T. Matsumura-Inoue, Y. Ru, A.W. Addison, K. Kano, Synthesis and proton transfer-linked redox tuning of ruthenium(II) complexes with tridentate 2,6-bis(benzimidazol-2-yl)pyridine ligands, J. Chem. Soc. Dalt. Trans. (1993) 2477. doi:10.1039/dt9930002477.

[77] M. HAGA, K. KOBAYASHI, K. TERADA, Fabrication and functions of surface nanomaterials based on multilayered or nanoarrayed assembly of metal complexes, Coord. Chem. Rev. 251 (2007) 2688–2701. doi:10.1016/j.ccr.2007.03.022.

[78] N. Matsushita, H. Kitagawa, T. Mitani, Counter-ion radius dependence of the mixed-valence state in MX chain platinum complexes, Synth. Met. 71 (1995) 1933–1934. doi:10.1016/0379-6779(94)03113-K.

[79] H. KATANO, Y. MURAYAMA, H. TATSUMI, Voltammetric Study of the Transfer of Fluoride Ion at the Nitrobenzene | Water Interface Assisted by Tetraphenylantimony, Anal. Sci. 20 (2004) 553–556. doi:10.2116/analsci.20.553.

[80] M. Haga, M.M. Ali, S. Koseki, K. Fujimoto, A. Yoshimura, K. Nozaki, T. Ohno, K. Nakajima, D.J. Stufkens, Proton-Induced Tuning of Electrochemical and Photophysical Properties in Mononuclear and Dinuclear Ruthenium Complexes Containing 2,2‘-Bis(benzimidazol-2-yl)-4,4‘-bipyridine: Synthesis, Molecular Structure, and Mixed-Valence State and Excited-State Proper, Inorg. Chem. 35 (1996) 3335–3347. doi:10.1021/ic950083y.

[81] M.-A. Haga, A. Tsunemitsu, The outer-sphere interactions in ruthenium and osmium complexes I. Spectrophotometric and voltammetric studies on the hydrogen bonding interactions of bis(2,2′-bipyridine)(2-(2′-pyridyl)-benzimidazole)ruthenium(II)cation and its derivatives with aromatic , Inorganica Chim. Acta. 164 (1989) 137–142. doi:10.1016/S0020-1693(00)83214-4.

[82] M. Haga, H. Hong, Y. Shiozawa, Y. Kawata, H. Monjushiro, T. Fukuo, R. Arakawa, Synthesis and Proton-Coupled Electron-Transfer Reaction of Self-Assembled Monolayers of a Ruthenium(II) Complex Containing Tridentate 2,6-Bis(benzimidazol-2-yl)pyridine on a Gold Surface: Comparison of Acid/Base Chemistry with Bulk Solution Chemistry, Inorg. Chem. 39 (2000) 4566–4573. doi:10.1021/ic990934s.

[83] I. Noviandri, K. N. Brown, D. S. Fleming, P. T. Gulyas, P. A. Lay, A. F. Masters, L. Phillips, The Decamethylferrocenium/Decamethylferrocene Redox Couple: A Superior Redox Standard to the Ferrocenium/Ferrocene Redox Couple for Studying Solvent Effects on the Thermodynamics of Electron Transfer, J. Phys. Chem. B. 103 (1999) 6713–6722. doi:10.1021/jp991381.

[84] O. Kohle, S. Ruile, M. Grätzel, Ruthenium(II) Charge-Transfer Sensitizers Containing 4,4‘-Dicarboxy-2,2‘-bipyridine. Synthesis, Properties, and Bonding Mode of Coordinated Thio- and Selenocyanates, Inorg. Chem. 35 (1996) 4779–4787. doi:10.1021/ic9515665.

[85] V. Palaniappan, S. Sathaiah, H.D. Bist, U.C. Agarwala, Electron mediation through the thiocyanate bridge: mono- and dinuclear ruthenium diimine complexes and their mixed-valence properties, J. Am. Chem. Soc. 110 (1988) 6403–6410. doi:10.1021/ja00227a021.

[86] J.C. Smith, N.J. Foecking, W.P. Barber, Solubility Data for Aniline-Nitrobenzene-Water System, Ind. Eng. Chem. 41 (1949) 2289–2291. doi:10.1021/ie50478a052.

Chapter 5. Three-phase ion transfer studies in microfluidic devices of different geometries

As discussed in the second chapter, a microdroplet based TPE configuration is easy to use; however, currents are not reproducible because the droplets deposited using a micropipette do not have the same circumference each time. In order to get a stable current, few methods such as using a cylindrical metal microelectrode, the production of the size-controlled organic droplet [1–3], and creating TPE in microfluidic systems have been developed [4–7].

In microfluidic devices, TPE configuration is formed by the parallel flow of the organic and aqueous phases across the gold band microelectrodes. Microfluidic TPE system has been used to study the anion transfer reactions in the hydrodynamic conditions [4–7]. Also, it allows us to use the water-miscible acetonitrile as the organic phase; the two-phase flow of acetonitrile|aqueous solution of 2 M NaCl is possible [5]. Section 2.5 in chapter 2 reviews the ion transfer reactions carried out in the microfluidic TPE configurations.

The two key factors which prove the ion transfer are the influence of ion hydrophobicity and concentration on the voltammetric peak potentials. These two effects are similar in the droplet-based and microfluidic TPE configurations. Also, our group has done the comparative anion transfer studies in the droplet-based and microfluidic TPE systems; studies indicate that the hydrophobicity and concentration effects are identical in both systems and the voltammetric peak potentials are not affected by the flow rate in the case of the microfluidic system [7].

However, ion transfer limiting current in the microfluidic TPE system behaves anomalously with the flow rate. In the case of flowing NOP|aqueous $NaClO_4$ interface; the oxidation current (ClO_4^- ion transfer) did not vary according to the Levich equation, current decreases as the flow increases [4]. In another instance of flowing acetonitrile|aqueous interface; the limiting current was independent of the flow rate [5]. Hence a detailed study was conducted by our group to investigate the flow rate behaviour, as explained in section 2.5 [6]. I believe that the ion transfer reactions using microfluidic TPE systems are not entirely understood since we do not know the effect of microfluidic geometry, flow rates, the viscosity of solvents, and ionophores on the ion transfer reaction. Some of these effects are well known for single-phase microfluidic electrochemistry but not for biphasic TPE ion transfer studies. I tried to investigate the ion transfer studies in microfluidic TPE systems of different geometries. Here, the different geometries refer to the T-junction types (where one phase is stationary, and the other is flowing), well-defined organic|aqueous interface (where flow rates of each phase are controlled) and surface modification of the microfluidic cell. I briefly summarised all the results.

5.1 Introduction and principles of microfluidics

Microfluidics involves the technology and systems to manipulate the small volume of fluids (micro to attoliter) using the microchannels (dimensions of ten to several hundred micrometers) on the substrates. During the subsequent years, microfluidic components for fluid transport, mixing, and separation have found applications in chemistry, biochemistry, biomedical devices, and analytical systems [8–10]. In the field of electrochemistry, microfluidic systems have been used in the biosensing [9], energy conversion systems [11], electrosynthesis [12], ion transfer across organic|aqueous interfaces [4–6] and others [13].

In microfluidics, the conventional properties of fluids (like viscosity, surface tension, and diffusion) are denoted in terms of dimensionless parameters like Reynold's number (**Re**) (Eq. 5.1), Capillary number (**Ca**) (Eq. 5.2) and Peclet number (**Pe**) (Eq. 5.3) [9]. In the following equations, ρ indicates the fluid density, l presents the length, υ represents the mean fluid velocity, μ denotes the dynamic fluid viscosity, γ is surface tension and D signifies the diffusion coefficient [9].

$$\mathrm{Re} = \frac{\rho l \upsilon}{\mu} \qquad 5.1$$

$$\mathrm{Ca} = \frac{\mu v}{\gamma} \qquad 5.2$$

$$\mathrm{Pe} = \frac{\upsilon l}{\mathrm{D}} \qquad 5.3$$

Re number is the relationship between inertial and viscous forces. It is a suitable parameter to predict the flow condition is laminar or turbulent. Low **Re** (viscous forces are dominant) means the flow is laminar, and larger **Re** indicates the flow is turbulent (inertial forces are dominating). The **Ca** number is the ratio of viscous force to surface tension force, and the **Pe** number is the ratio between the convection concerning diffusion. Usually, **Re**, **Ca**, and **Pe** numbers are low for the microfluidic system having the laminar flow [9]. These parameters are essential for designing electrochemical microfluidic devices.

5.2 Fabrication of the electrochemical microfluidic systems having T-junction

I used polydimethylsiloxane (PDMS) synthetic polymer to fabricate the microchannels. PDMS is a rubbery elastomer of siloxane; which is a hydrophobic, transparent, and non-toxic material. Also, its surface can be chemically modified; hence PDMS is an excellent material to make T-junction microchannels. The fabrication procedure for the microfluidic devices having the gold band electrodes contains the following steps: (1)

Designing the mask using CleWin (version 2.90) software and printing it on transparency (photomask), (2) Microchannel fabrication on a silicon wafer (master preparation by photolithography) and casting PDMS on the master to get microchannels in the PDMS (PDMS micro-molding), (3) Fabrication of the gold microband electrodes on a glass slide, and (4) Final assembly. The procedures followed for the fabrication are as follows [10]:

5.2.1 Photolithography

Designs were produced in the CleWin software and printed as the high-resolution transparent image on the dark background. This transparency works as the photomask in photolithography to deposit the photoresist on the silicon wafer. The epoxy-based negative photoresist (SU-8 2050, MicroChem Inc., target: 100 μm) was coated on the 4-inch silicon wafer by spin-coating. Then the coated silicon wafer was soft-baked for 7 minutes and exposed to UV radiation beneath the mask utilising a mask aligner. This negative photoresist crosslinks upon exposure to the UV radiation. The unexposed parts of the photoresist are soluble and can be eliminated during developing. After exposure, the wafer was baked for 7 minutes on the hot plate, cooled, and developed using the SU-8 developer. Later the silicon wafer was hard-baked for 3 minutes and rinsed with isopropyl alcohol to clean the residues.

5.2.2 PDMS micro-molding

PDMS precursor (Sylgard 184 Silicone Elastomer) and a crosslinking agent were mixed at 10:1 ratio (based on weight). After degassing, this mixture was poured on the SU-8 master mold and cured at 70 °C for 6 hours. Later the cured PDMS microchannel block was cut according to the size, detached from the master, and pierced holes at inlets and outlet of the microchannel.

5.2.3 Fabrication of gold band microelectrodes on the slide

Standard photolithography procedure was used to deposit (AZ ECI 3027, MicroChem Inc.) photoresist electrode bands on a glass slide, followed by speatureing of gold and washing with acetone.

5.2.4 Final assembly

The PDMS microchannel block and the glass slide having microband gold electrodes were treated with oxygen plasma. Plasma oxidises both PDMS and glass surfaces, PDMS surface becomes silanol (SiOH). Upon placing the oxidised PDMS on the oxidised glass; PDMS irreversibly binds to the glass surface by Si-O-Si covalent bonds.

5.3 T-junction microfluidic electrochemical device for the ion transfer studies

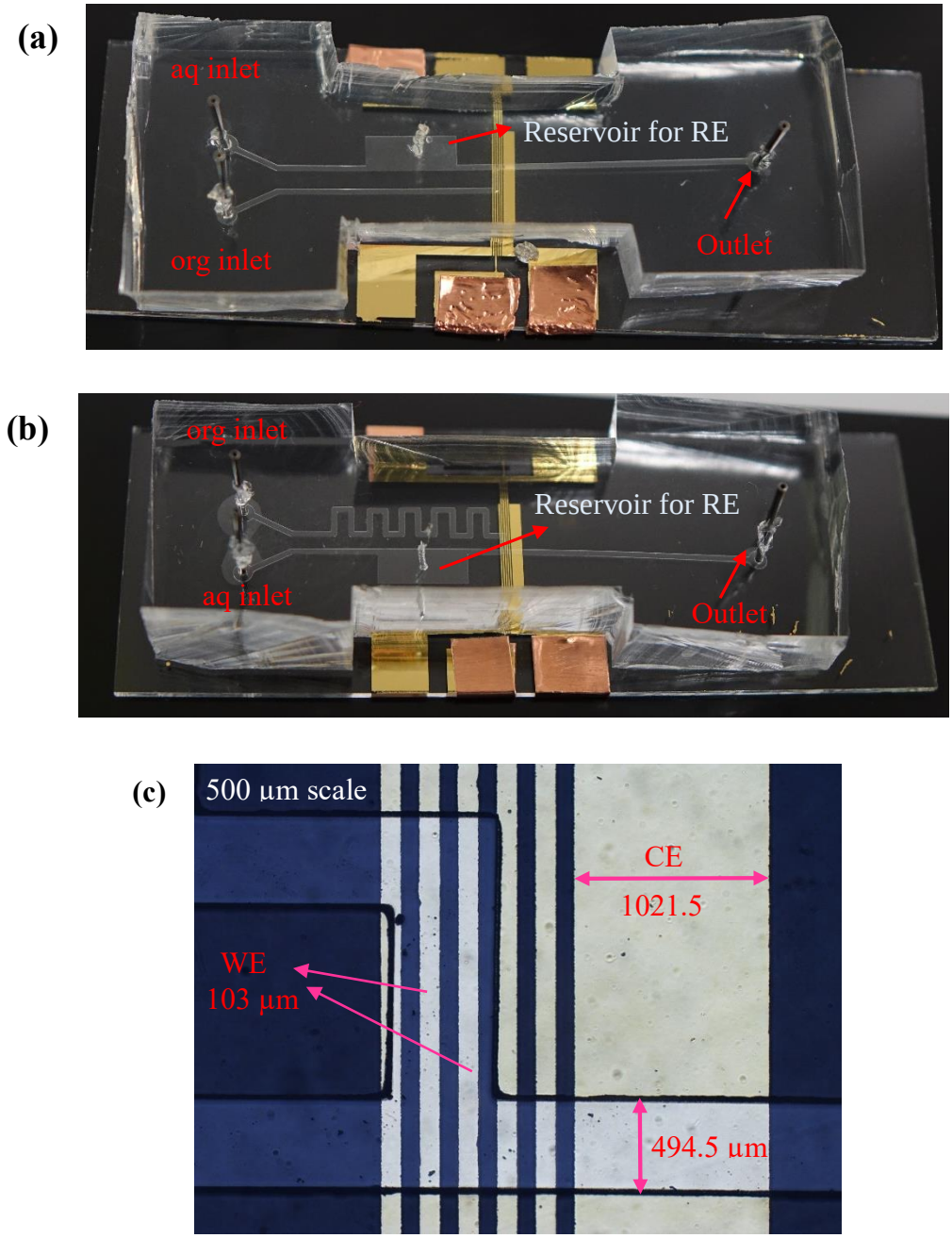

Figure 5.1 (a) and **(b)** Photographs of the microfluidic electrochemical devices having T-junction on the Au microband electrodes. **(c)** Photograph showing the microchannel placement on the Au microelectrodes.

The purpose of the T-junction microfluidic electrochemical system is to study the ion transfer with static organic and mobile aqueous phase or vice versa. **Fig 5.1a** and **b** show the photographs of microfluidic devices having T-junction. These cells were designed to study the ion transfer in the condition where the organic phase is static, and the aqueous phase is flowing. The intention was to have a stable organic|mobile aqueous interface at the T-junction (exactly where the organic microchannel meets the aqueous

one). Fabrication of such devices is quite complicated; however, it requires many attempts to have a proper working device.

Microchannels of width 500 μm were designed since the slimmer width will help to have a stable organic|mobile aqueous interface at the T-junction. A separate reservoir in contact with the aqueous channel was designed to mount the reference electrode (Pt//Ag/AgCl pseudo-reference electrode). A glass slide with Au WE (width ≈ 100 μm) and Au CE bands (width ≈ 1000 μm) was used as the substrate. **Fig 5.1c** shows the placement of the T-junction microchannel on the microband Au electrodes. The manual assembly of plasma-treated PDMS microchannel on the glass slide in alignment with microband Au electrodes is quite tricky (**Fig 5.1c**).

For T-junction anion transfer experiments, 10 mM dmfc dissolved in the NOP was used as the static organic phase. **Fig 5.2 a**–**d** show the instance where the aqueous phase is flowing at 5 μL min^{-1}, and the organic phase is static. As the aqueous phase starts flowing, gradually, the NOP|aqueous interface moves away from the T-junction. Moreover, the interface becomes unstable when potential is applied to the WE.

Fig 5.3 shows the ion transfer CVs measurements performed at T-junction microfluidic TPE systems. Since the NOP|aqueous interface is not stable when the aqueous phase is flowing, hence the CVs are not reproducible. When the NOP|aqueous interface was near to the T-junction (**Fig 5.2a**), I observed the red coloured CVs; while the interface is at the middle of T-junction (**Fig 5.2d**), black CVs were obtained.

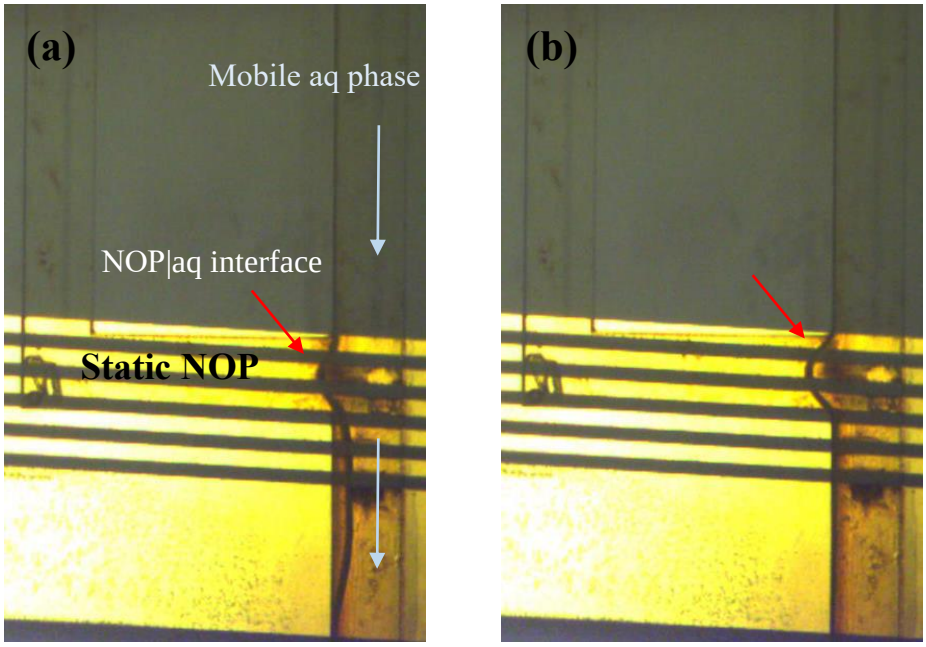

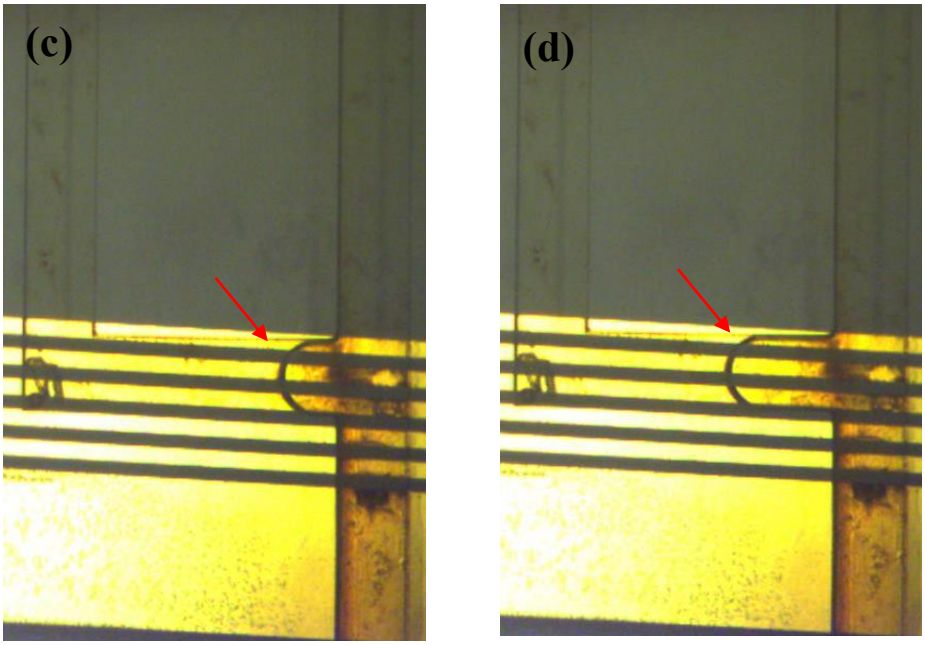

Figure 5.2 Photographs show the microfluidic TPE system where the NOP phase is in the static condition, and the aqueous phase is flowing at 5 µL min^{-1}. Photographs **a** to **d** display the instability of NOP|aqueous interface (red arrow), interface slowly moves away from the T-junction during the contentious flow of aqueous phase.

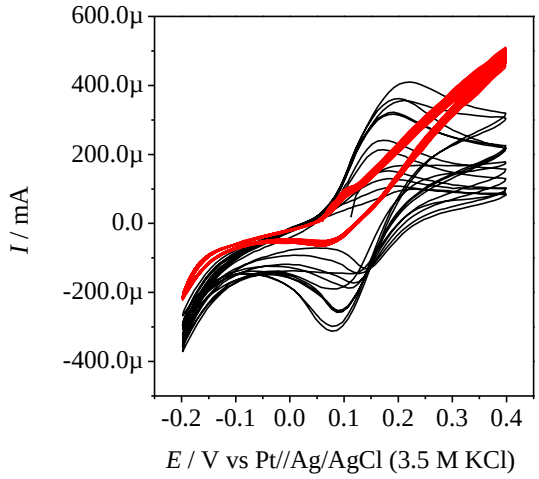

Figure 5.3 Continuous CV cycles of 10 mM dmfc in static NOP phase sharing interface at T-junction with 0.1 M $NaClO_4$ flowing at 5 µL min^{-1}. Red CVs were obtained when NOP|aqueous interface was near to the T-junction, and black CVs were produced when NOP|aqueous interface was away from the T-junction.

5.3.1 Modification of T-junction device with octadecyltrichlorosilane

Since NOP|aqueous interface is not stable at the T-junction, I tried to increase the hydrophobicity of the organic channel with octadecyltrichlorosilane (OTS). X. Lin and coworkers have shown that PDMS-glass channel can be hydrophobised by soaking with a 1 M NaOH, followed by washing with water, drying, and flowing 5% OTS dissolved in the mineral oil [14]. Treatment with NaOH makes both PDMS and glass substrate hydrophilic hence OTS coupling happens on PDMS-glass channel and makes it hydrophobic.

However, in my case, soaking the channel with 1 M NaOH was promoting to detach the PDMS from the glass substrate, which lead to the leakage of the microfluidic device. Hence, I used a different method. After bonding the plasma-treated PDMS channel and glass substrate; I filled the organic channel with 5% OTS-mineral oil solution and soaked for 5 mins. Upon silanisation, both PDMS and glass surfaces become hydrophobic by the attachment of octadecyl functionality.

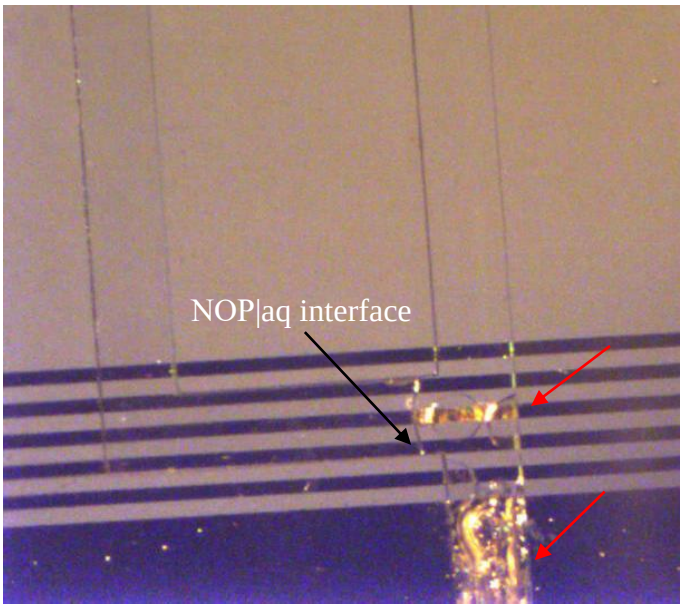

Figure 5.4 Photograph of the OTS treated microfluidic electrochemical devices. Red arrows show that the strange reaction happened on the WE and CE upon applying voltage.

Unfortunately, the silanisation process destroyed the Au band electrodes. As displayed in **Fig. 5.4**, upon applying the potential, both WE and CE reacted with the aqueous phase, and air bubbles were formed. Electrochemistry was not seen. Later, to protect the microband electrodes, the following modifications were done; (1) The distance between the organic inlet and microelectrodes was treated with OTS; (2) The organic microchannel of the PDMS block was silanised before the final assembly. However, the above changes did not help to keep the interface stable at the T-junction.

5.3.2 Other designs of the T-junction microfluidic devices

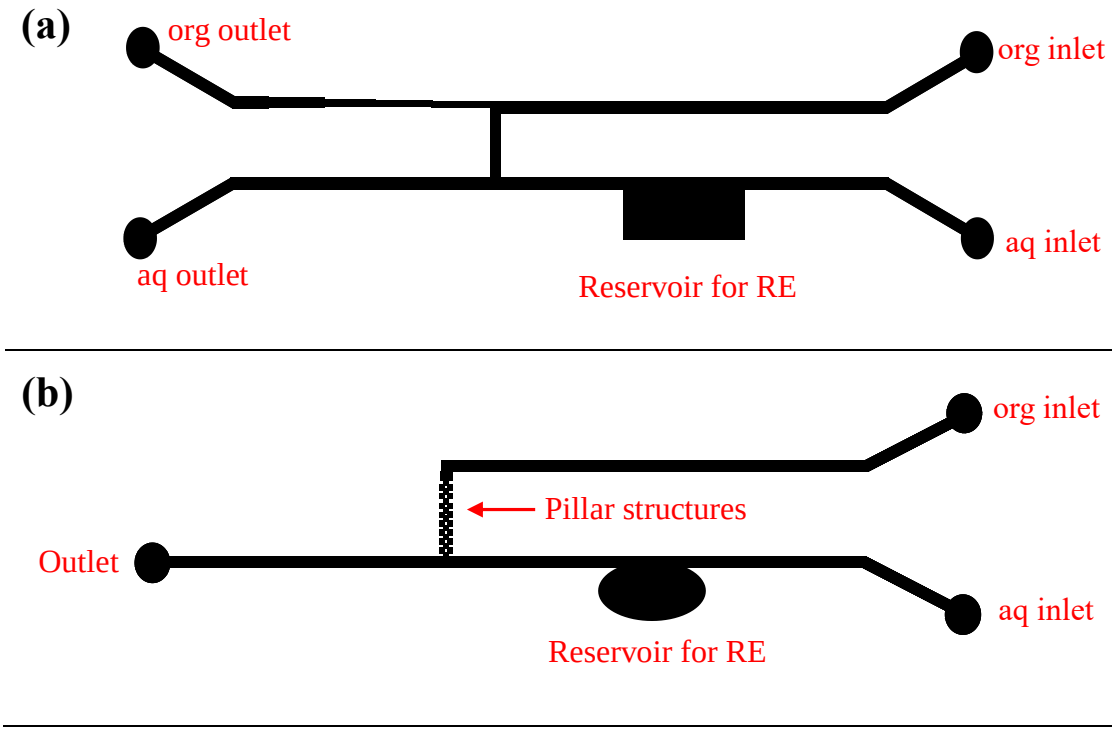

Figure 5.5 Microchannels designs used to create a small slit outlet for the organic phase **(a)** and the pillars at the T-junction **(b).**

After learning that the hydrophobised organic channel is not sufficient enough to keep the interface stable, several modifications were done to the basic design of the T-junction. These alterations were based on introducing the small slit to the organic channel (**Fig. 5.5a**) and the PDMS micropillars at the T-junction (**Fig. 5.5b**).

Along with the hydrophobised organic channel, the small slit (100 µm width) to the organic phase was introduced (**Fig. 5.5a**). In this case, to keep the NOP|aqueous interface stable at the T-junction, NOP phase flowed at a very less flow rate (0.5 to 3 µL min^{-1}) and the aqueous phase flowed at 5 to 30 µL min^{-1}. The optimised flow rates (aqueous 5 to 10 µL min^{-1} and NOP at 1 µL min^{-1}) can keep the interface near T-junction, but the interface keeps vibrating at the constant back-and-forth movement due to slight leaking of NOP along with the aqueous phase as shown in **Fig. 5.6**. CVs measured in this setup were not reproducible and almost look similar to **Fig. 5.3**.

An air bubble was formed during the final assembly of the device; however, it is away from the organic channel and can be neglected. An additional difficulty with the square-shaped aqueous reservoir is the formation of air bubbles during the insertion of a RE, and they reside at the corners of the reservoir.

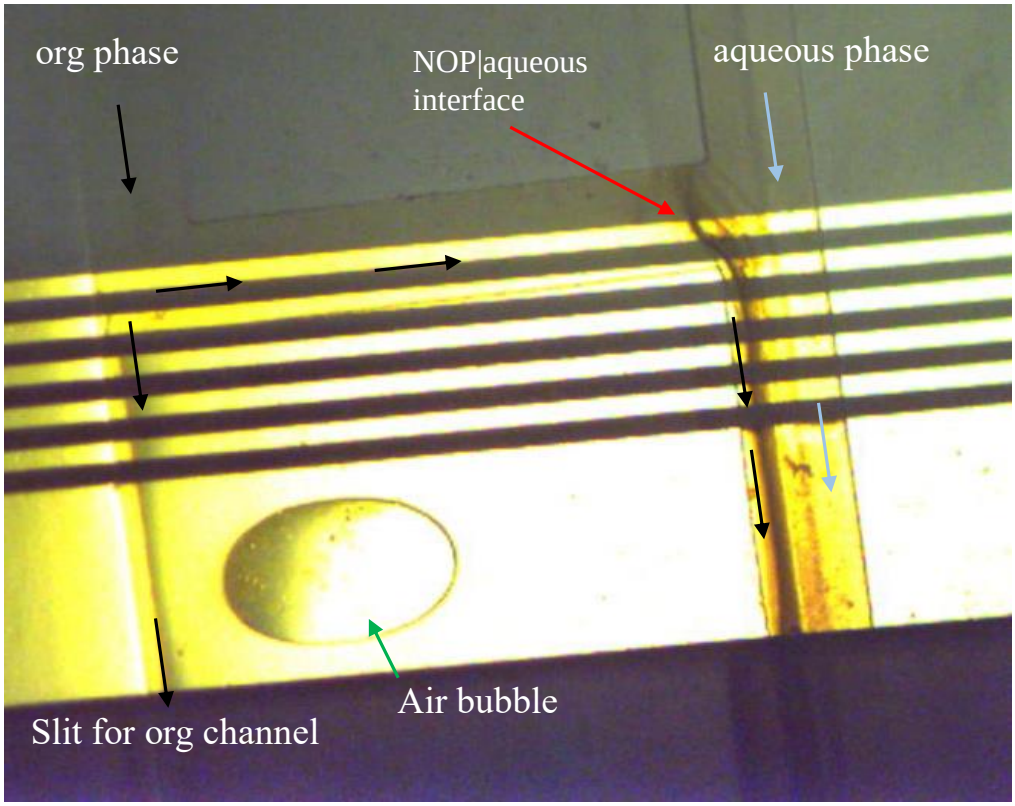

Figure 5.6 T-junction microfluidic electrochemical device with a slit in the organic channel. Black arrows show the flowing of NOP in the slit as well as leaking with the aqueous phase in the aqueous channel.

In another model, square-shaped micropillars (200 µm width) were created inside the PDMS microchannel, and the RE reservoir shape was changed to an oval using the design shown in **Fig. 5.5b**. The gentle press removes the air bubbles in the oval-shaped reservoir. Even the PDMS pillars could not stop the movement of the interface. Moreover, the slight movement of interface among the micropillars creates the droplets of the aqueous phase in NOP. Also, the leaking of NOP with the aqueous phase was observed.

5.4 Conclusion

I attempted to fabricate the T-junction microfluidic device to perform the TPE ion transfer CV studies where one phase is immobile, and the other is mobile.

The first difficulty was to the fabrication of leak-proof electrochemical microfluidic cell. Another challenge was the manual assembly of the T-junction PDMS block on the glass slide having Au band electrodes; so that 500 µm wide channel should

contain two WEs of 100 µm width placed 100 µm apart. The reason for this is in case one electrode fails to work; another one can be used as WE.

The principal problem for not getting the reproducible TPE ion transfer CVs at T-junction is the instability of the NOP|aqueous interface. Even hydrophobised PDMS and glass surface was not able to keep the interface stable. Further, other models, such as T-junction with slit and micropillars, also did not stabilise the interface.

5.5 References

[1] E. Bak, M. Donten, Z. Stojek, Three-phase electrochemistry with a cylindrical microelectrode, Electrochem. Commun. 7 (2005) 483–489. doi:10.1016/j.elecom.2005.03.005.

[2] E. Bak, M. Donten, Z. Stojek, Three-phase electrochemistry with cylindrical microelectrode crossing vertically the boundary of two immiscible liquids, J. Electroanal. Chem. 600 (2007) 45–53. doi:10.1016/j.jelechem.2006.02.022.

[3] E. Bak, M. Donten, Z. Stojek, F. Scholz, The punctured droplet electrode – A new three-phase electrode with well defined geometry, Electrochem. Commun. 9 (2007) 386–392. doi:10.1016/j.elecom.2006.09.032.

[4] S.M. MacDonald, J.D. Watkins, Y. Gu, K. Yunus, A.C. Fisher, G. Shul, M. Opallo, F. Marken, Electrochemical processes at a flowing organic solvent|aqueous electrolyte phase boundary, Electrochem. Commun. 9 (2007) 2105–2110. doi:10.1016/j.elecom.2007.05.031.

[5] J.D. Watkins, S.M. MacDonald, P.S. Fordred, S.D. Bull, Y. Gu, K. Yunus, A.C. Fisher, P.C. Bulman-Page, F. Marken, High-yield acetonitrile | water triple phase boundary electrolysis at platinised Teflon electrodes, Electrochim. Acta. 54 (2009) 6908–6912. doi:10.1016/j.electacta.2009.06.083.

[6] D. Kaluza, W. Adamiak, T. Kalwarczyk, K. Sozanski, M. Opallo, M. Jönsson-Niedziolka, Anomalous Effect of Flow Rate on the Electrochemical Behavior at a Liquid|Liquid Interface under Microfluidic Conditions, Langmuir. 29 (2013) 16034–16039. doi:10.1021/la403614z.

[7] D. Kaluza, W. Adamiak, M. Opallo, M. Jonsson-Niedziolka, Comparison of Ion Transfer Thermodynamics at Microfluidic and Droplet-Based Three Phase Electrodes, Electrochim. Acta. 132 (2014) 158–164. doi:10.1016/j.electacta.2014.03.105.

[8] G.M. Whitesides, The origins and the future of microfluidics, Nature. 442 (2006) 368–373. doi:10.1038/nature05058.

[9] D.G. Rackus, M.H. Shamsi, A.R. Wheeler, Electrochemistry, biosensors and microfluidics: a convergence of fields, Chem. Soc. Rev. 44 (2015) 5320–5340. doi:10.1039/C4CS00369A.

[10] J.C. McDonald, D.C. Duffy, J.R. Anderson, D.T. Chiu, H. Wu, O.J.A. Schueller, G.M. Whitesides, Fabrication of microfluidic systems in poly(dimethylsiloxane),

Electrophoresis. 21 (2000) 27–40. doi:10.1002/(SICI)1522-2683(20000101)21:1<27::AID-ELPS27>3.3.CO;2-3.

[11] M.A. Modestino, D. Fernandez Rivas, S.M.H. Hashemi, J.G.E. Gardeniers, D. Psaltis, The potential for microfluidics in electrochemical energy systems, Energy Environ. Sci. 9 (2016) 3381–3391. doi:10.1039/C6EE01884J.

[12] G.P. Roth, R. Stalder, T.R. Long, D.R. Sauer, S.W. Djuric, Continuous-Flow Microfluidic Electrochemical Synthesis: Investigating a New Tool for Oxidative Chemistry, J. Flow Chem. 3 (2013) 34–40. doi:10.1556/JFC-D-13-00002.

[13] W.B. Zimmerman, Electrochemical microfluidics, Chem. Eng. Sci. 66 (2011) 1412–1425. doi:10.1016/j.ces.2010.03.057.

[14] X. Lin, X. Hu, Z. Bai, Q. He, H. Chen, Y. Yan, Z. Ding, A microfluidic chip capable of switching W/O droplets to vertical laminar flow for electrochemical detection of droplet contents, Anal. Chim. Acta. 828 (2014) 70–79. doi:10.1016/j.aca.2014.04.023.

Summary and conclusions

This dissertation is dedicated to the electrochemical analysis of different redox probes at the organic|aqueous|electrode three-phase electrode (TPE) configuration. Till now, the following points have been adequately not addressed or rarely discussed in the literature of TPE ion transfer electrochemistry:

1) The redox behaviour of biologically essential compounds such as AQ and NQ are not investigated for inorganic cation transfer studies at the TPE setup. So far, Fe(III)TPP-Cl and LBPC metallorganic compounds were studied; however, the organic redox compounds (TCNQ and DPPH) investigated only for organic cation transfer reactions. In the case of metallorganic compound reduction, the central metal atom carries the negative charge, and the cation transfer depends on its lipophilicity. In quinones, the carbonyl functional groups obtain the charge when they undergo a redox reaction. The mechanism of ion transfer, when driven by the reduction of carbonyl functionality, is not known (**chapter 4.1**).

2) TCNQ redox probe was employed to investigate the different alkylammonium cations transfer studies at the TPE setup. The reduction potential of TCNQ depends on the lipophilicity of the transferring alkylammonium cation. On the other hand, TCNQ was not investigated for TPE inorganic cation transfer studies. We do not know whether TCNQ is sufficiently lipophilic for inorganic cations transfer or not. If TCNQ is adequately lipophilic, the ion transfer is based on the lipophilicity of the transferring cation or due to the ion-pair formation of the reduced TCNQ with the aqueous cation; because TCNQ derivatives form ion-pair with the inorganic supporting electrolytes in the single-phase electrochemistry (**chapter 4.2**).

3) Until now, DMFc and TPP-metal complexes (Mn, Fe, and Co) have used for anion transfer studies. DMFc is not suitable for highly hydrophilic anions, and TPP-metal complexes show interactions with the transferring nucleophilic anions. Consequently, a new, highly lipophilic non-interacting redox probe is required. (**chapter 4.3**).

4) TPE ion transfer voltammetry in the microfluidic condition where the parallel flow of the organic and aqueous phases on the microband electrode has studied. In addition to this, the voltammetry where one phase is stationary and the other is flowing has to be studied to get more insights into the ion transfer process in dynamic conditions (**chapter 5**).

The above-mentioned issues have been discussed in this thesis, and the most important outcomes are as follows:

1) Electrochemistry of biologically important quinones at GC|n-octyl pyrrolidone|aqueous interface.

- Both AQ and NQ displayed consecutive two-step one-electron reductions in NOP solvent ($Q \rightarrow Q^{\bullet -} \rightarrow Q^{2-}$).

- At the TPE configuration, AQ exhibited a single-step two-electron reduction (AQ to AQ^{2-}), which was followed by cation transfer from water to NOP. The cation transfer potential varied with the ionic potential of the aqueous cation due to the ion-pair formation between the AQ^{2-} and transferred cation in NOP.

- NQ reduction at TPE configuration happened in two steps ($NQ \rightarrow NQ^{\bullet -} \rightarrow NQ^{2-}$). In the first step, $NQ^{\bullet -}$ species expelled to the aqueous phase and also adsorbed on the NOP|aqueous interface or settled in an emulsion. Therefore, the first reduction potential was dependent on the hydrophilicity of the aqueous *anion* due to salting-out effects. The second reduction was accompanied by the cations transferred from water to NOP with the reduction potential dependent on the ionic potential of the aqueous cation.

- For both AQ and NQ, reduction potential changed with the ionic potential of the transferred cation, not with its hydrophobicity.

2) Electrochemistry of TCNQ at GC|n-octyl pyrrolidone|aqueous interface.

- TCNQ in the NOP solvent showed two subsequent one-electron reductions to $TCNQ^{\bullet -}$ and $TCNQ^{2-}$.

- At TPE configuration, reduced TCNQ anions ($TCNQ^{\bullet -}$ and $TCNQ^{2-}$) were expelled to the aqueous phase instead of cation transfer from water to NOP.

- Expulsion of the TCNQ redox probe was confirmed by the decrease in the current of continuous CVs and independency of the SWV peak potentials for different cations in the aqueous phase.

- TCNQ to $TCNQ^{\bullet -}$ reduction potential was dependent on the hydrophobicity of the aqueous *anion* due to salting-out effects.

3) Three-phase electrochemistry of a lipophilic neutral heteroleptic bis(tridentate) $[Ru^{II}(LR)(L)]^0$ complex at GC|NB|aqueous interface.

- A highly lipophilic neutral electroactive $[Ru^{II}(LR)(L)]^0$ complex was synthesised and characterised.

- The deprotonation of benzimidazole nitrogen sites of L ligand helped to isolate $[Ru^{II}(LR)(L)]^0$ as a neutral complex and lowered $Ru^{II/III}$ oxidation potential; so that one-electron oxidation of $[Ru^{II}(LR)(L)]^0$ to $[Ru^{III}(LR)(L)]^+$ happens before the water oxidation at the three-phase interface.

- At GC|NB|aqueous three-phase junction, the oxidation of $[Ru^{II}(LR)(L)]^0$ to $[Ru^{III}(LR)(L)]^+$ in NB is accompanied by the anion transfer from the aqueous to NB.

- Anion transfer potential depends on the hydrophobicity of the aqueous anion and its concentration.

4) TPE ion transfer voltammetry studies in T-junction microfluidic devices.

- TPE ion transfer voltammetry studies at T-junction in which the organic phase is stationary and the aqueous phase flowing were not reproducible due to the tiny back-and-forth vibration of the interface.

- The organic microchannel with the small slit outlet, increasing the hydrophobicity of the organic microchannel, and implementing PDMS micropillar structures at the T-junction did not stabilise the interface.

- PDMS based T-junction microfluidic devices and their surface modification are not suitable to study the TPE ion transfer voltammetry of one phase stationary and the other phase flowing configuration.

This research provides adequate information about the selection of compounds for three-phase ion transfer studies. Furthermore, it provides information regarding the ligand systems, which can lower the oxidation potential of the central metal ions, and also increase the lipophilic character of the complex.

IPC PAS, Warsaw, Poland.